LOW-RESOLUTION SPECTROSCOPY OF GAMMA-RAY BURST OPTICAL AFTERGLOWS: BIASES IN THE *SWIFT* SAMPLE AND CHARACTERIZATION OF THE ABSORBERS[*]

J. P. U. Fynbo[1,2], P. Jakobsson[2], J. X. Prochaska[3], D. Malesani[1], C. Ledoux[4], A. de Ugarte Postigo[4], M. Nardini[5], P. M. Vreeswijk[1,4], K. Wiersema[6], J. Hjorth[1], J. Sollerman[1,7], H.-W. Chen[8], C. C. Thöne[1,9], G. Björnsson[2], J. S. Bloom[10], A. J. Castro-Tirado[11], L. Christensen[12], A. De Cia[2], A. S. Fruchter[13], J. Gorosabel[11], J. F. Graham[13], A. O. Jaunsen[1,14], B. L. Jensen[1], D. A. Kann[15], C. Kouveliotou[16], A. J. Levan[17], J. Maund[1], N. Masetti[18], B. Milvang-Jensen[1], E. Palazzi[18], D. A. Perley[10], E. Pian[19], E. Rol[6], P. Schady[20], R. L. C. Starling[6], N. R. Tanvir[6], D. J. Watson[1], D. Xu[1], T. Augusteijn[21], F. Grundahl[22], J. Telting[21], AND P.-O. Quirion[22]

[1] Dark Cosmology Centre, Niels Bohr Institute, University of Copenhagen, Juliane Maries Vej 30, DK-2100 Copenhagen Ø, Denmark
[2] Centre for Astrophysics and Cosmology, Science Institute, University of Iceland, Dunhagi 5, IS-107 Reykjavík, Iceland
[3] Department of Astronomy and Astrophysics, UCO/Lick Observatory, University of California, 1156 High Street, Santa Cruz, CA 95064, USA
[4] European Southern Observatory, Alonso de Córdova 3107, Vitacura, Casilla 19001, Santiago 19, Chile
[5] SISSA, Via Beirut 2/4, I-34014 Trieste, Italy
[6] Department of Physics and Astronomy, University of Leicester, University Road, Leicester, LE1 7RH, UK
[7] Department of Astronomy, The Oskar Klein Centre, Stockholm University, 106 91 Stockholm, Sweden
[8] Department of Astronomy & Astrophysics and Kavli Institute for Cosmological Physics, University of Chicago, Chicago, IL 60637, USA
[9] INAF, Osservatorio Astronomico di Brera, Via Bianchi 46 I-23806 Merate, Italy
[10] Department of Astronomy, University of California, Berkeley, CA 94720-3411, USA
[11] IAA-CSIC, P.O. Box 03004, E-18080 Granada, Spain
[12] European Southern Observatory, Karl-Schwarzschildstrasse 2, D-85748 Garching, Germany
[13] Space Telescope Science Institute, Department of Physics and Astronomy, Johns Hopkins University, 3700 San Martin Drive, Baltimore, MD 21218, USA
[14] Institute of Theoretical Astrophysics, University of Oslo, P.O. Box 1029 Blindern, N-0315 Oslo, Norway
[15] Thüringer Landessternwarte Tautenburg, Sternwarte 5, D-07778 Tautenburg, Germany
[16] NASA Marshall Space Flight Center, Huntsville, AL 35805, USA
[17] Department of Physics, University of Warwick, Coventry CV4 7AL, UK
[18] INAF, Istituto di Astrofisica Spaziale e Fisica Cosmica di Bologna, via Gobetti 101, 40129 Bologna, Italy
[19] INAF-Trieste Astronomical Observatory, 34143 Trieste, Italy
[20] The UCL Mullard Space Science Laboratory, Holmbury St Mary, Dorking, Surrey RH5 6NT, UK
[21] Nordic Optical Telescope Apartado 474, 38700 Santa Cruz de La Palma, Santa Cruz de Tenerife, Spain
[22] Institute of Physics and Astronomy, University of Århus, Ny Munkegade, DK-8000 Århus C, Denmark
Received 2009 July 10; accepted 2009 October 15; published 2009 November 30

ABSTRACT

We present a sample of 77 optical afterglows (OAs) of *Swift* detected gamma-ray bursts (GRBs) for which spectroscopic follow-up observations have been secured. Our first objective is to measure the redshifts of the bursts. For the majority (90%) of the afterglows, the redshifts have been determined from the spectra. We provide line lists and equivalent widths (EWs) for all detected lines redward of Lyα covered by the spectra. In addition to the GRB absorption systems, these lists include line strengths for a total of 33 intervening absorption systems. We discuss to what extent the current sample of *Swift* bursts with OA spectroscopy is a biased subsample of all *Swift* detected GRBs. For that purpose we define an X-ray-selected statistical sample of *Swift* bursts with optimal conditions for ground-based follow-up from the period 2005 March to 2008 September; 146 bursts fulfill our sample criteria. We derive the redshift distribution for the statistical (X-ray selected) sample and conclude that less than 18% of *Swift* bursts can be at $z > 7$. We compare the high-energy properties (e.g., γ-ray (15–350 keV) fluence and duration, X-ray flux, and excess absorption) for three subsamples of bursts in the statistical sample: (1) bursts with redshifts measured from OA spectroscopy; (2) bursts with detected optical and/or near-IR afterglow, but no afterglow-based redshift; and (3) bursts with no detection of the OA. The bursts in group (1) have slightly higher γ-ray fluences and higher X-ray fluxes and significantly less excess X-ray absorption than bursts in the other two groups. In addition, the fractions of dark bursts, defined as bursts with an optical to X-ray slope $\beta_{OX} < 0.5$, is 14% in group (1), 38% in group (2), and >39% in group (3). For the full sample, the dark burst fraction is constrained to be in the range 25%–42%. From this we conclude that the sample of GRBs with OA spectroscopy is not representative for all *Swift* bursts, most likely due to a bias against the most dusty sight lines. This should be taken into account when determining, e.g., the redshift or metallicity distribution of GRBs and when using GRBs as a probe of star formation. Finally, we characterize GRB absorption systems as a class and compare them to QSO absorption systems, in particular the damped Lyα absorbers (DLAs). On average GRB absorbers are characterized by significantly stronger EWs for H I as well as for both low and high ionization metal lines than what is seen in intervening QSO absorbers. However, the distribution of line strengths is very broad and several GRB absorbers have lines with EWs well within the range spanned by QSO-DLAs. Based on the 33 $z > 2$ bursts in the sample, we place a 95% confidence upper limit of 7.5% on the mean escape fraction of ionizing photons from star-forming galaxies.

Key words: dust, extinction – galaxies: high-redshift – gamma rays: bursts

Online-only material: color figures

1. INTRODUCTION

The exploration of gamma-ray bursts (GRBs) has been among the most fascinating in the last decade of astrophysical research. After the breakthrough in 1997, when X-ray and optical afterglows (OAs) were discovered (Costa et al. 1997; van Paradijs et al. 1997), progress has been rapid. The connection between long-duration GRBs and star-forming galaxies has been empirically well established. There is an exclusive coincidence of long-duration GRBs with actively star-forming galaxies (e.g., Hogg & Fruchter 1999; Bloom et al. 2002; Fruchter et al. 2006), the majority of which show elevated specific star formation rates (Christensen et al. 2004). In several cases, long-duration GRBs have been directly associated with supernovae (SNe; e.g., Hjorth et al. 2003; Stanek et al. 2003; Campana et al. 2006; Woosley & Bloom 2006). Only a decade after the first afterglow detection, GRBs have allowed us to probe the universe from redshifts of almost 0 to larger than 8, representing larger look-back times than accessible with any other class of astrophysical objects (Jakobsson et al. 2006b; Tanvir et al. 2009; Salvaterra et al. 2009).

An important objective is to use GRBs as cosmological probes to study star formation primarily in the distant universe. GRBs may be ideal probes as each burst pinpoints the location of a single massive star. Hence, GRBs may allow a census of where massive stars are formed throughout the observable universe (e.g., Wijers et al. 1998). Through optical spectroscopy of the afterglows we can measure metallicities, molecular content, and kinematical properties of the sight lines to bursts within their hosts. After the bursts have faded away, imaging allows a detailed study of the host galaxies in emission, providing a census of the classes of galaxies contributing to the global star formation density as a function of redshift. There are three main issues to consider in this context: observational bias, intrinsic bias, and the influence the GRBs and their afterglows may have on their environments. Concerning intrinsic bias, it is believed that massive stars require low metallicity to retain enough angular momentum to form a GRB (e.g., Hirschi et al. 2005; Woosley & Heger 2006), and the GRBs hence are biased tracers of star formation (e.g., Guetta & Piran 2007; Kistler et al. 2008). Nevertheless, to establish if the evidence supports a low metallicity bias, it is necessary to first establish the importance and possible implications of observational bias, in particular as such a bias, if it exists, will unavoidably impact the measured distribution of metallicities for GRBs (see also Berger et al. 2007). Finally, concerning the issue of the impact of the GRBs and their afterglows on the gas along the line of sight, it is now well established that UV pumping affects intervening gas in the hosts (Dessauges-Zavadsky et al. 2006; Vreeswijk et al. 2007; D'Elia et al. 2009a, 2009b; Ledoux et al. 2009). It is also expected on theoretical grounds that GRB afterglows may destroy dust in the near environment of the burst, possibly out to as far as 100 pc from the GRB (Fruchter et al. 2001).

To address the issue of observational bias, it is necessary to build a sample of GRBs for which the incompleteness is well understood and can be quantified. In this paper, we present a spectroscopic sample of long-duration GRBs discovered by the *Swift* mission (Gehrels et al. 2004) for which follow-up optical spectroscopy has been secured. The purpose of the paper is twofold: (1) to discuss the GRB absorbers as a class and compare this class of absorbers with QSO absorbers, and (2) to discuss to which extent our current sample of GRBs with measured redshifts from OA spectroscopy is a biased subsample of all GRBs. GRB absorbers have been compared with other classes of absorbers in several papers in the literature (e.g., Jensen et al. 2001; Savaglio et al. 2003; Jakobsson et al. 2006c; Fynbo et al. 2006c; Savaglio 2006; Prochaska et al. 2007, 2008a; Fynbo et al. 2008d). However, most of these studies have been based on samples containing only few and/or predominantly optically bright afterglows. The issue of bias in the samples of GRBs with measured redshift has been discussed in the literature before (e.g., Bloom 2003; Fiore et al. 2007; Coward 2009). Fiore et al. (2007) discussed the importance of selection effects in the properties of the detection of the GRBs themselves, e.g., the sensitivity of the triggering detector as a function of energy. Coward (2009) argued that there is a learning curve at work in the following sense: over the years since the launch of *Swift*, the mean time taken to acquire spectroscopic redshifts for a GRB afterglow has evolved to shorter times. He also finds a correlation between the mean time before a spectroscopic redshift is secured and the measured redshift suggesting that low redshift bursts were preferentially missed in the first years of *Swift* operation. We have been following the same follow-up strategy since the launch of *Swift*. Furthermore, for the present study we only include *Swift* bursts detected after 2005 March where *Swift* operations were well established. Hence, for the present study there should be no significant issue with a learning curve. Here we will rather try to infer to which extent the sample of bursts with follow-up optical spectroscopy could be biased against, e.g., dusty sight lines.

The paper is organized in the following way: In Section 2, we define our sample and provide a list of the GRBs for which we present spectra in this paper. Section 3 describes our observations and data reduction. In Section 4.1, we present the redshift distribution of the statistical sample. In Section 4.2, we discuss biases in the sample of bursts with OA spectroscopy. In Section 4.3, we discuss GRB absorbers as a class and compare them to QSO absorbers. In Section 4.5, we briefly discuss the intervening absorbers in the sample. Finally, in Section 5, we offer our conclusions. In Appendices A and B, we provide line lists and plots of the spectra for the 77 optical GRB afterglows in our sample and provide notes on individual objects.

Throughout this paper we assume a flat cosmology with $\Omega_\Lambda = 0.70$, $\Omega_m = 0.30$, and a Hubble constant of $H_0 = 70$ km s^{-1} Mpc^{-1}.

2. THE SAMPLE

The aim of the sample selection is to construct a sample of long GRBs that is selected independent of the optical properties of the afterglows and at the same time has as high completeness in high quality optical follow-up as possible. We find that the optimal way to build such a sample is by including all *Swift* GRBs fulfilling the following criteria (Jakobsson et al. 2006b):

1. A Swift-detected GRB with observed duration $T_{90} > 2$ s.
   We wish to build a sample of long-duration GRBs known to be associated with massive stellar death. We could choose to make a stronger cut, e.g., $T_{90} > 5$ s, in order to avoid contamination from the long tail of the short-duration bursts. However, the number of bursts with 2 s $< T_{90} < 5$ s is so small that this would not make a significant difference for the statistical properties of the sample. Therefore, we choose to keep the standard operational definition of long GRBs (Kouveliotou et al. 1993).

2. XRT afterglow position distributed within 12 hr.
   With this criterion, we secure that a precise afterglow position is available quickly, which is crucial for efficient ground-based follow-up. This criterion also excludes bursts close to the Moon.

3. Small foreground Galactic extinction: $A_V < 0.5$ mag.
   With this criterion, we remove from the sample bursts with high Galactic extinction. These bursts are also typically located in very crowded fields. Removing these bursts from the sample does not introduce any bias in the intrinsic properties of the bursts.

4. Favorable declination: $-70° < \delta < 70°$.
   For bursts close to the poles, the probability of securing ground-based follow-up is smaller, and we therefore apply this declination cut to the sample.

5. Sun-to-field distance larger than $55°$.
   Bursts that are too close to the Sun cannot be observed from the ground for very long. With this criterion we will usually have at least 1 hr during night time to secure a spectrum within 24 hr after the burst.

About 50% of all *Swift* GRBs do not fulfill these criteria, primarily for two reasons: first, *Swift* has to point close to the Sun a significant fraction of the time, and second, the fraction of the sky with Galactic $A_V > 0.5$ mag is about 34%. For bursts fulfilling the above criteria, we have attempted to detect optical and near-infrared afterglows and to measure their redshifts. Also, these bursts will have a high probability of being well observed by other follow-up teams.

3. OBSERVATIONS AND DATA REDUCTION

In this paper, we include bursts in the time interval from 2005 March to 2008 September. In this period, 146 bursts fulfilled our sample criteria (see Table 73 in Appendix B). These we will refer to as the *statistical sample* in the following. For 69 of these, we present spectroscopic observations in this paper. Most of the spectra have been obtained through our target-of-opportunity programs, but we also include a few spectra that we have obtained from the ESO and Gemini archives.

The spectra were obtained using one of the following instruments: (1) the Nordic Optical Telescope (NOT) equipped with the Andalucia Faint Object Spectrograph and Camera (AlFOSC); (2) the ESO-VLT equipped with either one of the two FOcal Reducer and low dispersion Spectrographs (FORS1 and FORS2), or in rare cases the Ultraviolet and Visual Echelle Spectrograph (UVES); (3) one of the Gemini telescopes equipped with one of the Gemini Multi-Object Spectrographs (GMOS-N and GMOS-S); (4) the 3 m Shane Telescope at Lick Observatory equipped with the dual-channel Kast spectrometer; and (5) the Keck telescope equipped with the Low Resolution Imaging Spectrograph (LRIS; Oke et al. 1995). In Table 1, we provide further details of each of the instrumental setups applied in this work.

Table 1
Instrumental Setups Used for Spectroscopic Data Presented in this Work

Telescope	Instrument	Grating	Resolution	Range (Å)
VLT	FORS1/2	300V	440	3400–9500
VLT	FORS1/2	1400V	2100	4600–5900
VLT	FORS1/2	1200R	2140	5800–7300
VLT	FORS1/2	600I	1500	6600–9400
VLT	UVES		45000	
Gemini-S/N	GMOS-S/N	R831	2200	5300–9000
		R400	965	5300–9000
		R150	315	4500–10000
		B600	844	3400–6000
Keck 1	LRIS	R300	540	3900–8000
		R400	1100	5800–9200
	HIRES		45000	
Shane-3m	Kast	600/7500	1000	3800–10000
		800/3460	1500	3800–7310
NOT	AlFOSC	G4	355	3600–9000

Notes. Resolutions are given for a 1 arcsec slit even though we some times used a slightly wider slit.

The longslit spectra were reduced using standard methods for bias subtraction, flat-fielding, and wavelength calibration. Most of the spectra have been flux calibrated using observations of spectrophotometric standard stars observed with the same setup as the afterglow spectra. For a few of the spectra, no standard star spectra were secured, and here we instead provide normalized spectra. Afterglows observed with UVES will be discussed in detail elsewhere (see, e.g., Fox et al. 2008; Ledoux et al. 2009), and for these bursts, we only show here the spectra and provide equivalent width (EW) measurements of the Si II λ1526, and/or C IV lines.

The spectra have been obtained under very diverse observing conditions (see Table 2). Given the transient nature of GRBs, the afterglows often have to be observed at high airmass, with poor seeing, through clouds and/or with a large Moon phase. In a few cases, we observed the afterglows in twilight.

The full list of spectroscopic targets is given in Table 2. In the table, we also include eight bursts that do not fulfill the sample criteria for which we also have secured spectra. In the following, we refer to the bursts in Table 2 as the *spectroscopic sample*.

4. RESULTS

In Appendix A, we provide notes on each burst in our spectroscopic sample. In Tables 5–72 in Appendix B, we provide line lists for all lines detected redward of Lyα both from the GRB absorbers and from the intervening absorption systems. We provide measurements for all lines for which we can measure the EWs with a signal-to-noise ratio (S/N) higher than 2. The EWs are measured in normalized spectra using an aperture given by two times the resolution full-width-at-half-maximum (for unresolved lines) or from where the profile reaches 1 on each side of the profile (for resolved or blended lines). The error bar includes the statistical noise and the error from the normalization. For the Lyα lines we do not provide EWs. Instead, we provide in Table 3 the H I column densities derived from Voigt-profile fits to the Lyα lines. In cases where several lines are blended we provide the EWs for the full blend. In cases where three or more lines are blended we have drawn a line around the blend in the tables to ease the reading. In Figure 14 in Appendix B, we show one- and two-dimensional spectra of each of the 77 bursts listed in Table 2.

Table 2
Spectroscopic Sample

GRB	Instrument	Exptime (ks)	Airmass	Seeing (arcsec)	Δt (hr)	Mag_{acq}	Redshift	Ref.
050319	AlFOSC	2.4	1.1	1.3	34.5	21.0	3.2425	(1)
050401	FORS2	11.6	1.1–1.7	0.7	14.7	23.3	2.8983	(2)
050408	GMOS-N	3.6				21.0	1.2356	(3)
050730	FORS2	1.8	1.2	1.5	4.1	17.8	3.9693	(4)
050801	LRIS	1.8	1.9	. . .	5.7	20.7	1.38	(5)
050802	AlFOSC	4.8	1.2	0.7	11.4	20.5	1.7102	(6)
050820A	UVES	12.1	2.1	1.0	0.5	16.0	2.6147	(7)
050824	FORS2	3.0	1.8	0.7	9.5	20.6	0.8278	(8)
050908	FORS1	3.6	1.1	0.6	1.6	20.5	3.3467	(9)
050922C	AlFOSC	2.4	0.9	1.3	1.0	16.5	2.1995	(1)
060115	FORS1	3.6	1.3–1.6	0.7	8.9	22.0	3.5328	(10)
060124	LRIS	1.0	1.6	1.0	16.1	19.5	2.3000	(11)
060206	AlFOSC	2.4	1.0	1.2	0.3	17.5	4.0559	(12)
060210	GMOS-N	3.0	1.1	. . .	1.2	20.6	3.9133	(13)
060502A	GMOS-N	3.6	1.6	. . .	5.2	21.2	1.5026	(14)
060512	FORS1	3.6	2.5	1.6	3.0	19.9	2.1	(15)
060526	FORS1	9.9	1.1–1.4	1.3	8.8	19.5	3.2213	(1)
060604	AlFOSC	1.2	1.7	1.0	10.0	21.5	$\lesssim 3$	(16)
060607A	UVES	12.0	1.9–1.0	1.0	0.1	14.7	3.0749	(17)
060614	FORS2	1.8	1.2	0.7	21.1	19.8	0.1257	(18)
060707	FORS2	5.4	1.0	1.1	34.4	22.4	3.4240	(1)
060708	FORS2	3.6	1.2	0.6	43.0	22.9	1.92	(19)
060714	FORS1	5.4	1.1	0.7	8.5	20.4	2.7108	(1)
060719	FORS2	2.4	1.1	2.2	50.0	24.5	$\lesssim 4.6$	(5)
060729	FORS2	5.4	2.0–2.6	1.5	13.2	17.5	0.5428	(20)
060807	FORS1	7.2	1.8	0.8	9.5	22.9	$\lesssim 3.4$	(21)
060908	GMOS-N	1.8	1.2	1.6	2.0	19.8	1.8836	(22)
060927	FORS1	5.4	1.2	1.5	12.5	24.0	5.4636	(23)
061007	FORS1	5.4	1.2–1.3	0.9	17.4	21.5	1.2622	(24)
061021	FORS1	1.8	1.9	0.8	16.5	20.5	0.3463	(25)
061110A	FORS1	5.4	1.4–1.8	0.8	15.0	22.0	0.7578	(26)
061110B	FORS1	3.6	1.3–1.5	0.7	2.5	22.5	3.4344	(27)
061121	LRIS	1.2	1.2	. . .	0.2	17.8	1.3145	(28)
070110	FORS2	5.4	1.5–1.9	1.0	17.6	20.8	2.3521	(29)
070129	FORS2	1.8	2.2	1.0	2.2	21.3	$\lesssim 3.4$	(1)
070306	FORS2	5.4	1.2–1.3	1.0	34.0	23.1	1.4965	(30)
070318	FORS1	1.8	1.6	0.7	16.7	20.2	0.8397	(31)
070419A	GMOS-N	2.4	1.2–1.3	. . .	0.8	20.4	0.9705	(5)
070506	FORS1	2.7	1.6–1.8	1.1	4.0	21.0	2.3090	(32)
070611	FORS2	3.6	1.1–1.2	1.0	7.7	21.0	2.0394	(33)
070721B	FORS2	5.4	1.2–1.5	1.2	21.6	24.3	3.6298	(34)
070802	FORS2	5.4	1.2	0.5	1.9	21.9	2.4541	(35)
071020	FORS2	0.6	2.0	1.0	2.0	20.4	2.1462	(36)
071025	HIRES	1.8	1.35	. . .	. . .	. . .	5.2	(1)
071031	FORS2	1.8	1.2	1.0	1.2	18.9	2.6918	(37)
071112C	FORS1	3.6	1.7	1.2	9.0	21.9	0.8227	(38)
071117	FORS1	5.4	1.4	0.9	9.0	23.0	1.3308	(39)
080210	FORS2	1.2	1.8–2.4	1.4	0.7	18.8	2.6419	(40)
080310	Kast	1.8	. . .	. . .	. . .	17.0	2.4274	(41)
080319B	FORS2	3.6	2.1–2.3	1.0	26.0	20.5	0.9382	(42)
080319C	GMOS-N	3.6	1.2	1.7	2.4	21.1	1.9492	(43)
080330	AlFOSC	1.8	1.8	1.5	0.8	17.6	1.5119	(44)
080413B	FORS1	0.6	1.5	0.5	0.8	19.3	1.1014	(45)
080520	FORS2	5.4	1.2	0.7	7.3	23.0	1.5457	(46)
080523	FORS2	5.4	1.8–2.0	1.0	10.9	23.	$\lesssim 3.0$	(47)
080603B	AlFOSC	2.0	1.3	1.0	2.0	17.5	2.6892	(48)
080604	GMOS-N	1.8	1.3	1.0	1.6	21.9	1.4171	(49)
080605	FORS2	0.6	1.4–1.9	0.9	1.7	20.4	1.6403	(50)
080607	LRIS	5.1	1.0	0.8	0.2	18.9	3.0368	(51)
080707	FORS1	2.4	2.1–2.5	2.2	1.1	19.6	1.2322	(52)
080710	GMOS-S	2.4	1.6	. . .	2.2	. . .	0.8454	(53)
080721	FORS1	1.2	1.5	1.7	10.2	20.0	2.5914	(54)
080804	UVES	4.7	2.1–2.5	0.9	0.8	19.0	2.2045	(55)
080805	FORS2	1.2	1.7	1.0	1.0	21.5	1.5042	(56)
080810	AlFOSC	2.4	1.8	1.0	10.6	19.1	3.3604	(57)

Table 2
(Continued)

GRB	Instrument	Exptime (ks)	Airmass	Seeing (arcsec)	Δt (hr)	Mag$_{acq}$	Redshift	Ref.
080905B	FORS2	0.6	1.3	1.7	8.3	20.2	2.3739	(58)
080913	FORS2	1.8	1.0	1.1	2.0	24.2	6.7	(59)
080916A	FORS2	3.6	1.2	0.9	17.1	22.3	0.6887	(60)
080928	FORS2	1.8	1.6	1.1	15.5	20.4	1.6919	(61)
060904B[a]	FORS1	3.6	1.1–1.3	0.7	5.1	19.9	0.7029	(62)
060906[a]	FORS1	4.8	2.0	0.9	1.0	20.0	3.6856	(1)
060926[a]	FORS1	4.8	1.7–2.4	1.0	7.7	23.0	3.2086	(1)
070125[a]	FORS2	1.8	1.8	0.8	21.0	18.8	1.5471	(5)
070411[a]	FORS2	3.0	1.4–1.7	1.0	5.0	20.8	2.9538	(63)
070508[a]	FORS1	5.4	1.7	1.3	3.8	22.0	$\lesssim 3.0$	(64)
080411[a]	FORS1	0.6	2.3–2.6	1.1	2.4	17.5	1.0301	(65)
080413A[a]	UVES	2.7	1.2–1.6	0.7	3.7	19.0	2.4330	(66)

Notes. We list here the burst names and details of the spectroscopic observations. The column Δt shows the time after trigger when the spectroscopic observation was started. Mag$_{acq}$ gives the approximate magnitude (typically in the R-band) of the afterglow in the acquisition image.
[a] Not part of the statistical sample.

References. (1) Jakobsson et al. 2006c; (2) Watson et al. 2006; (3) Foley et al. 2007; (4) D'Elia et al. 2005; (5) This work; (6) Fynbo et al. 2005; (7) Ledoux et al. 2005; (8) Sollerman et al. 2007; (9) Fugazza et al. 2005; (10) Piranomonte et al. 2006a; (11) Prochaska et al. 2006b; (12) Fynbo et al. 2006c; (13) Cucchiara et al. 2006b; (14) Cucchiara et al. 2006a; (15) Starling et al. 2006a; (16) Castro-Tirado et al. 2006; (17) Ledoux et al. 2006b; (18) Della Valle et al. 2006; (19) Jakobsson et al. 2006d; Oates et al. 2009; (20) Thöne et al. 2006c; (21) Piranomonte et al. 2006b; (22) Rol et al. 2006; (23) Ruiz-Velasco et al. 2007; (24) Jakobsson et al. 2006a; (25) Thöne et al. 2006a; (26) Thöne et al. 2006b; Fynbo et al. 2007; (27) Fynbo et al. 2006b; (28) Bloom et al. 2006b; (29) Jaunsen et al. 2007b; (30) Jaunsen et al. 2008; (31) Jaunsen et al. 2007a; (32) Thöne et al. 2007b; (33) Thöne et al. 2007a; (34) Malesani et al. 2007; (35) Elíasdóttir et al. 2009; (36) Jakobsson et al. 2007c; (37) Ledoux et al. 2008; (38) Jakobsson et al. 2007a; (39) Jakobsson et al. 2007e; (40) Jakobsson et al. 2008b; (41) Prochaska et al. 2008c; (42) Vreeswijk et al. 2008c; (43) Wiersema et al. 2008a; (44) Guidorzi et al. 2009; (45) Vreeswijk et al. 2008d; (46) Jakobsson et al. 2008a; (47) Fynbo et al. 2008c; (48) Fynbo et al. 2008e; (49) Wiersema et al. 2008b; (50) Jakobsson et al. 2008c; (51) Prochaska et al. 2009; (52) Fynbo et al. 2008f; (53) Perley et al. 2008; (54) Starling et al. 2009; (55) Thöne et al. 2008d; (56) Jakobsson et al. 2008e; (57) de Ugarte Postigo et al. 2008; (58) Vreeswijk et al. 2008a; (59) Fynbo et al. 2008a; Greiner et al. 2009; (60) Fynbo et al. 2008b; (61) Vreeswijk et al. 2008e; (62) Fugazza et al. 2006; (63) Jakobsson et al. 2007b; (64) Jakobsson et al. 2007d; (65) Thöne et al. 2008a; (66) Thöne et al. 2008c.

4.1. Redshift Distribution

Our first objective is to measure the true redshift distribution of *Swift* GRBs and in particular to constrain the fraction of *Swift* bursts that could be at very high redshifts (here, $z > 6$–7). The error on the redshifts is typically a few permille.

As mentioned in Section 2, 146 *Swift* bursts fulfill our selection criteria for the statistical sample in Section 2. Table 73 in Appendix B includes all 146 bursts and their redshift constraints. The optical and/or near-IR afterglow is detected for 108 of the bursts. This completeness of 74% is much higher than for pre-*Swift* samples where only about 30% of the bursts have detected optical/near-IR afterglows (e.g., Fynbo et al. 2001; Lazzati et al. 2002). For the full sample of all *Swift* bursts observed in the same period from 2005 March to 2008 September, 198 out of 371 (53%) have detected optical/near-IR afterglows, and this difference between the statistical sample and the full *Swift* sample illustrates the motivation for our sample criteria.

The redshift is determined from the OA for 72 bursts in the statistical sample (five of these are photometric redshifts based on the detection of the Lyman limit or Lyα forest in the spectral energy distribution of the afterglow). For an additional 12, the redshift is determined from the likely host galaxy. For 25 bursts, an upper limit can be placed on the redshift through detection of the OA and hence establishing an upper limit to the position of the Lyman limit or Lyα forest breaks. For the remaining 37, we have no constraints on the redshift from the OA or host galaxy (four of these are detected in the J, H, and/or K bands, but these detections do not provide useful redshift limits, i.e., $z < 10$). For these bursts we follow Grupe et al. (2007) and assign a redshift upper limit to bursts with excess (over Galactic) X-ray absorbing column density above an equivalent H I column density of 2×10^{21} cm^{-2} (also taking uncertainty into account).

Grupe et al. (2007) used an upper limit of $z = 2$, but we will be slightly more conservative and assign an upper limit of $z = 3.5$ to these bursts (corresponding to an upper limit on the intrinsic absorbing column of about 10^{23} cm^{-2} for Solar metallicity). 10 bursts fulfill this criterion at 90% confidence. We will return to the issue of X-ray absorption in Section 4.2 below. In Figure 1, we show the resulting redshift distribution for the full sample of 146 bursts. Both the median and the mean of the measured redshifts are 2.2. The fraction of $z > 6$ bursts is constrained to be in the range 1%–23% (2–34 out of 146) and the fraction of $z > 7$ bursts is less than about 18% (27 out of 146). Based on detections of likely host galaxies of dark bursts,[23] Perley et al. (2009b) constrain the fraction of $z > 7$ bursts further to <7% at 90% confidence. A similar conclusion is reached from a study of a complete sample of GRB host galaxies (J. Hjorth et al. 2010, in preparation). It has been argued that the redshift measurements of *Swift* GRBs show evidence for a "learning curve" in the sense that the mean time before a spectrum is secured is decreasing and that the mean redshift is also decreasing as a function of time since the launch of *Swift* (Coward 2009). In Figure 2, we plot the magnitude of the afterglow at acquisition against the time since burst and color code the points by redshift. The mean (median) times after burst at the start of integration are 9.7 (9.5) hr, 9.6 (8.5) hr, 10.4 (7.7) hr, and 5.3 (2.0) hr for 2005, 2006, 2007, and 2008, respectively. The corresponding median redshifts are 2.9, 2.7, 2.0, and 2.0. Hence, there does seem to be a tendency for the bursts to be spectroscopically observed earlier and for the median redshift to decrease. However, the effect is very small and the scatter is large. If we simply split the sample

---

[23] Note that this work uses a somewhat different definition of dark bursts than the one we use in Section 4.2.3.
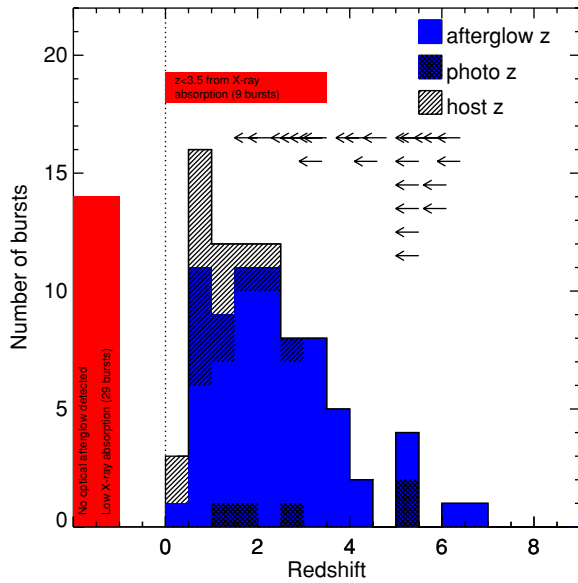
Figure 1. Redshift distribution of 146 *Swift* GRBs localized with the X-ray telescope and with low foreground extinction ($A_V < 0.5$). We indicate with different colors and shading bursts depending on whether the redshift is based on afterglow spectroscopy, host emission lines (or both), or a photometric redshift based on the OA broadband colors. Bursts for which only an upper limit on the redshift could be established from photometry of the OA are indicated by arrows. The red histogram at the left indicates the 28 bursts with no OA detection, weak or absent X-ray absorption, and no redshift measurement from the underlying host galaxy. For these bursts no redshift constraint could be inferred. The red block at the top indicates the 10 bursts for which the OA was not detected, but an upper limit of $z = 3.5$ could be placed based on excess X-ray absorption.
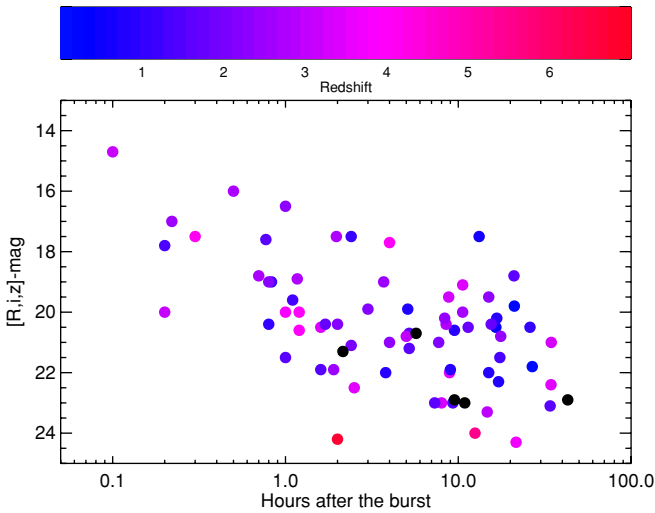

Figure 2. R-, i-, or z-band magnitude of the OAs in the acquisition image for the spectroscopy as a function of the time when the spectroscopic observations were started. The color bar in the top indicates the color code for the measured redshifts. Black points represent spectra for which we were not able to determine the redshift.

in two at the median time after trigger of 5 hr then we find that the mean redshifts and standard deviations for triggers before and after 5 hr are $\langle z \rangle = 1.9$, $\sigma(z) = 1.2$, and $\langle z \rangle = 2.5$, $\sigma(z) = 1.2$, respectively.

4.2. How Biased Is the Optical Afterglow Spectroscopy Sample?

Whereas there is evidence that the QSO-DLAs (damped Lyα absorbers) drawn from samples of optically selected QSOs are
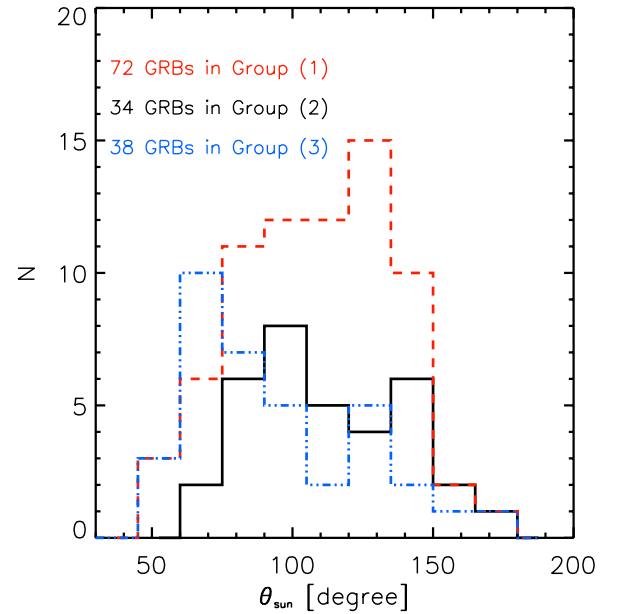

Figure 3. Sun angle distribution for members of the statistical sample.

fairly representative for the full underlying population (Ellison et al. 2001; Akerman et al. 2005; Ellison et al. 2008), this may well not be the case for the sample of GRB absorbers with OA spectroscopy. It was found soon after the discovery of OAs that some bursts are very faint in the optical (e.g., Groot et al. 1998). There is growing evidence that such bursts are mainly associated with dusty sight lines (e.g., Levan et al. 2006; Watson et al. 2006; Berger et al. 2007; Jaunsen et al. 2008; Tanvir et al. 2008b; Elíasdóttir et al. 2009; Prochaska et al. 2009; Perley et al. 2009; Zheng et al. 2009). Due to its high fraction of optical follow-up (and X-ray selection), our statistical sample is ideal to address this issue quantitatively.

In the following, we divide our statistical sample into three groups: (1) bursts with redshifts measured from optical spectroscopy of the afterglow; (2) bursts with a detected OA, but no afterglow-based redshift measurement; and (3) bursts with no detection of the OA.

4.2.1. Distribution of the Sun Angle

As described in Section 2, we have defined our sample to only contain bursts with good conditions for optical/near-IR follow-up conditions. Nevertheless, it is clear that all the bursts in the statistical sample did not have equally good conditions for being observed from ground. In Figure 3, we compare the Sun angle distribution for the three samples. The Sun angle is a good measure for how long a burst can be observed during night time from the ground. It is clear that bursts with no OA detections tend to be closer to the Sun and hence are more difficult to observe. This is one of the contributing reasons why these bursts do not have detected OAs.

4.2.2. Distributions of High-energy Properties

In addition to the observational differences, we are interested in revealing astrophysical differences between the bursts in the statistical sample. Essentially all long GRBs have an X-ray afterglow. In particular, in our statistical sample all bursts have available X-ray spectra from *Swift* (e.g., Evans et al. 2009). It is therefore interesting to compare the X-ray properties such as excess absorption and flux at fixed observed times for the sample
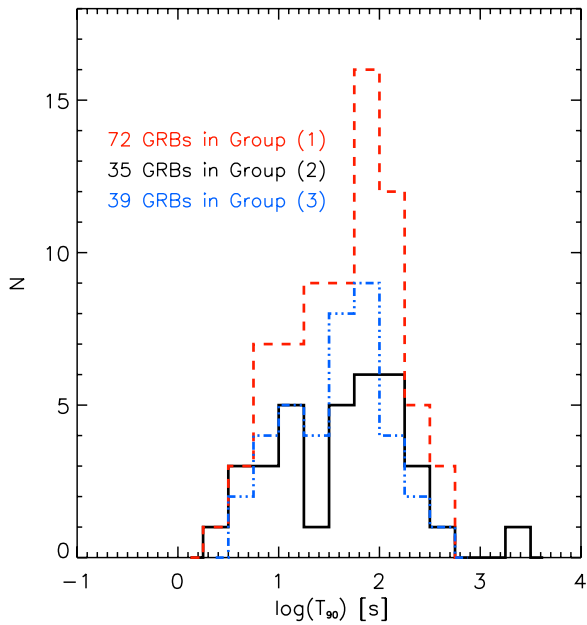
Figure 4. BAT T_{90} distribution for members of the statistical sample.
(A color version of this figure is available in the online journal.)

Figure 6. XRT flux distribution at 20,000 s post burst for members of the statistical sample.
(A color version of this figure is available in the online journal.)

Figure 5. BAT fluence distribution for members of the statistical sample.
(A color version of this figure is available in the online journal.)
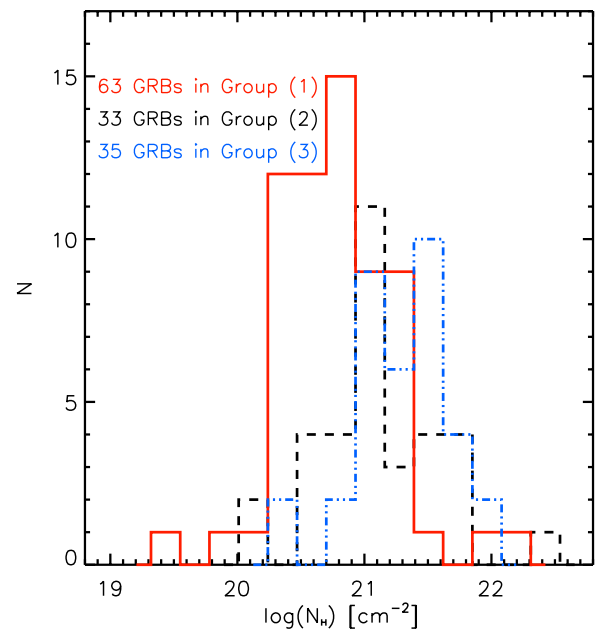
Figure 7. XRT excess absorption distribution (assuming $z = 0$) for members of the statistical sample.
(A color version of this figure is available in the online journal.)

of GRBs with follow-up optical spectroscopy with those that do not. It has been found that the fluence of the prompt emission correlates with the flux of the X-ray afterglow at fixed rest-frame times (Nysewander et al. 2009). We therefore compare both gamma-ray and X-ray properties of the three subsamples. The results are shown in Figures 4–7 (note that the number of bursts in each group is slightly different in the three plots as some of the measurements were unavailable for a few of the bursts). In Table 4, we provide the Kolmogorov–Smirnov (KS) test based probabilities that these three subsamples are drawn from the same underlying distributions. It is clear that bursts in groups (2) and (3) have fainter afterglows and in particular more excess absorption than bursts in group (1). The most striking difference is the X-ray excess for which it is firmly excluded that groups

(1) and (3) are drawn from the same underlying distribution. A similar conclusion was reached by Schady et al. (2007a) based on a smaller sample.

4.2.3. Dark Bursts

We follow the definition of dark bursts advocated by Jakobsson et al. (2004), whereby dark bursts are defined as bursts with an optical to X-ray spectral slope $\beta_{OX} < 0.5$. The fact that group (1) is not representative for all bursts in the statistical sample is confirmed by the fraction of dark bursts in the three subsamples (see Figure 8). For four bursts in the sample, it was not possible to calculate β_{OX} due to insufficient data (three from group (2)
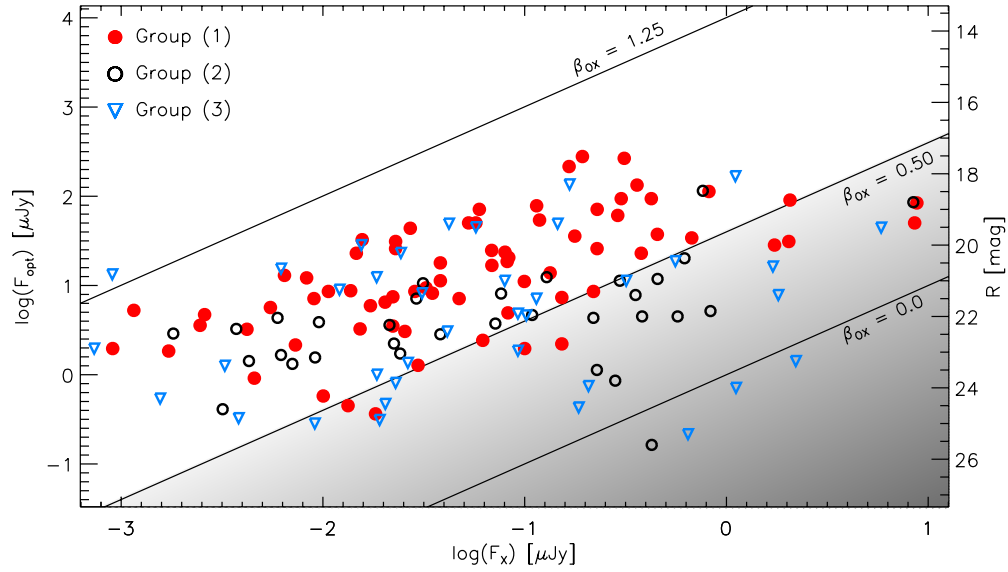
Figure 8. Dark burst diagram (F_{opt} vs. F_X), first presented in Jakobsson et al. (2004), for the statistical sample. GRBs with $\beta_{OX} < 0.5$ are defined as dark bursts. The β_{OX} values were calculated in an almost identical way as in Jakobsson et al. (2004). The only difference is that here we did not use 11 hr as a reference time. Rather, when possible, we selected measurements obtained a few hr after a burst to avoid the early stage of the X-ray canonical behavior. For low-z bursts we also avoided late-time measurements to prevent any host contamination in the OA flux.

(A color version of this figure is available in the online journal.)

and one from group (3)). In group (1) the fraction of dark bursts is 14% (10/72), in group (2) it is 38% (12/32), and in group (3) the fraction has a lower limit of 39% (15/38). In the full statistical sample, the fraction of dark bursts is constrained to be in the range 25%–42%. Note that the $\beta_{OX} < 0.5$ definition of dark bursts is conservative in the sense that a burst with an intrinsic $\beta_{OX} = 1.25$ can suffer from ~ 6 mag extinction in the observed R-band and still have an observed $\beta_{OX} > 0.5$.

A contributing factor to the increasing "darkness" from groups (1) to (3) could be a different fraction of bursts with cooling breaks between the optical and X-ray bands (Pedersen et al. 2006). However, the fact that GRBs in groups (2) and (3) have more excess absorption than bursts in group (1) shows that dust extinction of the optical light is most likely the dominating factor for the higher dark burst fraction in groups (2) and (3). This is made clearer from Figure 9 where we plot β_{OX} against excess absorption for the full statistical sample. Bursts with $\beta_{OX} < 0.5$ also have higher excess absorption than bursts with $\beta_{OX} > 0.5$. The nine dark bursts in group (1) are GRBs 050401, 050904, 060210, 070802, 080319C, 080605, 080607, 080805, and 080913. Two of these are dark due to high redshifts ($z > 6$) and the rest probably due to a combination of high hydrogen column densities and high metallicities and hence, high dust column densities.

4.3. GRB Absorption Systems Compared to QSO Absorption Systems

QSO absorption systems have been studied since the discovery of QSOs, and for these systems, a classification is well established (Weymann et al. 1981). Weymann et al. (1981) divided the QSO absorbers into four classes: (A) associated broad absorption line systems, (B) associated narrow line systems, (C) intervening narrow metal line systems, and (D) intervening Lyα forest systems. Classes C and D are further divided into subclasses such as Mg II absorbers, C IV absorbers, DLAs, sub-DLAs, etc. Clearly, these classes are not disjunct, i.e., DLAs are also Mg II and C IV absorbers, but the opposite is generally not true. The physical selection mechanism behind GRB absorption

Table 3
H I Column Densities from Spectroscopic Sample

GRB	z	$\log(N_{H I}/cm^{-2})$
050319	3.240	20.90 ± 0.20
050401	2.899	22.60 ± 0.30
050730	3.968	22.10 ± 0.10
050820A	2.612	21.10 ± 0.10
050908	3.344	17.60 ± 0.10
050922C	2.198	21.55 ± 0.10
060115	3.533	21.50 ± 0.10
060124	2.30	18.5 ± 0.5
060206	4.048	20.85 ± 0.10
060210	3.913	21.55 ± 0.15
060526	3.221	20.00 ± 0.15
060607A	3.075	16.95 ± 0.03
060707	3.425	21.00 ± 0.20
060714	2.711	21.80 ± 0.10
060906	3.686	21.85 ± 0.10
060926	3.206	22.60 ± 0.15
060927	5.464	22.50 ± 0.15
061110B	3.433	22.35 ± 0.10
070110	2.351	21.70 ± 0.10
070411	2.954	19.30 ± 0.30
070506	2.308	22.00 ± 0.30
070611	2.041	21.30 ± 0.20
070721B	3.628	21.50 ± 0.20
070802	2.455	21.50 ± 0.20
071020	2.145	< 20.30
071031	2.692	22.15 ± 0.05
080210	2.641	21.90 ± 0.10
080310	2.427	18.70 ± 0.10
080413A	2.433	21.85 ± 0.15
080603B	2.690	21.85 ± 0.05
080607	3.037	22.70 ± 0.15
080721	2.591	21.60 ± 0.10
080804	2.205	21.30 ± 0.15

systems is fundamentally different from those of intervening QSO absorbers. Hence, the fact that GRB absorbers in many ways appear similar to mainly DLAs provides interesting new
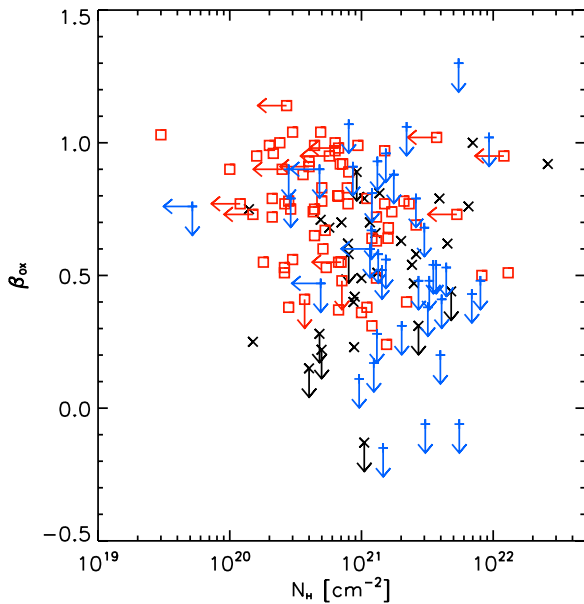
Figure 9. β_{OX} plotted against X-ray excess absorption (assuming $z = 0$). Dark bursts (defined by $\beta_{OX} < 0.5$) tend to have large X-ray excess absorption consistent with the interpretation that these bursts are obscured by dust. GRBs in groups (1), (2), and (3) are identified by red squares, black crosses, and blue plus symbols, respectively.

(A color version of this figure is available in the online journal.)

Table 4
KS Test Probabilities that Bursts in Group (2) (OA Detected, but no OA Based Redshift) and Group (3) (no OA Detection) are Drawn from Same Distribution as Group (1)[a]

Property	Group	
	(2)	(3)
0.3–10 keV flux a* 20000 s	6.1×10^{-2}	4.8×10^{-4}
X-ray excess absorption	2.1×10^{-3}	7.0×10^{-7}
15–350 keV fluence	0.21	3.5×10^{-2}
15–350 keV peak flux	0.20	0.29
T_{90}	0.76	0.71

Note. [a] Bursts with OA-based redshift measurement.

information not only of the properties of the GRB host galaxies, but also about the physical origin of intervening QSO absorbers. Specifically, the fact that QSO-DLAs and GRB absorbers look so similar strongly suggests that DLAs also originate from the interstellar medium of high-redshift galaxies.

Interestingly, GRB absorbers have overlapping properties not only with class C of Weymann et al. (1981), but also with their class B. There are even similarities between the afterglow spectrum of GRB 021004 and associated QSO absorbers from class A, namely both very high blueshifts and evidence for line locking (Savaglio et al. 2002; Møller et al. 2002, but see also Chen et al. 2007b).

Using our large sample we will here try to characterize the GRB absorbers as a class in terms of their absorption line strengths. The low resolution of most of our data prevents us from comparing properties such as metallicity or kinematical structure.

4.3.1. Comparison of GRB and QSO-DLA Absorption Systems

The issue of the distribution of H I column densities in *Swift* detected long-duration GRBs has already been addressed
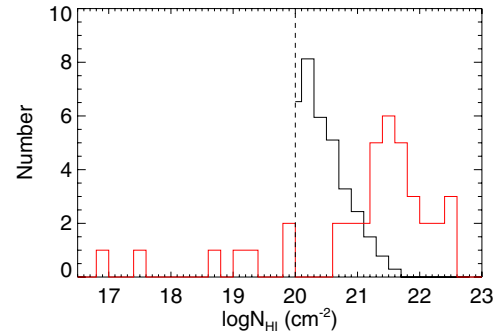
Figure 10. Distribution of H I column densities. Black: QSO-DLAs from the sample of Noterdaeme et al. (2009). Red: GRB absorbers from the spectroscopic sample. The numbers of QSO-DLAs have been renormalized to the same number of objects as the GRB absorbers.

(A color version of this figure is available in the online journal.)

in Jakobsson et al. (2006c). Compared to that study, we provide here 14 additional measurements. In addition, we have improved measurements for some of the bursts in Table 3 of Jakobsson et al. (2006c), e.g., GRB 060607A and GRB 060124. The column densities for all 33 Lyα lines detected in our spectroscopic sample are listed in Table 3 and plotted in Figure 10. The H I distribution covers five orders of magnitude from 10^{17} cm^{-2} to $\lesssim 10^{23}$ cm^{-2}. Roughly 80% of the systems have measured H I column densities above 2×10^{20} cm^{-2}, which is the classical definition of a DLA system (e.g., Wolfe et al. 2005). There is evidence that the true distribution may extend to somewhat higher column densities, namely the fact that the three bursts with the highest column densities are dark bursts. The upper range of the distribution may also reflect the transition where the bulk of the hydrogen is in molecular form (Schaye 2001; Krumholz et al. 2009). We will return to this point in Section 4.2. The distribution of H I column densities for GRB absorbers has recently been successfully reproduced in a high-resolution simulation of galaxy formation simulation (Pontzen et al. 2009).

Given that the majority of the bursts have column densities above 10^{20} cm^{-2}, it is natural primarily to compare GRB absorbers with the QSO-DLAs.

In Figures 10–12, we compare the distributions of H I and metal-line strengths for QSO-DLAs and GRB absorbers in the spectroscopic sample (the histogram for QSO absorbers is renormalized to have the same number of systems as GRB absorbers with log $N_{HI} > 20.0$). In the two latter plots, we only include GRB absorbers with log $N_{HI} > 20.0$ where we have comparison data from Sloan. We have used the original QSO-DLA sample from Noterdaeme et al. (2009) based on the Sloan Digital Sky Survey Data Release 6 (SDSS-DR6) database of QSO spectra. These authors automatically searched for DLA lines, refining their Lyα fits whenever metal lines are detected redward of the Lyα forest. We have selected all systems from their list with log $N(HI) \geqslant 20$ and redshifts in the range $2.2 < z_{abs} \leqslant 3.2$, located at least 5000 km s^{-1} from a background QSO with $R < 21$.

The EWs of two metal transition lines, namely, Si II $\lambda 1526$ and C IV $\lambda 1549$ (i.e., the blend of the 1548 and 1550 Å lines), were measured. These lines are strong so that they are detected in most cases and the risk of overestimating their EWs due to blending with unrelated absorption is minimal. For the measurements themselves, intervals of rest-frame widths 2 Å (3.5 Å) centered on the Si II $\lambda 1526$ (C IV $\lambda 1549$) were used. However, those

Figure 11. Black: QSO-DLAs measurements. Red: GRB absorbers from the spectroscopic sample with $\log N_{\rm H\,I} > 20$. Encircled points are dark bursts. The histograms are normalized to have the same area. Open diamonds: LBGs. The LBG point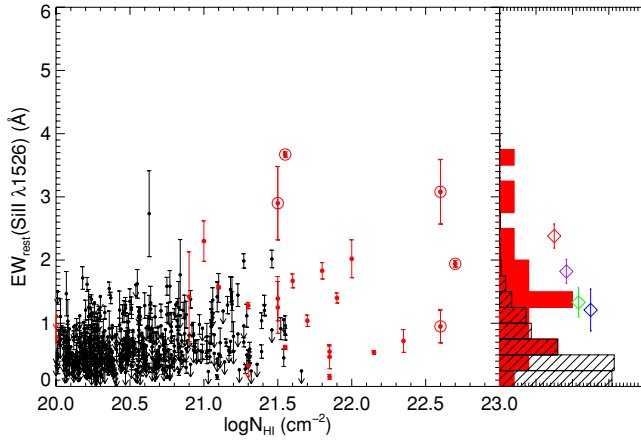s are displaced horizontally for visibility reasons. The LBG measurements represent mean values of four composite spectra representing the quartiles of increasing Lyα EW from blue to red.
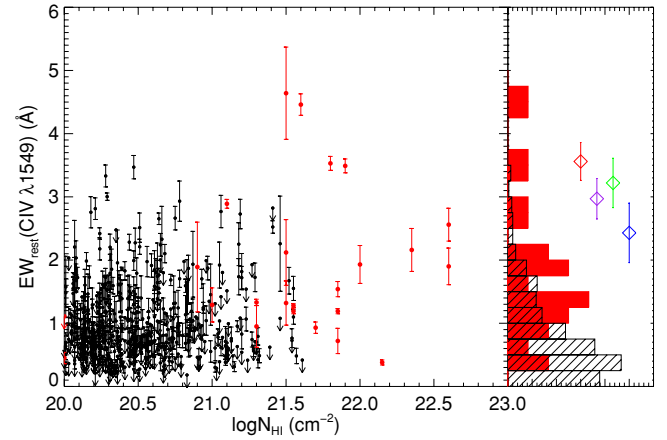
Figure 12. Black: QSO-DLAs measurements. Red: GRB absorbers from the spectroscopic sample with $\log N_{\rm H\,I} > 20$. The histograms are normalized to have the same area. Open diamonds: LBGs. The LBG points are displaced horizontally for visibility reasons. The LBG measurements represent mean values of four composite spectra representing the quartiles of increasing Lyα EW from blue to red.

systems where these metal lines lie inside the Lyα forest were not considered any further.

Among all EW measurements, only those satisfying the following two criteria were used: $\chi_{\rm r}^2 < 1.5$ (where $\chi_{\rm r}^2$ is the reduced χ^2) and err$_{\rm EW} < 0.3$ Å. These thresholds were determined from the distribution of data points in the χ_r^2 versus err$_{\rm EW}$ plane in order to reject unreliable measurements. Among the remaining measurements, we provide 3σ upper limits when the S/N is below 3.

Figures 11 and 12 compare the rest-frame EWs of Si II and C IV for the GRB-DLAs and QSO-DLAs. We also show measurements of the strength of these interstellar lines from Lyman-break galaxies (LBGs) from Shapley et al. (2003). These measurements represent mean values of four composite spectra representing the quartiles of increasing Lyα EW from blue to red. Note that the C IV EWs for LBGs also contain a stellar contribution so they should be considered upper limits. For GRB-DLAs and QSO-DLAs, we plot these values against the N(H I) estimates that separate the GRB-DLAs from the majority of QSO-DLAs. In all of these comparisons, there is significant overlap between the QSO-DLA and GRB-DLA EW distributions, but the GRB-DLA measurements extend to significantly higher EW values than what is seen in the much larger QSO-DLA sample. The large data set presented here confirms the results of systematically larger Si II and C IV EWs in GRB-DLAs reported by Prochaska et al. (2008a). Similar results were found by Savaglio et al. (2004) in a comparison of Fe II, Si II, and Mn II lines between GRB absorbers and QSO-DLAs. The LBG measurements fall at the high end of the of GRB-DLA distribution. The LBG systems with the largest line strengths (both Si II and C IV) are those that have the strongest Lyα absorption. These systems also have the highest dust contents (Shapley et al. 2003; Noll et al. 2004).

To understand the difference between the GRB-DLA and QSO-DLA distributions, it is natural to focus on the different ways the two absorber classes probe their host galaxies (see also Vreeswijk et al. 2004; Prochaska et al. 2007; Fynbo et al. 2008d). GRB-DLAs probe the sight line to the location of a massive star with a random orientation relative to the geometry of the galaxy (ignoring for now the issue of bias). QSO-DLAs probe H I cross-section-selected random sight lines through their

host galaxies. The distribution of orientations of the host galaxy relative to the sight line is not random, but weighted with the selection function. If the QSO-DLAs have a flattened geometry, this will tend to produce a shorter sight line through the host than for a random distribution of orientations. On the other hand, the GRB absorbers do not probe the full sight line through their hosts; in particular, for some systems located in the outskirts of their hosts toward us only a small fraction of the absorbing material will be probed. An additional piece of evidence is the distance between the location of the GRB and the bulk of the absorbing material which has been inferred for a few GRBs based on modeling of fine-structure line variability (Dessauges-Zavadsky et al. 2006; Vreeswijk et al. 2007; D'Elia et al. 2009a, 2009b; Ledoux et al. 2009). These studies have found that the bulk of the absorbing material probed by the variable fine-structure lines are at distances of 50–100 pc, 1.7 kpc, 0.7–6 kpc, 280 pc, and a 5 kpc for the GRBs 020813, 060418, 080319B, 080330, and 050730, respectively. The nearly ubiquitous detection of strong Mg I absorption also indicates that a substantial quantity of neutral gas in GRB-DLAs is located at distances exceeding 100 pc (Prochaska et al. 2006a). Finally, vibrationally excited H_2 lines have also been used to infer a distance in the range 230–940 pc between GRB 080607 and the bulk of the absorbing material (Sheffer et al. 2009).

For strong and saturated lines like those presented in Figures 11 and 12, the EW is weakly sensitive to the abundance of the ion. Instead, the EW values trace the kinematics of these ions along the sight line. Prochaska et al. (2008a) have argued, based on comparisons of resonance and fine-structure transitions of Si II and Fe II, that the large EWs in GRB-DLAs reflect motions in the "halos" of these galaxies, i.e., in gas at distances exceeding several kpc. The data presented here indicate that such motions are a generic property of gas in the galactic environment of GRBs. Of principal interest is whether these motions reflect gravitational dynamics (as argued by Prochaska et al. 2008a) or galactic-scale outflows driven by star formation, active galactic nucleus (AGN), etc. Independent of the mechanism, the fact that both the Si II and C IV histograms extend significantly beyond the range spanned by QSO-DLA (Figures 11 and 12) indicates the gas is either predominantly ionized or multi-phase. In other words, if C IV absorption was mainly produced in a roughly

spherical, hot halo whereas the low-ionization lines were produced in a central, colder component, then we would expect the C IV plot to be different from the Si II plot. Hence, C IV seems to probe the same volume as the low-ionization lines. The same conclusion has been reached by Prochaska et al. (2008a).

For QSO-DLAs the Si II λ1526 line can be used as a proxy for metallicity through the relation [M/H] = −0.92 + 1.41 log (EW/Å) (Prochaska et al. 2008a). The underlying physical reason for this is believed to be a velocity width versus metallicity relation (Ledoux et al. 2006a; Prochaska et al. 2008a). Roughly, a rest-frame EW of 1 Å corresponds to a metallicity of 0.1 solar. We do not know yet if GRB absorbers follow this correlation, but there is some indication that they do (Prochaska et al. 2008a). The metallicities have been measured for GRBs 050401, 050730, 050820A, 050922C, 070802, 071031, 080310, 080413A, and 080607 in our spectroscopic sample (Watson et al. 2006; Fox et al. 2008; Elíasdóttir et al. 2009; Prochaska et al. 2009; Ledoux et al. 2009), and these bursts seem to follow the correlation although possibly with a somewhat steeper slope.

As seen in Figure 11, slightly more than half of the GRB absorbers have $\mathrm{EW_{rest}}$(Si II λ1526) > 1 Å, suggesting that about half of GRBs with afterglow spectroscopy at these redshifts have metallicity above 0.1 solar. This is consistent with the metallicity distribution of GRB-DLAs based on direct estimates of N(H I) and a metal column density (e.g., Prochaska et al. 2007). The true fraction could well be higher due to the bias against bursts with high X-ray-absorbing columns in the sample of GRBs with OA spectroscopy.

4.4. Implication for the Escape Fraction of Ionizing Photons in Star-forming Galaxies at z > 2

An important utility of the spectroscopic sample of *Swift* GRBs in Table 4 is to constrain the escape fraction of ionizing photons f_{esc} in distant star-forming galaxies (Chen et al. 2007a; Gnedin et al. 2008), which specifies the fraction of stellar-origin ionizing photons ($h\nu$ > 1 Ryd) that escape from star-forming regions into the intergalactic medium (IGM). A traditional approach to obtain empirical constraints of f_{esc} is to search for high-energy photons detected at wavelengths below the Lyman limit transition of a distant galaxy. However, such measurements are subject to a number of systematic uncertainties that are difficult to quantify, including background subtraction, intrinsic spectral shape at ultraviolet wavelengths of star-forming galaxies, and line-of-sight variations of IGM Lyα absorption (see Chen et al. 2007a for a brief review).

Chen et al. (2007a) introduced a new approach that determines f_{esc} in high-redshift star-forming galaxies based on the range of neutral hydrogen column density N(H I) found in the hosts of long-duration GRBs. The observed N(H I) in the host of each GRB from early-time afterglow spectra represents a measure of the integrated optical depth of Lyman limit photons along the line of sight away from the parent star-forming region where the progenitor resides. Considering the N(H I) distribution function of an ensemble of GRBs together therefore yields an estimate of the mean f_{esc} averaged over random lines of sight. Adopting a sample of 28 GRBs at $z \gtrsim 2$, Chen et al. (2007a) found $\langle f_{\mathrm{esc}} \rangle = 0.02 \pm 0.02$ with a 95% c.l. upper limit $\langle f_{\mathrm{esc}} \rangle \leqslant 0.075$. Although the best-estimated $\langle f_{\mathrm{esc}} \rangle$ is among the lowest value reported for $z > 2$ star-forming galaxies, the subluminous nature of the majority of GRB host galaxies (e.g., Jakobsson et al. 2005; Chen et al. 2009) in combination with a steep faint-end slope of the distant galaxy population (e.g., Reddy & Steidel 2008) indicates that sub-$L*$ galaxies with $\langle f_{\mathrm{esc}} \rangle = 1\%$–2% can already
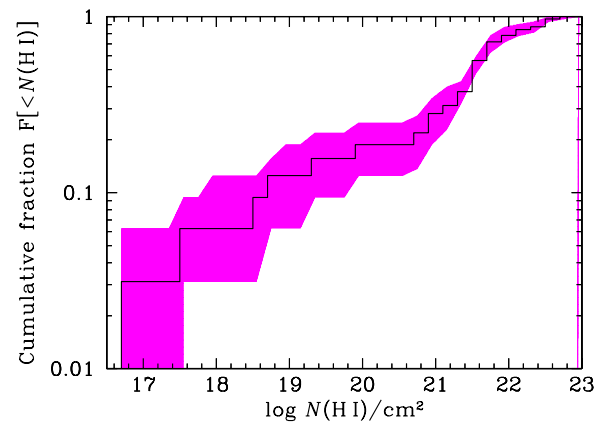
Figure 13. Cumulative distribution of neutral hydrogen column density $\mathcal{F}[< N(\mathrm{H\,I})]$ observed in the host galaxies of 32 long-duration GRBs discovered at $z \geqslant 2$ by *Swift* (solid histogram). The shaded area shows the 1σ uncertainties evaluated using a bootstrap re-sampling method that accounts for both N(H I) measurement uncertainties and sampling errors.

(A color version of this figure is available in the online journal.)

contribute a comparable amount of ionizing photons as QSOs to the ultraviolet background radiation at $z \sim 3$.

While the new approach of constraining f_{esc} based on the observed N(H I) distribution is not affected by the same systematic uncertainties that bias the f_{esc} measurements from the traditional method (see Chen et al. 2007a for related discussion), the accuracy of $\langle f_{\mathrm{esc}} \rangle$ depends on an unbiased sample of GRB hosts. Specifically, if some fraction of optically thin sight lines are missed due to a lack of S/N in the afterglow spectra for identifying weak absorption features, then the estimated $\langle f_{\mathrm{esc}} \rangle$ would be biased toward a lower value. Chen et al. (2007a) considered a sample of 28 GRBs at $z \gtrsim 2$ with available early-time afterglow spectra for constraining the N(H I), eight of which are from the pre-*Swift* era when rapid localizations of the optical transients were challenging. It is not clear how significant the bias is due to missed optical transients.

The 33 GRBs discussed in this paper represent a uniform spectroscopic sample of *Swift* bursts with rapid localizations and allow us to obtain an accurate measurement of $\langle f_{\mathrm{esc}} \rangle$. Figure 13 presents the cumulative N(H I) distribution, $\mathcal{F}[<N(\mathrm{H\,I})]$, from the sample of 32 GRB host galaxies (excluding GRB 071020 due to the uncertain N(H I)), together with the 1σ uncertainties determined based on a bootstrap re-sampling method (see Chen et al. 2007a for further illustrations). Adopting this sample of 32 GRBs at $z \gtrsim 2$, we find $\langle f_{\mathrm{esc}} \rangle = 0.02 \pm 0.02$ with a 95% c.l. upper limit $\langle f_{\mathrm{esc}} \rangle \leqslant 0.07$, in excellent agreement with the finding of Chen et al. (2007a). We note that while the two samples are comparable in size, only roughly half of the new sample overlaps with those considered by Chen et al. (2007a). In addition, including GRB 071020 and assuming a host N(H I) of log N(H I) = 16.85 (matching the lowest N(H I) found so far for a GRB host) would double the estimated value to $\langle f_{\mathrm{esc}} \rangle = 0.04$. Our new measurement confirms that the mean escape fraction of ionizing photons in distant star-forming galaxies is small.

4.5. Intervening Absorption Systems

The issue of intervening absorbers is interesting for two main reasons. The first is the puzzling result that there are more intervening Mg II absorbers along GRB sight lines than along QSO sight lines (Prochter et al. 2006; Vergani et al. 2009; Cucchiara et al. 2009). However, there is no excess of
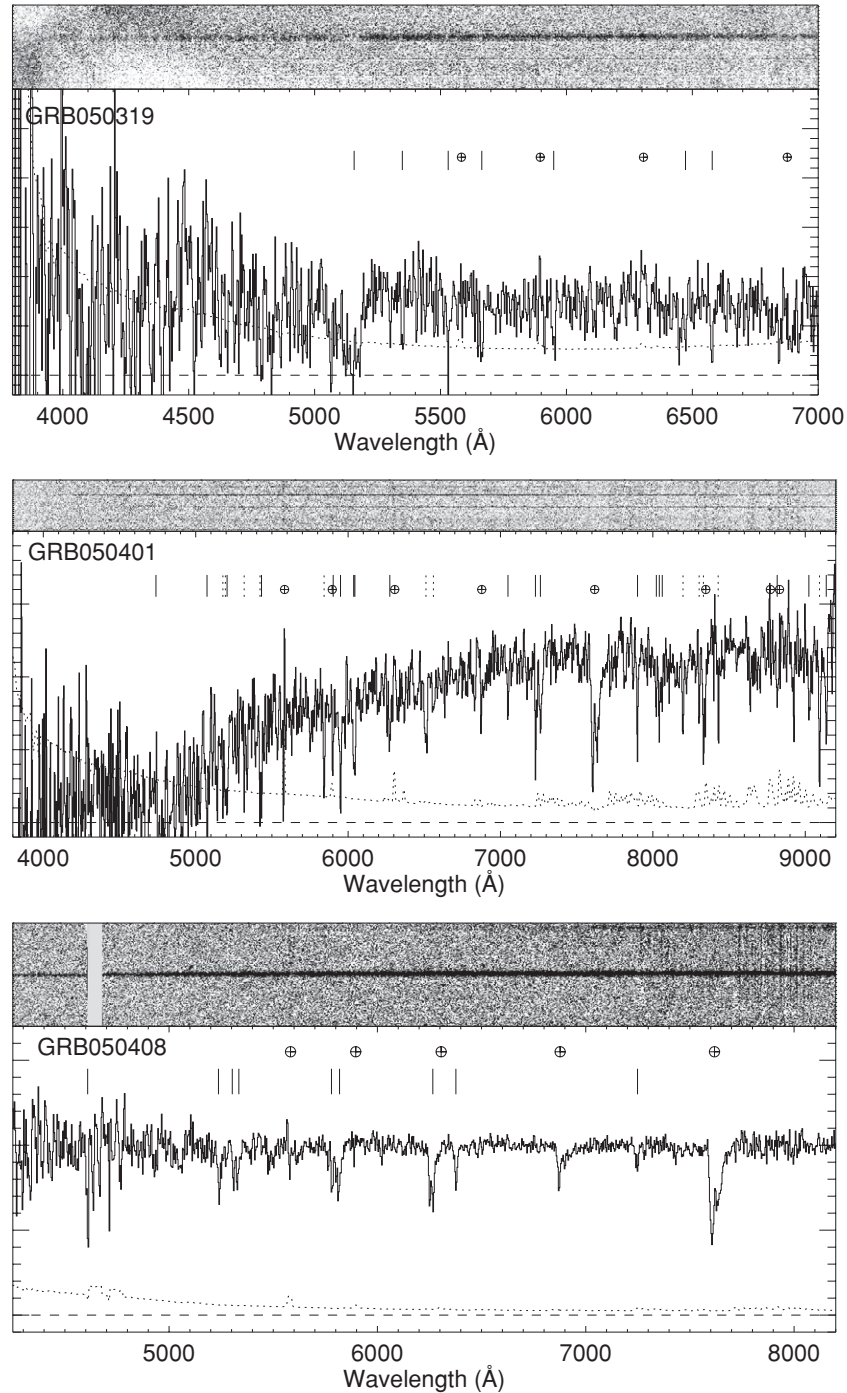
Figure 14. Shown are one- and two-dimensional spectra for GRBs 050319–080928. Lines from the GRB absorption systems are marked with vertical lines, whereas unidentified lines or lines from intervening systems are marked with vertical dashed lines. Telluric features are marked with a telluric symbol. The error spectrum is plotted as a dotted line. When in the spectral range, we also plot the position of the Lyman limit as a vertical dashed line.

C IV systems along GRB sight lines (Sudilovsky et al. 2007; Tejos et al. 2007). The other reason is that the search for galaxy counterparts of the absorbers is much easier along GRB sight lines as the OA quickly fades away (Vreeswijk et al. 2003).

In our sample, we detect several very strong intervening Mg II absorbers, i.e., 12 systems with $\mathrm{EW_{rest}} > 2$ Å. For a full statistical analysis of the excess we refer to S. D. Vergani et al. (2010, in preparation).

We also detect a few strong intervening Lyα absorbers, e.g., along the sight lines to GRB 050730, GRB 050908,

and GRB 070721B (see B. Milvang-Jensen et al. 2010, in preparation). It is interesting to note that the $z = 2.62$ sub-DLA toward GRB 050908 also has remarkably strong metal lines (e.g., an $\mathrm{EW_{rest}}$ of 2.2 Å for the Si II λ1526 line). Also, the $z = 3.09$ sub-DLA toward GRB 070721B has very strong lines ($\mathrm{EW_{rest}}$ 1.7 Å for the Si II λ1526 line). QSO-DLAs with $\mathrm{EW_{rest}}$ larger than 1.5 Å for the Si II λ1526 line are quite rare (see Prochaska et al. 2008a and Figure 11 below). Unfortunately, our sample is too small to judge if the intervening Lyα absorbers toward GRB sight lines are also statistically different from those along QSO sight lines.
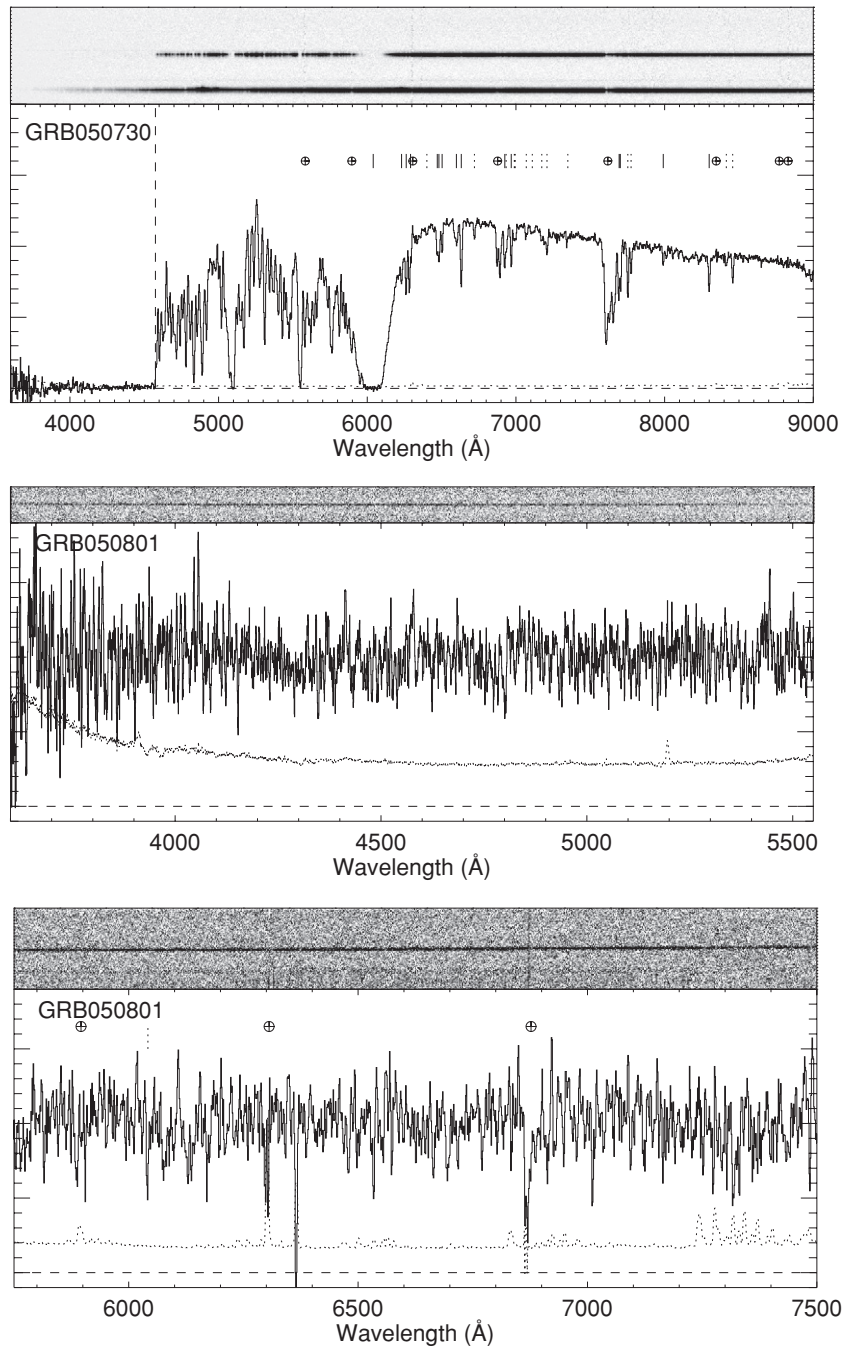
Figure 14. (Continued)

5. CONCLUSIONS

GRB afterglow spectroscopy provides a detailed analysis of the ISM of actively star-forming galaxies. In this work, we have presented a large sample of GRBs detected by *Swift* for which primarily low-resolution spectroscopic observations have been secured. The majority ($\sim$ 80%) of the GRB host absorbers bear strong resemblance to high-column density QSO absorbers like DLAs and sub-DLAs. However, the GRB absorbers are characterized by a broader range of line strengths extending to significantly stronger lines (both for H I, Si II, and C IV) than what is seen for high-column density QSO absorbers.

We find that the sample of GRBs for which optical spectroscopy is secured is a significantly biased subsample. In the statistical sample, only about 50% have OA spectroscopy, and this subsample has substantially smaller X-ray excess absorption and a substantially smaller fraction of dark bursts (by the Jakobsson et al. 2004 definition) than the other half of the sample.

The implication of this work is that the metallicity distribution we derive from OA spectroscopy likely is skewed toward low metallicities compared to the true underlying distribution (see also Ledoux et al. 2009). This is important to take into account, e.g., when establishing how well GRBs trace star formation and when inferring to which extent GRB progenitors may be restricted to massive stars with low metallicities.

This work also shows that if we can secure optical and/ or near-IR spectroscopy for a much larger fraction of an
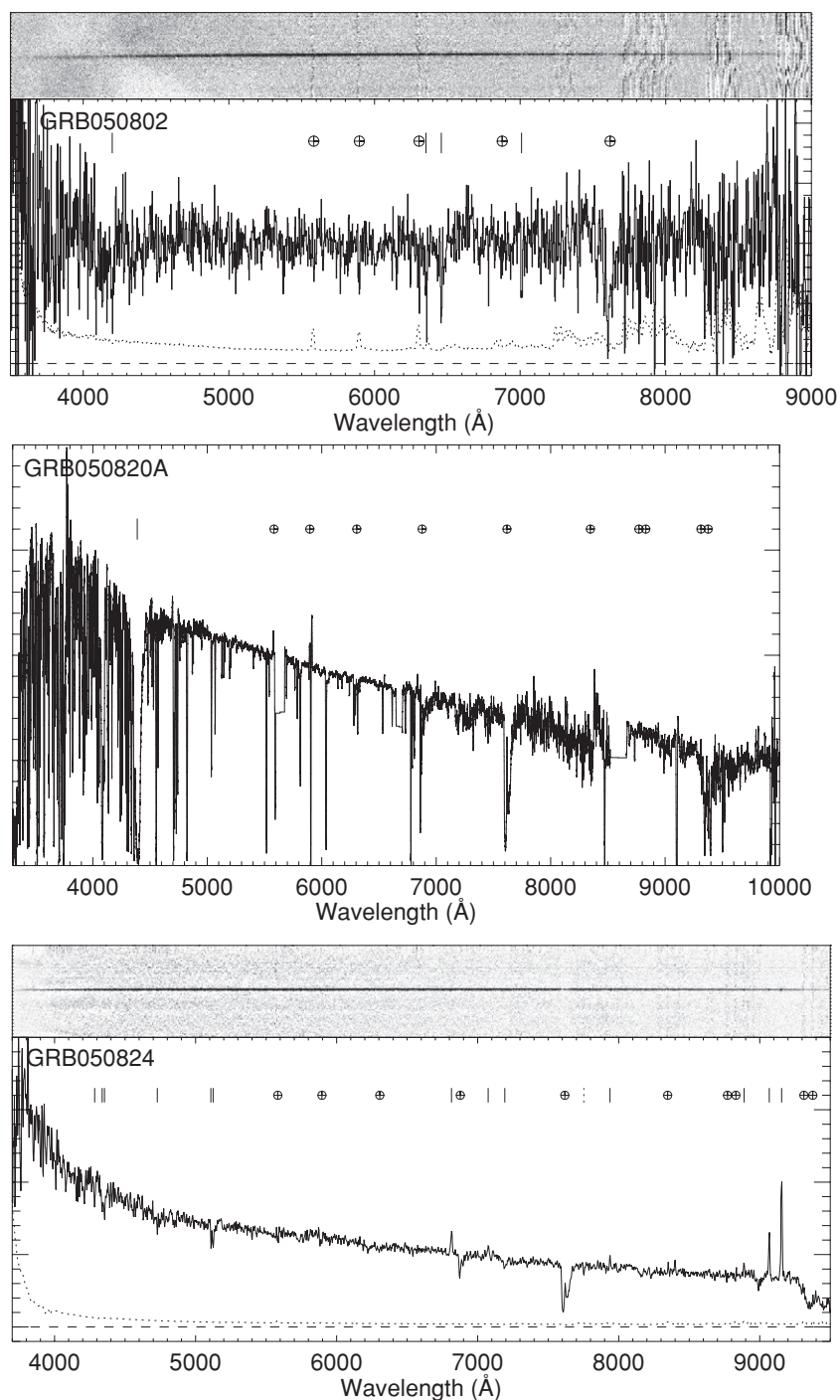
Figure 14. (Continued)

X-ray-selected sample, it is likely that we will pick up sight lines with significantly higher dust contents, molecular fractions, and higher metallicities. A similar conclusion was reached by Ledoux et al. (2009). Such studies will be ideal to study extinction curves and properties of star-forming regions, in particular at high redshifts. In the current sample, dusty bursts like GRBs 070802, 080605, and 080607 were observed under fortunate conditions, i.e., very soon after the bursts and in good observing conditions. It is plausible that bursts for which the current search strategy and instrumentation cannot secure a redshift are similar to or even more dust obscured than these bursts.

Currently, most GRB error circles are only observed in optical bands. For further progress, systematic near-IR follow-up of an X-ray-selected sample will be important. Such systematic near-IR follow-up is currently carried out by a few teams using, e.g., GROND, UKIRT, and PAIRITEL (e.g. Greiner et al. 2009; Krühler et al. 2008; Tanvir et al. 2008b; Prochaska et al. 2009). For the spectroscopic follow-up, instruments like the newly commissioned X-shooter spectrograph that cover the full near-UV to near-IR range in a single shot (Kaper et al. 2009) will be important, but it is likely that we will have to wait for the advent of 30–40 m telescopes with similar instrumentation before we will reach a spectroscopic completeness of, e.g., 90%.

Figure 14. (Continued)

APPENDIX A

NOTES ON INDIVIDUAL OBJECTS

A.1. GRB 050319 ($z = 3.2425$)

The data presented here have previously been published in Jakobsson et al. (2006c). The spectrum has a low S/N, but due to the presence of the strong hydrogen Lyα line, the redshift is secure.

A.2. GRB 050401 ($z = 2.8983$)

The data presented here have previously been published in Watson et al. (2006). This burst has one of the highest H i
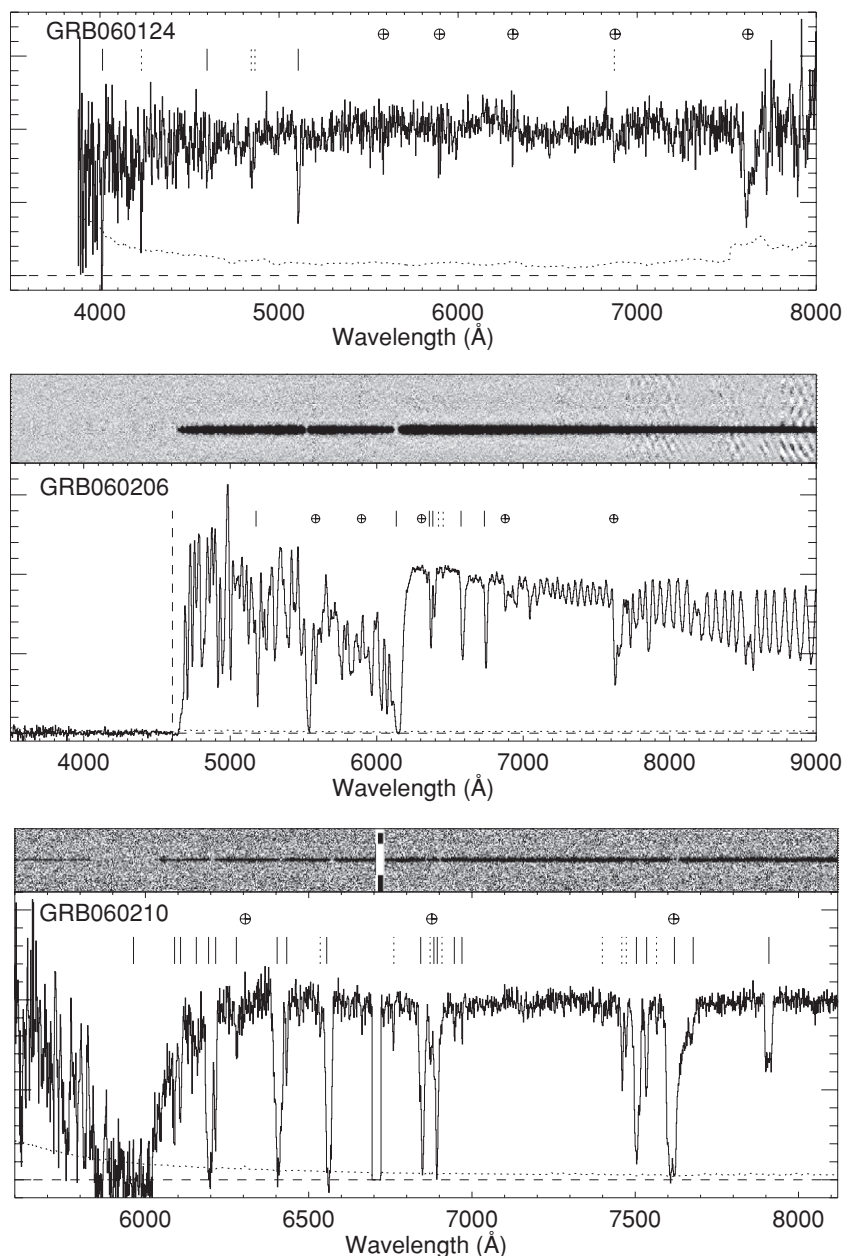
Figure 14. (Continued)

column densities measured along any sight line. The redshift is based on numerous metal lines including fine-structure lines. The spectrum also shows evidence for substantial SMC-type reddening and classifies as a dark burst by the definition of Jakobsson et al. (2004).

A.3. GRB 050408 ($z = 1.2356$)

The data presented here have previously been published in Foley et al. (2007). The redshift is based on numerous metal lines (including fine-structure lines).

A.4. GRB 050730 ($z = 3.9693$)

The data presented here have previously been published only in the GCN circulars (D'Elia et al. 2005). Spectra of this burst were also presented by Chen et al. (2005), Starling et al. (2005), D'Elia et al. (2007), and Ledoux et al. (2009). In the 2D spectrum, we detect a foreground QSO ($z = 3.02$) at an impact parameter of 20 arcsec (153 kpc). This QSO is possibly associated with the $z = 3.022$ absorption system seen in the spectrum of GRB 050730.

A.5. GRB 050801 ($z = 1.38$)

The data presented here have not been published earlier. No standard star was observed and therefore no flux calibration has been attempted for this spectrum (the plotted spectrum is normalized to 1 in the continuum). We only detect a single unidentified line in the spectrum. The upper limit on the redshift based on the absence of a Lyα forest is about 2.3. Based on UVOT colors, a photometric redshift of 1.38 has been determined for this burst (Oates et al. 2009).

A.6. GRB 050802 ($z = 1.7102$)

The data presented here have previously been published only in the GCN circulars (Fynbo et al. 2005). No standard star was
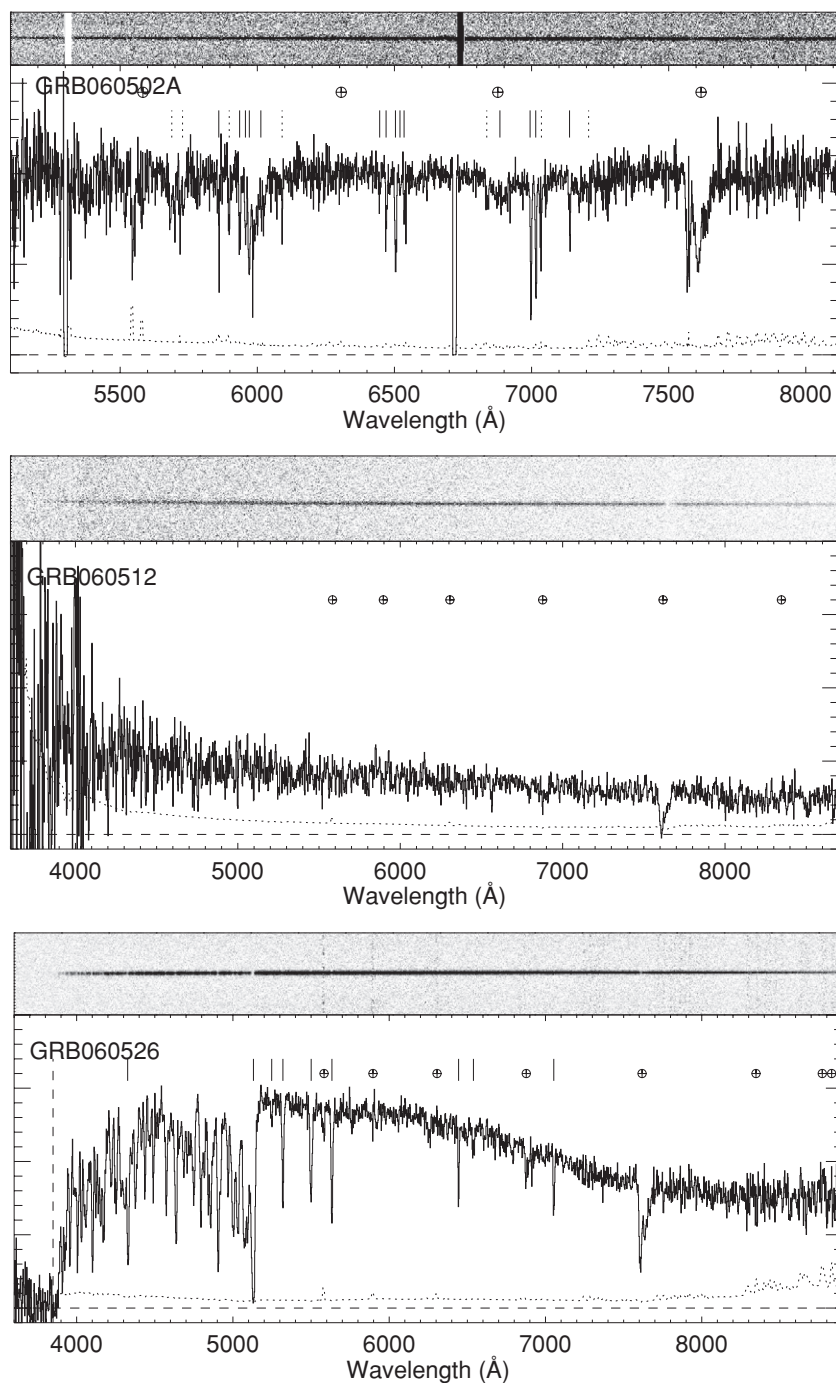
Figure 14. (Continued)

observed and therefore no flux calibration has been attempted for this spectrum (the plotted spectrum is normalized to 1 in the continuum). The redshift is based on several weak metal lines. The upper limit on the redshift based on the absence of the Lyα forest is about 2.3.

A.7. GRB 050820A ($z = 2.6147$)

The UVES data for this burst are discussed in Ledoux et al. (2005) and Fox et al. (2008).

A.8. GRB 050824 ($z = 0.8278$)

GRB 050824 is an X-ray flash (XRF). The data presented here have previously been published in Sollerman et al. (2007).

That work also established evidence for an associated supernova (SN) and detected the host galaxy of the burst. Here, the data have been re-reduced and reanalyzed and more lines have been identified. The redshift is based both on metal absorption lines and emission lines from the underlying host galaxy.

A.9. GRB 050908 ($z = 3.3467$)

The data presented here have previously been published only in the GCN circulars (Fugazza et al. 2005). The spectra will be discussed in more detail in A. Smette et al. (2010, in preparation) where an H I column density of $\log N_{\rm H I} = 17.60 \pm 0.10$ is derived. This system is interesting due to its low H I column
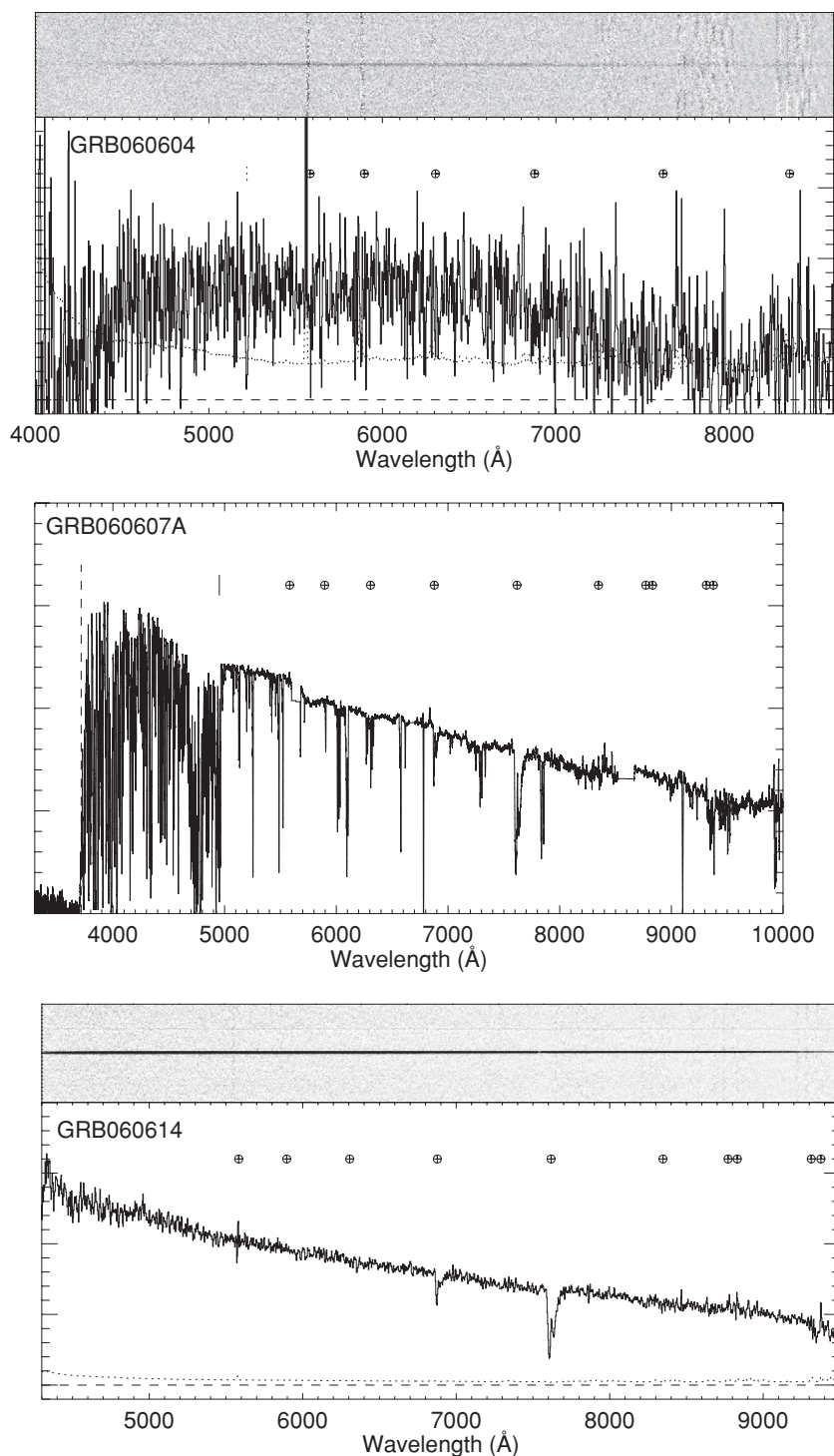
Figure 14. (Continued)

density and the detection of escaping ionizing radiation along its line of sight. Furthermore, there is an intervening sub-DLA at $z = 2.62$ with very strong metal lines.

A.10. GRB 050922C ($z = 2.1995$)

The data presented here have previously been published in Jakobsson et al. (2006c). For this burst, high-resolution spectra have been presented in Piranomonte et al. (2006b). The plotted spectrum is normalized.

A.11. GRB 060115 ($z = 3.5328$)

The data presented here have previously been published only in the GCN circulars (Piranomonte et al. 2006a). The redshift is based on both Lyα and fine-structure lines and is hence secure.

A.12. GRB 060124 ($z = 2.3000$)

The data presented here have previously been published only in the GCN circulars (Prochaska et al. 2006b). The GRB system is characterized by a low H I column density and the absence
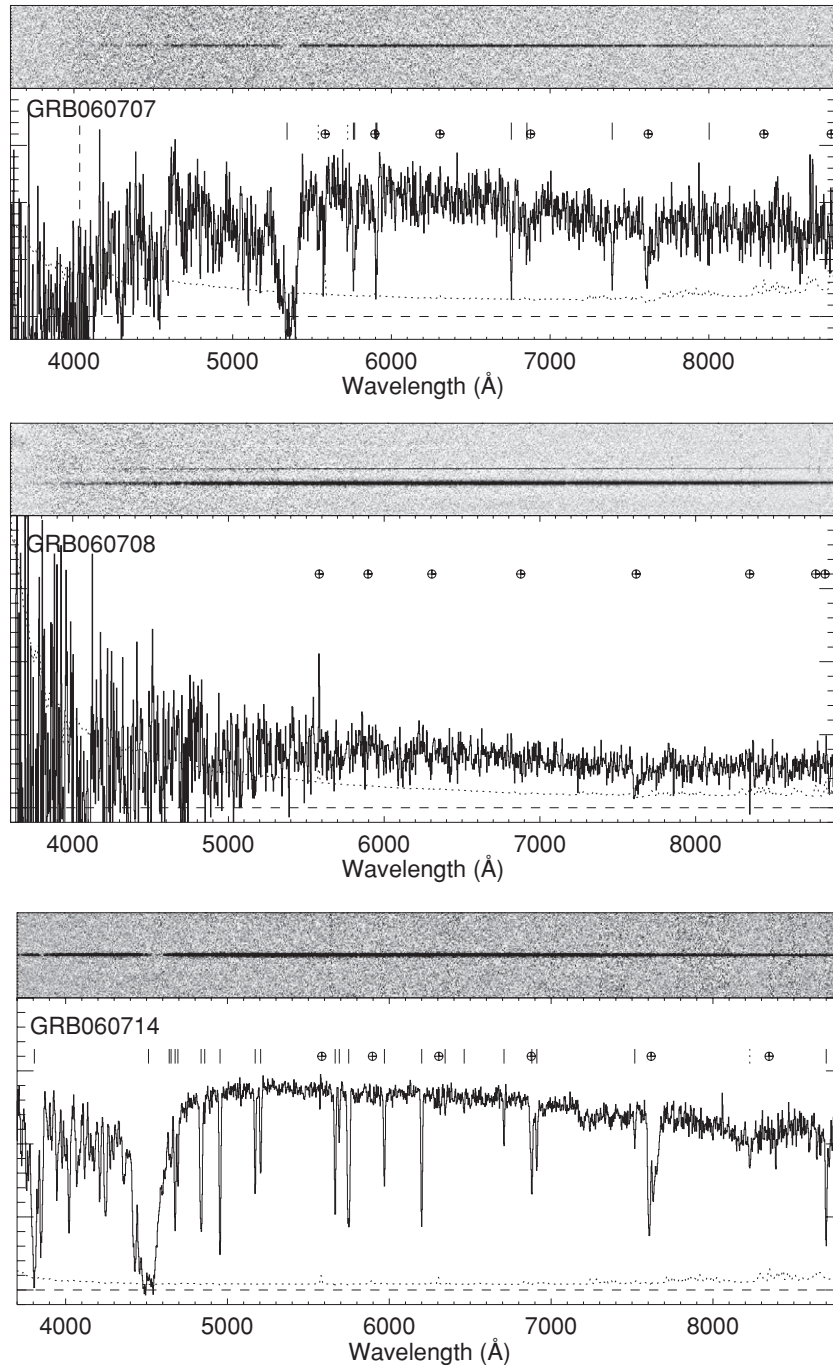
Figure 14. (Continued)

of low-ionization lines. A detailed discussion of the prompt emission and afterglow of this burst can be found in Romano et al. (2006).

A.13. GRB 060206 ($z = 4.0559$)

The data presented here have previously been published in Fynbo et al. (2006c) and Thöne et al. (2008b). Spectroscopic observations of this afterglow have also been published by Hao et al. (2007), who claimed variable absorption lines in the intervening system. This was subsequently falsified by Aoki et al. (2008) and Thöne et al. (2008b). There is tentative evidence for molecular absorption in this spectrum (Fynbo et al. 2006c; see also Prochaska et al. 2009). No standard star was observed

at the night of the observation so we show here a normalized spectrum. The spectrum is strongly affected by fringing redward of 7000 Å.

A.14. GRB 060210 ($z = 3.9122$)

The data presented here have previously been published only in the GCN circulars (Cucchiara et al. 2006b). We do not confirm their identification of an intervening system at $z = 1.47$. The burst has very strong low-ionization lines and classifies as a dark burst by the Jakobsson et al. (2004) definition. A detailed discussion of the prompt emission and afterglow of this burst can be found by Curran et al. (2007), who also infer substantial reddening based on broadband modeling of the afterglow.
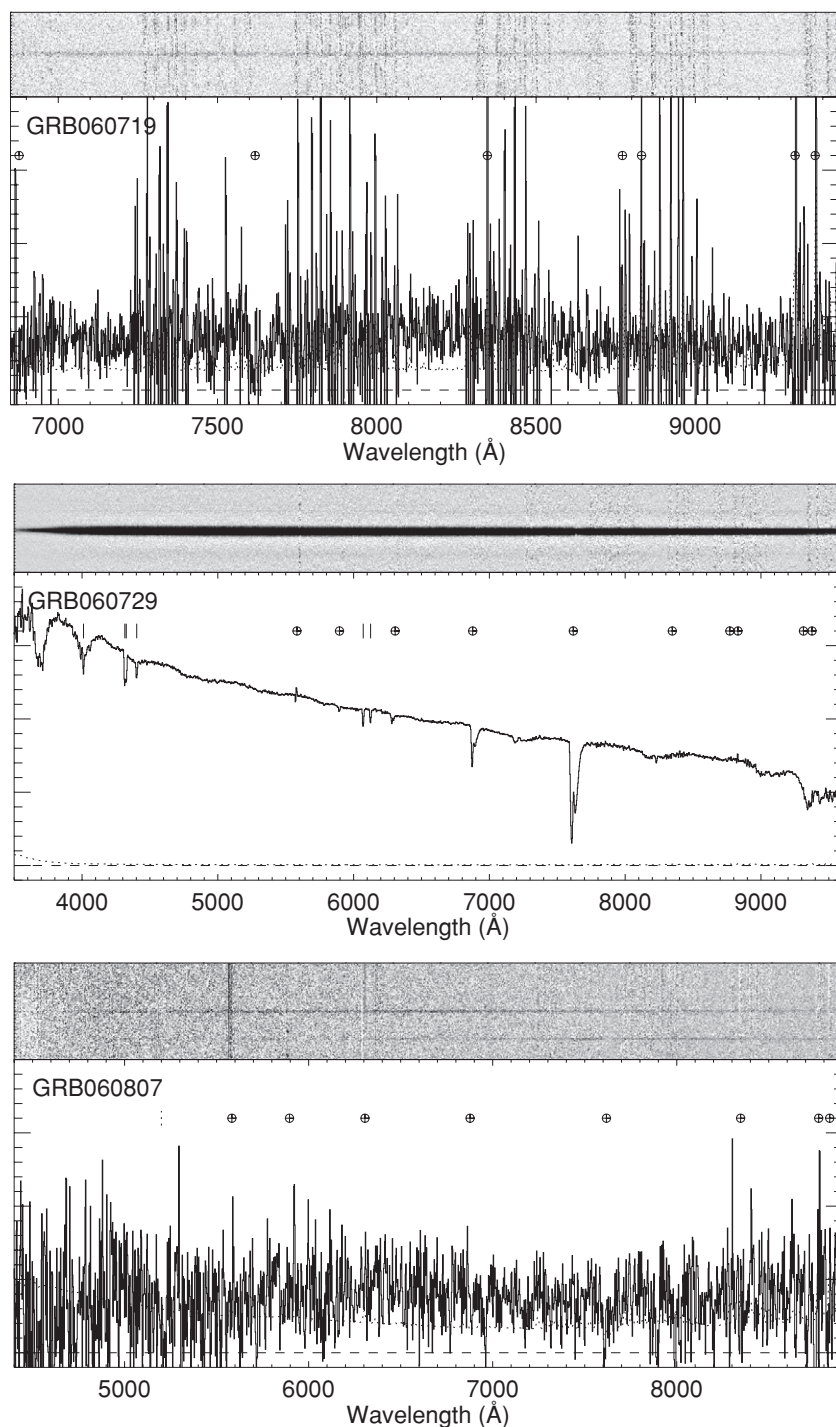
Figure 14. (Continued)

A.15. GRB 060502A ($z = 1.5026$)

The data presented here have previously been published only in the GCN circulars (Cucchiara et al. 2006a). The redshift is based on a rich spectrum of low-ionization (including fine-structure) absorption lines.

A.16. GRB 060512 ($z = 2.1?$)

GRB 060512 is an XRF. The data presented here have previously been published only in the GCN circulars (Starling et al. 2006a). For this burst there is uncertainty about the redshift in the GCN reports. An afterglow spectrum taken at the Telescopio Nazionale Galileo indicates a redshift of around 2.1 (Starling et al. 2006b), which is supported by a spectral break detected by UVOT (De Pasquale & Cummings 2006; Oates et al. 2009), and which is supported by modeling of the broad band spectral energy distribution of the burst (Schady et al. 2007a). Bloom et al. (2006a) measure a redshift of 0.44 from a galaxy close to the afterglow position. This galaxy is offset by about 0.7 arcsec from the position of the afterglow. Based on a binning of the spectrum shown here, we confirm the presence of a broad absorption line around 3750 Å consistent with a redshift of around 2.1 if interpreted as Lyα. This suggests that the $z = 0.44$ galaxy close to the line of sight is a foreground
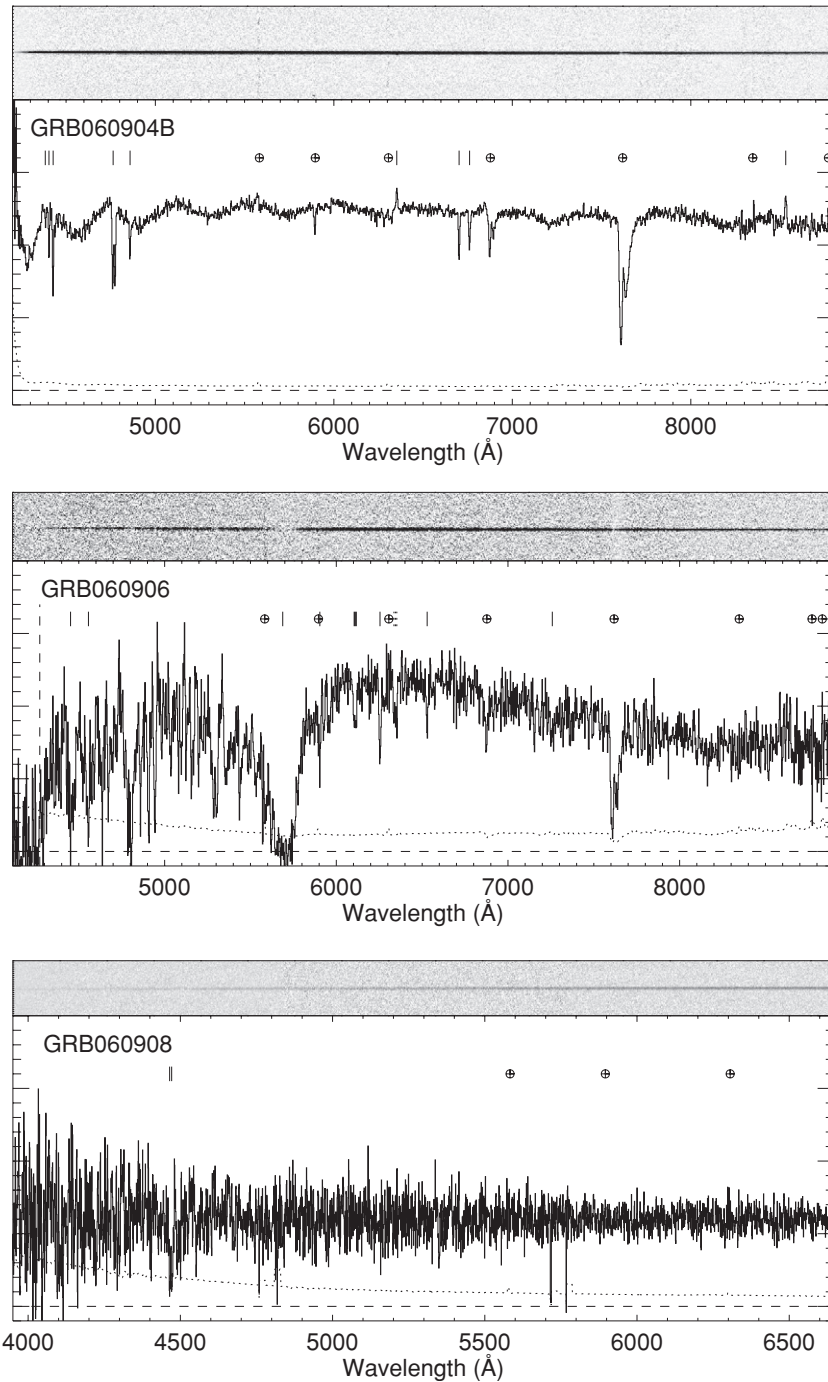
Figure 14. (Continued)

object. We do not detect significant metal lines in the afterglow spectrum.

A.17. GRB 060526 (z = 3.2213)

The data presented here have previously been published in Jakobsson et al. (2006c). Additional medium resolution spectra are discussed in Thöne et al. (2008e). The redshift is based on Lyα and metal absorption lines.

A.18. GRB 060604 (z ≲ 3)

The data presented here have previously been published only in circulars (Castro-Tirado et al. 2006). In the spectrum, we

detect a single absorption line at 5219 Å. The origin of the line is unclear. The line appears too narrow to be Mg II at $z = 0.864$. A possibility is Al II at $z = 2.124$. This would be compatible with the tentative break detected by UVOT (Blustin & Page 2006). From the absence of the onset of the Lyα forest we infer an approximate upper limit on the redshift of ~3. We do not confirm the tentative redshift of $z = 2.68$ proposed by Castro-Tirado et al. (2006).

A.19. GRB 060607A (z = 3.0749)

For this burst, UVES spectra were obtained starting only about 7.5 minutes after the burst (Ledoux et al. 2006b). For a
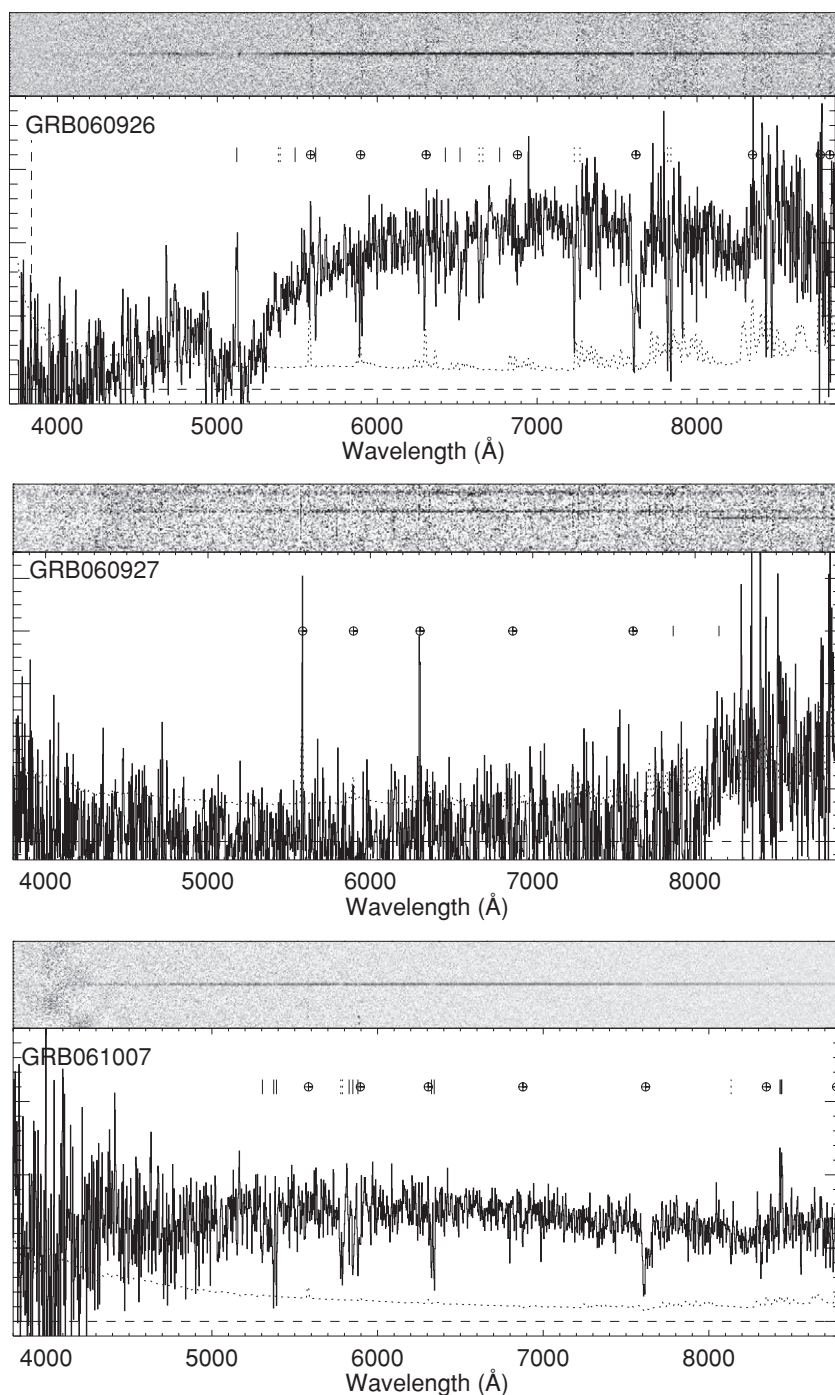
Figure 14. (Continued)

full analysis of the UVES data, see Fox et al. (2008), Prochaska et al. (2008b), and A. Smette et al. (2010, in preparation).

A.20. GRB 060614 ($z = 0.1257$)

The data presented here have previously been published in Della Valle et al. (2006). This is the lowest redshift burst in our spectroscopic sample. However, from the present spectrum no lines (either absorption or emission) are significantly detected. The upper limit on the redshift based on the absence of a Lyα forest is about 2.6. The redshift was later found to be $z = 0.1257$ based on emission lines from the underlying host galaxy (Della Valle et al. 2006). GRB 060614 is remarkable in being a long

burst without an associated (bright) SN (Fynbo et al. 2006d; Della Valle et al. 2006; Gal-Yam et al. 2006).

A.21. GRB 060707 ($z = 3.4240$)

The data presented here have previously been published in Jakobsson et al. (2006c). The burst is remarkable in having very strong metal lines while showing no sign of extinction.

A.22. GRB 060708 ($z = 1.92$)

The data presented here have previously been published only in the GCN circulars (Jakobsson et al. 2006d). The spectrum does not display any significant absorption or emission lines.
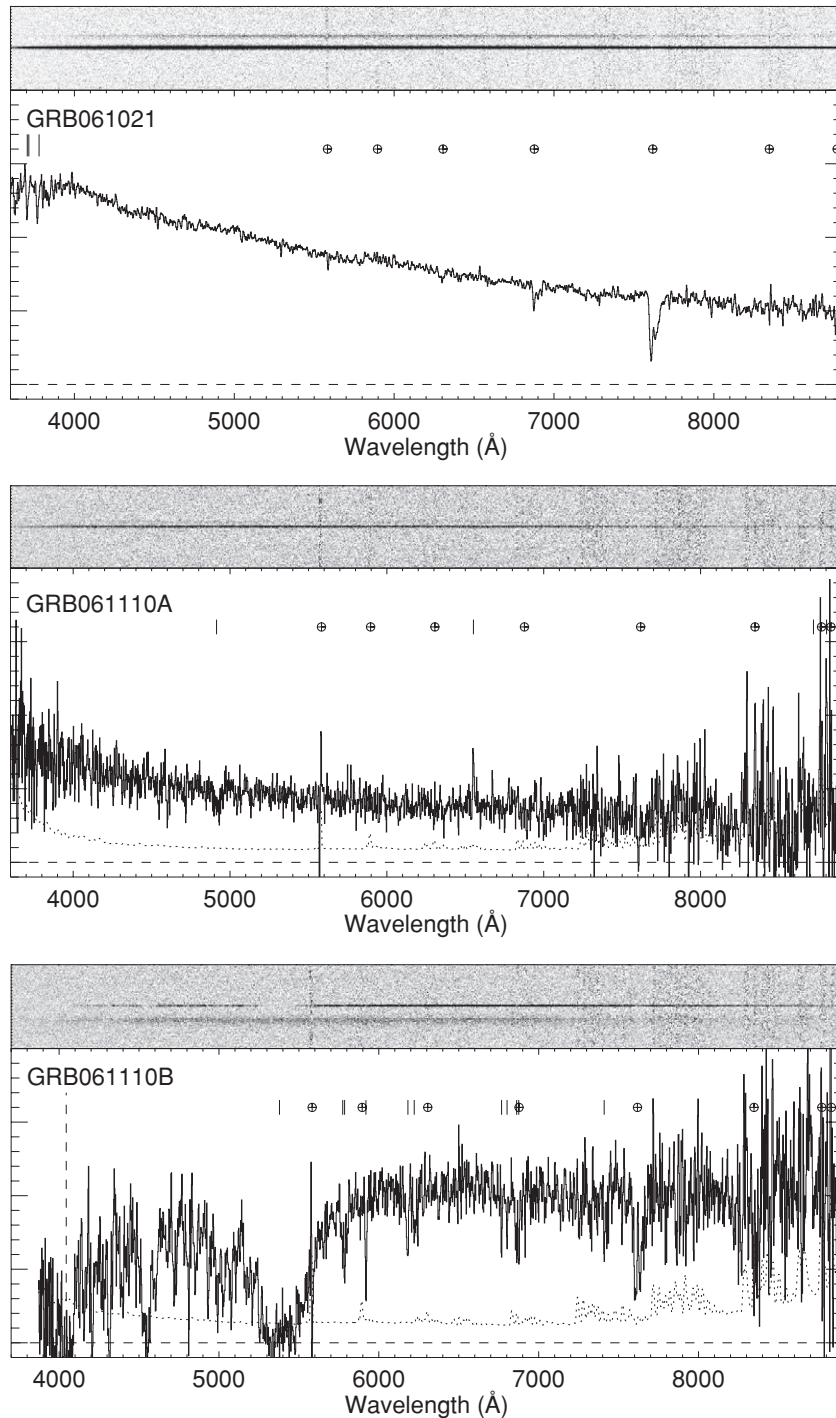
Figure 14. (Continued)

An upper limit of $z \lesssim 2.8$ can be placed on the redshift of GRB 060708 from the lack of significant Lyα forest lines in the spectrum of the afterglow redward of 4600 Å. Blueward of 4600 Å, there is very marginal evidence for broad absorption lines in the spectrum, but the spectrum is too noisy to establish a precise redshift. The *Swift* team has established a photometric redshift of 1.92 for this burst based on the UVOT imaging of the OA (Schady & Moretti 2006).

A.23. GRB 060714 ($z = 2.7108$)

The data presented here have previously been published in Jakobsson et al. (2006c). In the trough of the DLA line of the host absorption system, Lyα emission is detected, presumably from the underlying host galaxy.

A.24. GRB 060719 ($z \lesssim 4.6$)

The data presented here have not been published earlier. This afterglow was extremely red with an $R-K$ color of about 4.5 (Malesani et al. 2006) and the burst was considered a candidate high-redshift burst. Our spectrum, taken with the 600I grating, shows a featureless continuum in the range 6800–9400 Å, thereby placing an upper limit of ~4.6 on the redshift. Hence, this is most likely a dust obscured burst.
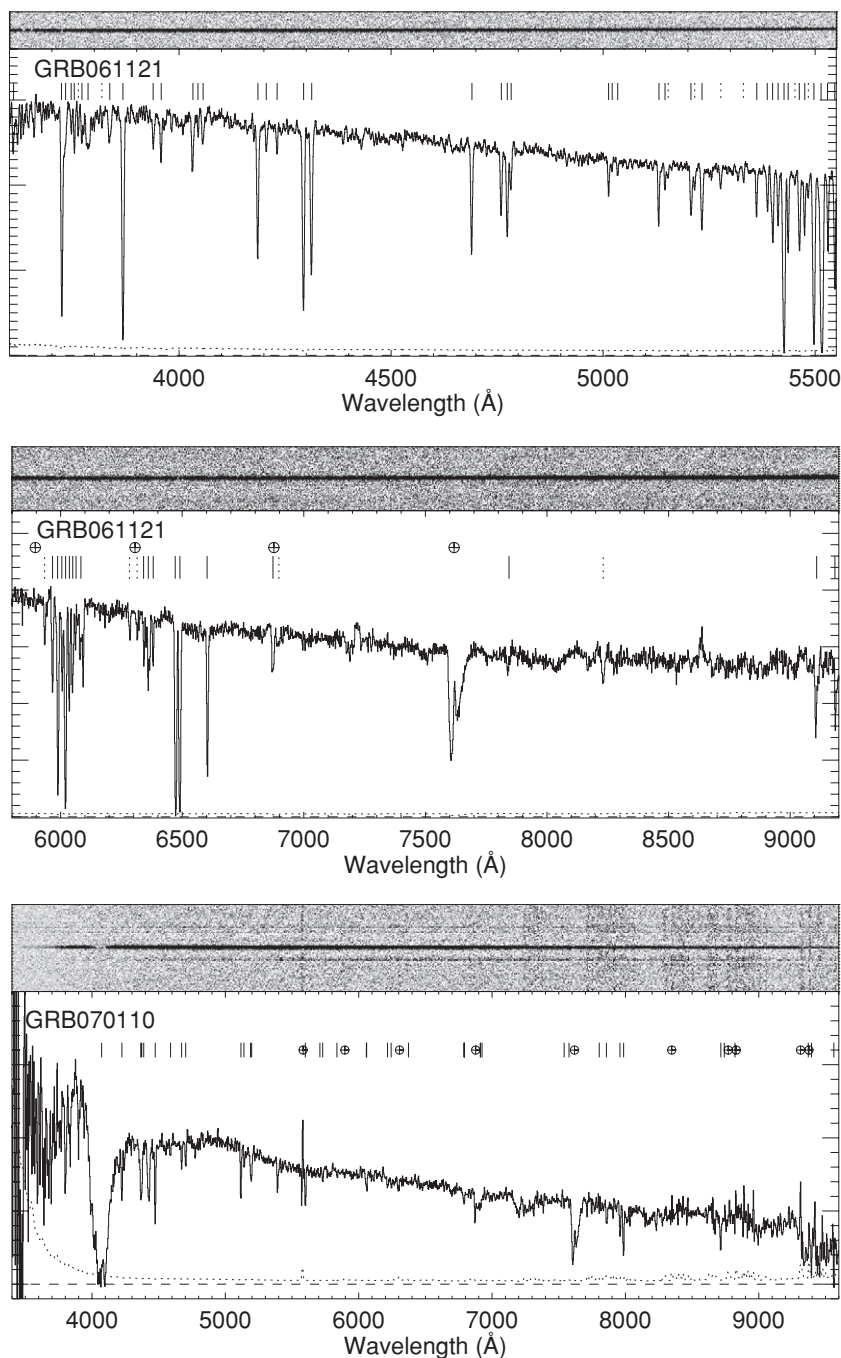
Figure 14. (Continued)

A.25. GRB 060729 ($z = 0.5428$)

The data presented here have previously been published only in the GCN circulars (Thöne et al. 2006c). The broad undulations seen in the blue end of the spectrum are caused by systematic errors in the flux calibration due to the high airmass of the observation. All of the observed strong spectral lines can be associated with a single absorption system. We associate the GRB redshift with this gas. The upper limit on the redshift based on the absence of a Lyα forest is about 2.1.

A.26. GRB 060807 ($z \lesssim 3.4$)

The data presented here have not been published elsewhere. We retrieved the data from the ESO archive. There is a single marginal line at 5200 Å in the spectrum. If it is due to Lyα, then the redshift of the burst would be 3.28. From the absence of a spectral break we set a conservative upper limit of $z < 3.4$. For this burst there is evidence for emission lines in the X-ray spectrum (Butler 2006).

A.27. GRB 060904B ($z = 0.7029$)

The data presented here have previously been published only in the GCN circulars (Fugazza et al. 2006). The burst is not included in the statistical sample as it has too high foreground extinction ($A_V = 0.57$, Schlegel et al. 1998). The broad undulations seen in the spectrum are due to errors in the flux calibration. All of the observed strong, spectral lines can be associated with a single absorption system. We associate the

Figure 14. (Continued)

GRB redshift with this gas. The upper limit on the redshift based on the absence of a Lyα forest is about 2.5.

A.28. GRB 060906 (z = 3.6856)

The data presented here have previously been published in Jakobsson et al. (2006c). The spectrum was obtained in twilight just before sunrise. We do not include this burst in the statistical sample due to its too high foreground extinction of $A_V = 0.54$ (Schlegel et al. 1998). The redshift is based on both Lyα and metal absorption lines.

A.29. GRB 060908 (z = 1.8836)

The data presented here have previously been published only in the GCN circulars (Rol et al. 2006). The redshift is based on a single C IV doublet and is confirmed by the detection of the Lyα emission line from the underlying host galaxy (B. Milvang-Jensen et al. 2010, in preparation). Hence, we do not confirm the tentative redshift of $z = 2.43$ reported by Rol et al. (2006). The redshift we infer is also consistent with the UVOT constraints (Morgan et al. 2006).
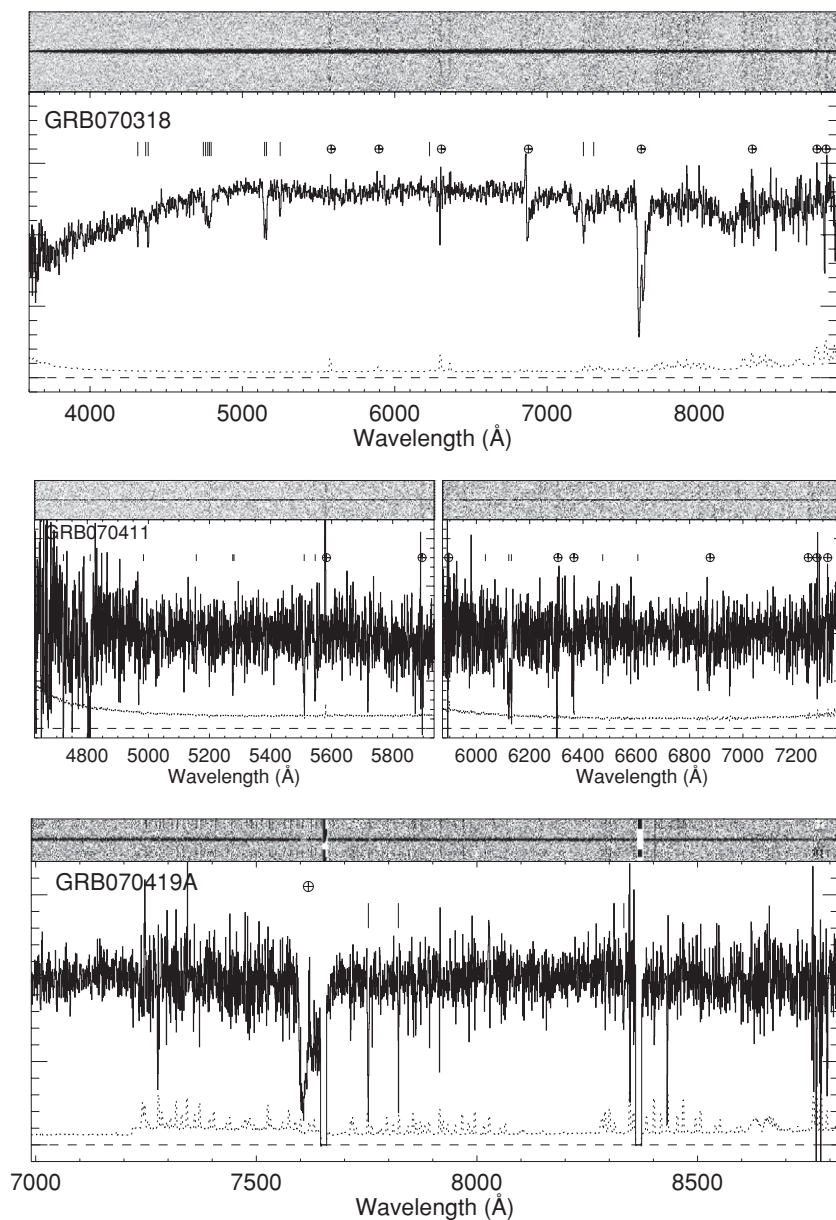
Figure 14. (Continued)

A.30. GRB 060926 ($z = 3.2086$)

The data presented here have previously been published in Piranomonte et al. (2006b). We do not include this burst in the statistical sample due to its too high foreground extinction of $A_V = 0.52$. In the trough of the DLA line of the host absorption system, Lyα emission from the underlying host galaxy is detected. The H I column density is among the highest detected and there is evidence for substantial reddening.

A.31. GRB 060927 ($z = 5.4636$)

The data presented here have previously been published in Ruiz-Velasco et al. (2007). The precise redshift is based on a single low-S/N Si II line. Based alone on the onset of the Lyα forest the redshift can be estimated to be in the range 5.5–5.6, the second highest in the spectroscopic sample.

A.32. GRB 061007 ($z = 1.2622$)

The data presented here have previously been published only in circulars (Jakobsson et al. 2006a). This burst is one of the brightest in γ-rays observed by *Swift*, and its afterglow was also very luminous both in the X-ray and optical bands (Schady et al. 2007b; Mundell et al. 2007). The redshift is based on both metal absorption lines and emission lines from the underlying host galaxy.

A.33. GRB 061021 ($z = 0.3463$)

The data presented here have previously been published only in circulars (Thöne et al. 2006a). In the GCN circular, no redshift measurement was reported. It was only after measuring the redshift from the underlying host galaxy (J. Hjorth et al. 2010, in preparation) that we identified Mg II absorption lines in the very blue end of the afterglow spectrum. This is the second lowest redshift in our spectroscopic sample.

GRB070506

GRB070508

GRB070611
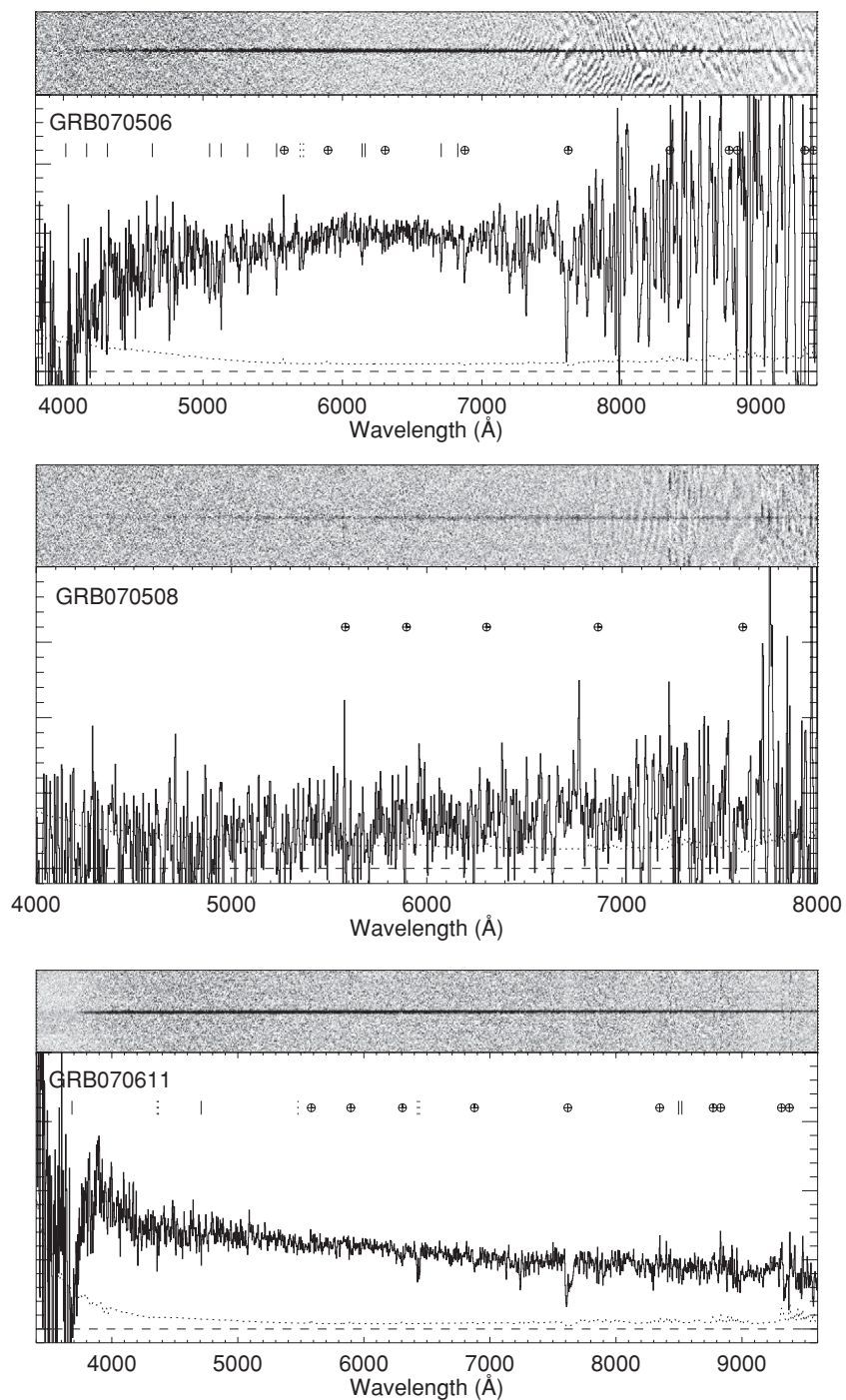
Figure 14. (Continued)

A.34. GRB 061110A ($z = 0.7578$)

The data presented here have previously been published only in circulars (Fynbo et al. 2007). The redshift is mainly based on emission lines from the underlying host galaxy. We also identify a broad absorption feature consistent with the Mg II doublet at the same redshift.

A.35. GRB 061110B ($z = 3.4344$)

The data presented here have previously been published only in circulars (Fynbo et al. 2006b). The redshift is based on both a very strong Lyα line and metal absorption lines, including fine-structure lines.

A.36. GRB 061121 ($z = 1.3145$)

The data presented here have previously been published only in the GCN circulars (Bloom et al. 2006b). The redshift is based on a rich spectrum of low-ionization (including fine-structure) absorption lines.

A.37. GRB 070110 ($z = 2.3521$)

The data presented here have previously been published only in circulars (Jaunsen et al. 2007b). In the trough of the DLA line of the host absorption system, Lyα emission from the underlying host galaxy is detected.

A.38. GRB 070125 ($z = 1.5471$)

The data presented here have not previously been published and will be presented in A. De Cia et al. (2010a, in preparation). The redshift of the burst was determined from Gemini data (Cenko et al. 2008). The burst is peculiar in being very bright and having very weak absorption lines in its afterglow spectrum. For a typical fainter OA, the redshift for such an absorption system would be very difficult to establish. The burst is not included in the statistical sample as the XRT position was distributed later than 12 hr after the burst. The upper limit on the redshift based on the absence of Lyα forest lines is about 2.3. The broad undulations in the blue end of the spectrum are due to systematics in the flux calibration.

A.39. GRB 070129 ($z \lesssim 3.4$)

The data presented here have not previously been published. A redshift could not be established as no significant lines are detected in the spectrum. We place a conservative upper limit of $z \lesssim 3.4$ from the upper limit on wavelength of the onset of the Lyα forest.

A.40. GRB 070306 ($z = 1.4965$)

The data presented here have previously been published in Jaunsen et al. (2008). The redshift is based on a single oxygen emission line. The identification with [O II] is secure as the doublet is resolved in a higher resolution spectrum (Jaunsen et al. 2008). The burst is remarkable in having a highly extinguished afterglow only detected in the K and H bands while being located in a blue host galaxy (Jaunsen et al. 2008).

A.41. GRB 070318 ($z = 0.8397$)

The data presented here have previously been published only in circulars (Jaunsen et al. 2007a). The afterglow spectrum displays a spectral break around 5000 Å (or about 2700 Å in the rest frame), the nature of which is currently not understood. All of the observed strong, spectral lines can be associated with a single absorption system. We associate the GRB redshift with this gas. The upper limit on the redshift based on the absence of Lyα forest features is about 2.1.

A.42. GRB 070411 ($z = 2.9538$)

The data presented here have previously been published only in circulars (Jakobsson et al. 2007b). The spectra were obtained with the two medium resolution gratings, 1400V and 1200R. The burst is not included in our statistical sample as the foreground Galactic extinction is too high ($A_V = 0.76$, Schlegel et al. 1998). The GRB absorption system has one of the lower H I column densities in our sample (see Table 3).

A.43. GRB 070419A ($z = 0.9705$)

The data presented here have not been published before. All of the observed strong, spectral lines can be associated with a single absorption system. We associate the GRB redshift with this gas.

A.44. GRB 070506 ($z = 2.3090$)

The data presented here have previously been published only in circulars (Thöne et al. 2007b). Redward of 7000 Å, the spectrum is strongly affected by fringing. The redshift is based on both Lyα and metal absorption lines.

A.45. GRB 070508 ($z \lesssim 3.0$)

The data presented here have previously been published only in circulars (Jakobsson et al. 2007d). No lines are detected in the spectrum, and an upper limit of $z \lesssim 3$ is placed on the redshift from the upper limit on wavelength of the onset of the Lyα forest. The burst is not included in the statistical sample as the declination is too low ($-78°$). The burst classifies as a dark burst by the definition of Jakobsson et al. (2004).

A.46. GRB 070611 ($z = 2.0394$)

The data presented here have previously been published only in circulars (Thöne et al. 2007a). The redshift is based on both Lyα and metal absorption lines. Also detected in the spectrum are two intervening Mg II systems.

A.47. GRB 070721B ($z = 3.6298$)

The data presented here have previously been published only in circulars (Malesani et al. 2007). A bright Lyα emitter is located 20 arcsec from the GRB position at the same redshift as the GRB. A $z = 3.09$ intervening sub-DLA is detected in both the spectrum of the afterglow and in the spectrum of the neighbor Lyα emitter. A possible galaxy counterpart of the absorber is detected in emission 2 arcsec from the afterglow position. The spectrum will be discussed in more detail in B. Milvang-Jensen et al. (2010, in preparation).

A.48. GRB 070802 ($z = 2.4541$)

The data presented here have previously been published in Elíasdóttir et al. (2009). The spectrum is remarkable, showing a strong 2175 Å dust extinction feature at the GRB redshift of $z = 2.45$ (see also Krühler et al. 2008). The burst classifies as a dark burst by the definition of Jakobsson et al. (2004). There are also two intervening Mg II systems in the spectrum, one of which is very strong.

A.49. GRB 071020 ($z = 2.1462$)

The data presented here have previously been published only in circulars (Jakobsson et al. 2007c). The spectrum will be discussed in more detail in M. Nardini et al. (2009, in preparation). All of the observed strong spectral lines can be associated with a single absorption system. We associate the GRB redshift with this gas.
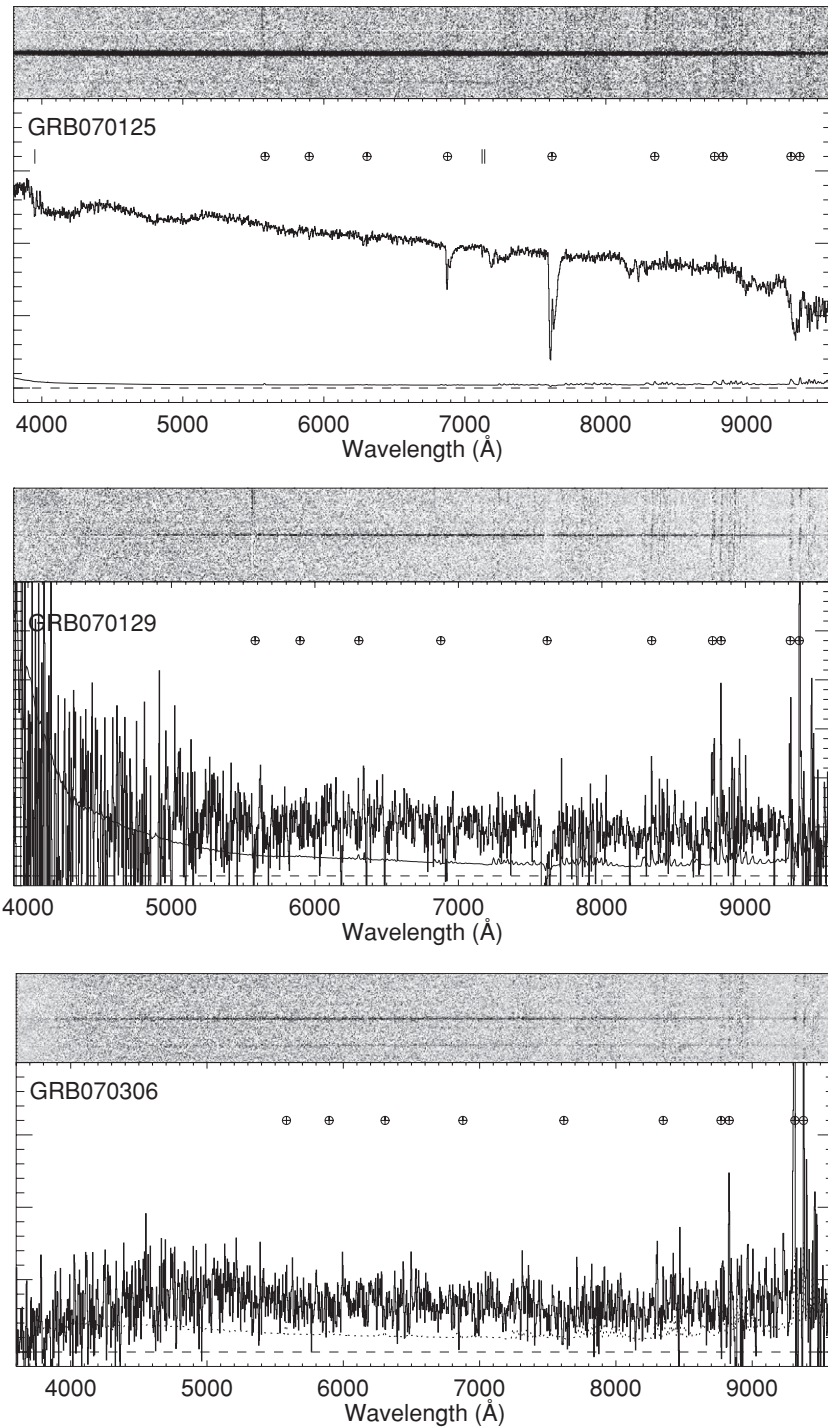
The upper limit on the redshift based on the absence of a Lyα forest is about 3.

A.50. GRB 071025 ($z = 5.2?$)

The data presented here have not previously been published. The data were obtained with the high resolution HIRES spectrograph. Weak continuum flux is detected from the afterglow at wavelengths $\lambda > 7500$ Å, but no emission is detected at shorter wavelengths. This flux "decrement" may be associated with the IGM at $z \approx 5.2$ but could also be associated with a significant reddening of the afterglow. If one presumes the latter, the burst is still very likely to be at high redshift ($z > 2.5$) because a sharp decrement from dust is only expected at ultraviolet wavelengths. This redshift of $z \approx 5.2$ is consistent with the photometry which displays a break between the R and I bands (e.g., Rykoff et al. 2007). We do not show a figure of this spectrum.

A.51. GRB 071031 (z = 2.6918)

The data presented here have previously been published only in circulars (Ledoux et al. 2008). In addition to the 300V spectrum shown here, spectra were secured with a range of higher resolution gratings and with the high-resolution UVES spectrograph (e.g., Fox et al. 2008). In the trough of the DLA line at the host redshift Lyα emission from the underlying host galaxy is detected. In the medium and high resolution spectra, a large number of Fe II fine-structure and metastable lines are detected.

A.52. GRB 071112C (z = 0.8227)

The data presented here have previously been published only in circulars (Jakobsson et al. 2007a). The redshift is based on both absorption lines from the GRB host system as well as emission lines from the underlying host galaxy.

A.53. GRB 071117 (z = 1.3308?)

The data presented here have previously been published only in circulars (Jakobsson et al. 2007e). The redshift is based on a single emission line at 8687 Å, which we interpret as [O II] at z = 1.331. The spectrum is affected by fringing redward of about 7000 Å, and the line is only seen after subtracting two of the individual exposures where the source has been offset along the slit from each other. Hence, we consider the significance of this redshift measurement to be marginal.

A.54. GRB 080210 (z = 2.6419)

The data presented here have previously been published only in circulars (Jakobsson et al. 2008b). The spectrum will be discussed in more detail in A. De Cia et al. (2010b, in preparation). There is evidence for substantial reddening. The redshift is based on both Lyα and metal absorption lines.

A.55. GRB 080310 (z = 2.4274)

This burst was observed both with the VLT/UVES spectrograph (Vreeswijk et al. 2008b) and the Kast spectrograph. Here we show the Kast spectrum previously published in Prochaska et al. (2008c). The GRB absorber is characterized by a low H I column density and several high ionization lines (see also Fox et al. 2008; Ledoux et al. 2009; A. De Cia et al. 2010c, in preparation).

A.56. GRB 080319B (z = 0.9382)

This is the famous "naked eye burst" (e.g., Racusin et al. 2008; Woźniak et al. 2009; Bloom et al. 2009). The FORS2 spectrum presented here was obtained quite late, 26 hr after the burst. We retrieved the data from the ESO archive.

A.57. GRB 080319C (z = 1.9492)

The data presented here have previously been published only in circulars (Wiersema et al. 2008a). The data were obtained in poor conditions with cloud cover. The plotted spectrum is normalized. The redshift is based on the highest redshift metal line system in the spectrum. We also detect an intervening Mg II system. The upper limit on the redshift based on the absence of significant Lyα forest lines is about 2.7. The burst classifies as a dark burst by the Jakobsson et al. (2004) definition.

A.58. GRB 080330 (z = 1.5119)

GRB 080330 is an XRF. The data presented here have previously been published in Guidorzi et al. (2009). The burst was also observed with the VLT-UVES spectrograph (D'Elia et al. 2009b). All of the observed strong spectral lines can be associated with a single absorption system. We associate the GRB redshift with this gas.

A.59. GRB 080411 (z = 1.0301)

The data presented here have previously been published only in circulars (Thöne et al. 2008a). The burst is not included in the statistical sample as it has too high foreground extinction (A_V = 0.54, Schlegel et al. 1998). The burst is remarkable in having a bright X-ray afterglow visible for more than three weeks after the burst (Marshall et al. 2008). The OA spectrum has a fairly strong unidentified line at 4439 Å.

A.60. GRB 080413A (z = 2.4330)

This burst was observed with VLT/UVES. The burst is not included in the statistical sample as it has too high foreground extinction (A_V = 0.52, Schlegel et al. 1998).

A.61. GRB 080413B (z = 1.1014)

The data presented here have previously been published only in circulars (Vreeswijk et al. 2008d). Spectra were also secured in a number of higher resolution gratings. The broad undulations in the blue end of the spectrum are due to systematics in the flux calibration.

A.62. GRB 080520 (z = 1.5457)

The data presented here have previously been published only in circulars (Jakobsson et al. 2008a). The afterglow was very faint at the time of observation, but the redshift is based on both host emission lines and afterglow metal absorption lines and hence is secure.

A.63. GRB 080523 (z ≲ 3.0)

The data presented here have previously been published only in circulars (Fynbo et al. 2008c). The afterglow was very faint at the time of observation and due to the lack of significant lines or breaks, we can only place an upper limit of about 3.0 on the redshift.

A.64. GRB 080603B (z = 2.6892)

The data presented here have previously been published only in circulars (Fynbo et al. 2008e). The redshift is on both Lyα and metal (including fine-structure) absorption lines. We also detect an intervening Mg II system in the spectrum.

A.65. GRB 080604 (z = 1.4171)

The data presented here have previously been published only in circulars (Wiersema et al. 2008b). The plotted spectrum is normalized. All of the observed strong, spectral lines can be associated with a single absorption system. We associate the GRB redshift with this gas. The upper limit on the redshift is about 3.1 based on the absence of a Lyα forest in the spectrum.

A.66. GRB 080605 ($z = 1.6403$)

The data presented here have previously been published only in circulars (Jakobsson et al. 2008c). Spectra were also secured with a number of higher resolution gratings. This spectrum, like the spectrum of GRB 070802, shows both C I absorption and evidence for the 2175 Å extinction feature. Spectroscopy of this afterglow will be further discussed in D. Xu et al. (2010, in preparation).

A.67. GRB 080607 ($z = 3.0368$)

The data presented here have previously been published in Prochaska et al. (2009). The spectrum is characterized by a very strong Lyα line and by the detection of both H$_2$ and CO molecular lines (Prochaska et al. 2009; Sheffer et al. 2009). The spectrum shows evidence for substantial reddening. Based on the broadband photometry, there is also evidence for the presence of the 2175 Å extinction bump (Prochaska et al. 2009). The burst classifies as a dark burst by the Jakobsson et al. (2004) definition. In the figure of this spectrum we only show the R400 spectrum. For the blue grating spectrum covering Lyα we refer to Prochaska et al. (2009).

A.68. GRB 080707 ($z = 1.2322$)

The data presented here have previously been published only in circulars (Fynbo et al. 2008f). The spectrum was obtained under quite poor conditions with bad seeing and at high airmass. A spectrum was also secured with a higher resolution grating. All of the observed strong spectral lines can be associated with a single absorption system. We associate the GRB redshift with this gas. The upper limit on the redshift is about 2.2 based on the absence of a Lyα forest.

A.69. GRB 080710 ($z = 0.8454$)

The data presented here have previously been published only in circulars (Perley et al. 2008). All of the observed strong, spectral lines can be associated with a single absorption system. The system also shows fine-structure lines. We associate the GRB redshift with this gas. The plotted spectrum has been normalized.

A.70. GRB 080721 ($z = 2.5914$)

The data presented here have previously been published in Starling et al. (2009). Spectra were also secured with a number of higher resolution gratings. The spectrum is affected by fringing redward of about 7000 Å. The redshift is on both Lyα and metal (including fine-structure) absorption lines.

A.71. GRB 080804 ($z = 2.2045$)

The data presented here have previously been published only in circulars (Thöne et al. 2008d). The spectrum was obtained with the high resolution UVES spectrograph.

A.72. GRB 080805 ($z = 1.5042$)

The data presented here have previously been published only in circulars (Jakobsson et al. 2008e). The strongest line in the spectrum is from a very strong intervening Mg II system. The proposed GRB redshift of 1.504 is based on a higher redshift weaker metal absorption line system. There is evidence for the presence of the 2175 Å extinction feature in the shape of the spectrum at the proposed GRB redshift. The burst classifies as a dark burst according the Jakobsson et al. (2004) definition.

A.73. GRB 080810 ($z = 3.3604$)

The data presented here have previously been published only in circulars (de Ugarte Postigo et al. 2008). A higher resolution spectrum was secured at the Keck telescope, and this can be inspected in Page et al. (2009). The host absorber is remarkable in having a relatively low H I column density. There is evidence for Lyα emission presumably from the underlying host galaxy.

A.74. GRB 080905B ($z = 2.3739$)

The data presented here have previously been published only in circulars (Vreeswijk et al. 2008a). The light from the afterglow is blended with light from another object on the slit. Spectra were also secured with a number of higher resolution gratings. The redshift is based on metal absorption lines including fine-structure lines.

A.75. GRB 080913 ($z = 6.7$)

The data presented here have previously been published in Greiner et al. (2009). The redshift is based on the detection of the onset of the Gunn-Peterson trough at 9400 Å. No absorption or emission lines are detected in the spectrum. This is the most distant GRB for which the redshift has been determined in our spectroscopic sample. The burst classifies as a dark burst by the Jakobsson et al. (2004) definition.

A.76. GRB 080916A ($z = 0.6887$)

The data presented here have previously been published only in circulars (Fynbo et al. 2008b). The redshift is based on both absorption lines and emission lines from the underlying host galaxy.

A.77. GRB 080928 ($z = 1.6919$)

The data presented here have previously only been published in circulars (Vreeswijk et al. 2008e). This is another good example of a spectrum where the lines from the intervening absorber are significantly stronger than in the likely GRB absorber. The proposed GRB system is the highest redshift, but weaker, of two metal line systems detected in the spectrum. The upper limit on the redshift based on the absence of Lyα forest features is about 2.1.

APPENDIX B

LINE LISTS AND SPECTRA OF GRB AFTERGLOWS

In Figure 14, we show one- and two-dimensional spectra of each of the 77 bursts listed in Table 2.

Table 5
GRB 050319 ($z = 3.2425$)

λ_{obs} (Å)	λ_{rest} (Å)	z	Feature	EW$_{obs}$ (Å)
5157	1215.7		Lyα	
5348.2	1260.4	3.2425	Si II	8 ± 3
5530.5	1302.2	3.2425	O I	9 ± 3
	1304.4	3.2425	Si II	
5663.8	1334.5	3.2425	C II	9 ± 3
5913.2	1393.7	3.2425	Si IV	5 ± 3
5949.9	1402.7	3.2425	Si IV	9 ± 3
6472.8	1526.7	3.2425	Si II	6 ± 3
6578.9	1548.2	3.2425	C IV	8 ± 3
	1550.8	3.2425	C IV	

Table 6
GRB 050401 ($z = 2.8983$)

λ_{obs} (Å)	λ_{rest} (Å)	z	Feature	EW_{obs} (Å)
4739.0	1215.7	2.8983	Lyα	
5074.4	1302.2	2.8983	O I	14 ± 4
	1304.4	2.8983	Si II	
5180.0				6 ± 3
5194.7				14 ± 4
5205.0	1334.5	2.8983	C II	12 ± 3
	1335.7	2.8983	C II*	
5422.2	1548.2	2.4982	C IV	14 ± 2
5431.9	1550.8	2.4982	C IV	
	1393.8	2.8983	Si IV	
5842.6	1670.8	2.4982	Al II	8 ± 2^{a}
5900.0				5.5 ± 1.6
5950.4	1526.7	2.8983	Si II	12 ± 2
6036.5	1548.2	2.8983	C IV	10.0 ± 1.0
6044.6	1550.8		C IV	
6273.9	1608.4	2.8983	Fe II	8.5 ± 1.5
6510.9	1670.8	2.8983	Al II	7.0 ± 1.4
6559.9				3.2 ± 0.9
7049.0	1808.0	2.8983	Si II	3.2 ± 0.7
7229.5	1854.7	2.8983	Al III	7.5 ± 0.7
7262.0	1862.8	2.8983	Al III	7.5 ± 0.8
7899.2	2026.1	2.8983	Zn II	5.7 ± 0.8
	2026.5	2.8983	Mg I	
8020.8	2056.3	2.8983	Cr II	3.5 ± 0.9
8042.2	2062.2	2.8983	Cr II	5.6 ± 0.9
	2062.7	2.8983	Zn II	
8055.0	2066.2	2.8983	Cr II	3.0 ± 0.9
8197.9	2344.2	2.4982	Fe II	3.7 ± 0.8
8303.8	2374.5	2.4982	Fe II	2.3 ± 1.0
8331.5	2382.8	2.4982	Fe II	7.4 ± 0.7
8428.5	2411.3	2.4982	Fe II	3.8 ± 1.1
8815.8	2260.8	2.8983	Fe II	3.7 ± 0.9
9023.8	2316.7	2.8983	Ni II**	5.4 ± 0.9
9093.7	2600.2	2.4982	Fe II	9.2 ± 0.8
9137.6	2344.2	2.8983	Fe II	5.5 ± 0.7
9254.8	2374.5	2.8983	Fe II	6.2 ± 1.0
9289.9	2382.8	2.8983	Fe II	6.2 ± 1.0

Note. ^{a} Likely blended with another line.

Table 7
GRB 050408 ($z = 1.2356$)

λ_{obs} (Å)	λ_{rest} (Å)	z	Feature	EW_{obs} (Å)
		GMOS/R150		
4610.4	2056.25	1.2356	Cr II	6.17 ± 1.51
	2062.2	1.2356	Cr II	
	2062.7	1.2356	Zn II	
	2066.2	1.2356	Cr II	
5241.4	2333.5	1.2356	Fe II*	5.49 ± 0.77
	2338.7	1.2356	Fe II*	
	2344.2	1.2356	Fe II	
	2345.0	1.2356	Fe II*	
	2349.0	1.2356	Fe II*	
5310.0	2365.6	1.2356	Fe II*	3.00 ± 0.67
	2374.5	1.2356	Fe II	
5328.7	2381.5	1.2356	Fe II*	4.22 ± 0.65
	2382.8	1.2356	Fe II	
	2383.8	1.2356	Fe II*	
	2389.4	1.2356	Fe II*	

Table 7
(Continued)

λ_{obs} (Å)	λ_{rest} (Å)	z	Feature	EW_{obs} (Å)
5782.9	2586.7	1.2356	Fe II	3.55 ± 0.43
5812.7	2594.5	1.2356	Mn II	7.83 ± 0.55
	2599.2	1.2356	Fe II*	
	2600.2	1.2356	Fe II	
	2606.5	1.2356	Mn II	
	2607.9	1.2356	Fe II*	
	2612.7	1.2356	Fe II*	
6261.7	2796.4	1.2356	Mg II	10.90 ± 0.66
	2803.5	1.2356	Mg II	
6377.9	2853.0	1.2356	Mg I	3.48 ± 0.39
7246.3	3240.0	1.2356	Ti II*	2.24 ± 0.48
	3242.9	1.2356	Ti II	
		GMOS/R831		
6378.1	2853.0	1.2356	Mg I	3.02 ± 0.29
6752.7	3021.5	1.2356	Fe I	0.69 ± 0.19
6875.1	3073.9	1.2356	Ti II	2.91 ± 0.30
7566.9	3384.7	1.2356	Ti II	1.11 ± 0.21

Table 8
GRB 050730 ($z = 3.9693$)

λ_{obs} (Å)	λ_{rest} (Å)	z	Feature	EW_{obs} (Å)
4889.3	1215.7	3.022	Lyα	
5549.2	1215.7	3.5680	Lyα	
6040.	1215.7	3.9693	Lyα	
6230.6	1253.8	3.9693	S II	1.38 ± 0.16
6261.9	1259.5	3.9693	S II	5.5 ± 0.3
	1260.4	3.9693	Si II	
6291.1	1264.7	3.9693	Si II*	
6400.8	1402.7	3.5680	Si IV	0.65 ± 0.13
6470.9	1302.2	3.9693	O I	
6481.7	1304.4	3.9693	Si II	7.1 ± 0.2
6503.4	1309.3	3.9693	Si II*	
	2344.2	1.7728	Fe II	
6599.4	1334.5	3.9693	C II	3.0 ± 0.2
	1549.5	3.25	C IV	
6632.3	1334.5	3.9693	C II	4.9 ± 0.2
6720.9	1670.7	3.0222	Al II	0.99 ± 0.11
6925.0	1393.7	3.9693	Si IV	7.1 ± 0.2
6934.	1402.7	3.9693	Si IV	
6968.4	1402.7	3.9693	Si IV	4.6 ± 0.2
	1526.7	3.5680	Si II	
6989.	1548.2	3.514	C IV	
6995.	1550.8	3.514	C IV	
7069.5	1548.2	3.5680	C IV	1.1 ± 0.2
	1550.8	3.5680	C IV	
7110.1				1.2 ± 0.2
7173.8	2586.7	1.7728	Fe II	4.2 ± 0.2
7208.7	2600.2	1.7728	Fe II	
7348.9	1608.4	3.5680	Fe II	0.34 ± 0.16
7694.1	1548.2	3.9693	C IV	1.1 ± 0.2
7702.0	1550.8	3.9693	C IV	
7752.6	2796.3	1.7728	Mg II	7.1 ± 0.3
7774.4	2803.5	1.7728	Mg II	
7990.7	1608.4	3.9693	Fe II	1.3 ± 0.2
8299.7	1670.7	3.9693	Al II	3.1 ± 0.3
8415.0	2586.7	2.2533	Fe II	1.0 ± 0.3
8457.8	2600.2	2.2533	Fe II	2.4 ± 0.3
9097.6	2796.3	2.2533	Mg II	2.6 ± 0.2
9121.7	2803.5	2.2533	Mg II	1.4 ± 0.2

Table 9
GRB 050801

λ_{obs} (Å)	λ_{rest} (Å)	z	Feature	EW$_{obs}$ (Å)
		LRISb/B600		
		LRISr/R600		
6040.7				2.32 ± 0.76

Table 10
GRB 050802 ($z = 1.7102$)

λ_{obs} (Å)	λ_{rest} (Å)	z	Feature	EW$_{obs}$ (Å)
4199.4	1548.2	1.7102	C IV	7.4 ± 1.5
4199.4	1550.8	1.7102	C IV	
6353.5	2344.2	1.7102	Fe II	7.1 ± 0.9
6458.7	2382.8	1.7102	Fe II	7.3 ± 0.9
7009.8	2586.7	1.7102	Fe II	5.0 ± 1.1

Table 11
GRB 050820A ($z = 2.6147$)

λ_{obs} (Å)	λ_{rest} (Å)	z	Feature	EW$_{obs}$ (Å)
5518.6	1526.7	2.6147	Si II	5.68 ± 0.05
5596.3	1548.2	2.6147	C IV	5.44 ± 0.04
5605.7	1550.8	2.6147	C IV	5.01 ± 0.05

Table 12
GRB 050824 ($z = 0.8278$)

λ_{obs} (Å)	λ_{rest} (Å)	z	Feature	EW$_{obs}$ (Å)
4284.7	2344.2	0.8278	Fe II	1.8 ± 0.5
4337.9	2374.5	0.8278	Fe II	4.5 ± 0.8
4354.2	2382.8	0.8278	Fe II	
4728.6	2586.7	0.8278	Fe II	1.5 ± 0.4
5108.6	2796.3	0.8278	Mg II	1.7 ± 0.3
5124.5	2803.5	0.8278	Mg II	2.3 ± 0.3
6814.5	3727.7	0.8278	[O II]	Emission
7074.4	3869.8	0.8278	[Ne III]	Emission
7192.4	3934.8	0.8278	Ca II	3.0 ± 0.5
7752.9				1.2 ± 0.4
7938.4	4341.7	0.8278	Hγ	Emission
8889.2	4862.7	0.8278	Hβ	Emission
9067.6	4960.3	0.8278	[O III]	Emission
9155.0	5008.2	0.8278	[O III]	Emission

Table 13
GRB 050908 ($z = 3.3467$)

λ_{obs} (Å)	λ_{rest} (Å)	z	Feature	EW$_{obs}$ (Å)
4402.7	1215.7	2.6208	Lyα	
5280.6	1215.7	3.3467	Lyα	
5527.8	1526.7	2.6208	Si II	8.1 ± 0.2
5607.4	1548.2	2.6208	C IV	3.2 ± 0.2
	1550.8	2.2613	C IV	
5627.8	1393.7	3.0383	Si IV	1.9 ± 0.2
5664.9	1402.7	3.0383	Si IV	0.80 ± 0.15

Table 13
(Continued)

λ_{obs} (Å)	λ_{rest} (Å)	z	Feature	EW$_{obs}$ (Å)
5683.8	1302.2	3.3467	O I	1.3 ± 0.2
	1304.4	3.3467	Si II	
5695.0	1309.3	3.3467	Si II*	1.28 ± 0.15
5796.8	1334.5	3.3467	C II	0.62 ± 0.18
5824.8	1608.4	2.6208	Fe II	1.47 ± 0.13
5973.0	2344.2	1.5481	Fe II	0.90 ± 0.14
6052.4	1393.7	3.3467	Si IV	6.53 ± 0.14
	2374.5	2.6208	Fe II	
	1670.7	1.5481	Al II	
6070.9	2382.8	1.5481	Fe II	1.45 ± 0.14
6093.2	1402.7	3.3467	Si IV	1.85 ± 0.15
6470.1				0.8 ± 0.2
6256.1	1548.2	3.0383	C IV	3.57 ± 0.15
	1550.8	3.0383	C IV	
6591.0	2586.6	1.5481	Fe II	1.15 ± 0.15
6625.0	1526.7	3.3467	Si II	1.85 ± 0.15
	2600.2	1.5481	Fe II	
6729.8	1548.2	3.3467	C IV	13.99 ± 0.20
	1550.8	3.3467	C IV	
7124.9	2796.3	1.5481	Mg II	2.10 ± 0.17
7144.6	2803.5	1.5481	Mg II	2.08 ± 0.17
8489.0	2344.2	2.6208	Fe II	3.70 ± 0.40
8594.4	2374.5	2.6195	Fe II	4.60 ± 1.0
8625.7	2382.8	2.6208	Fe II	8.5 ± 1.0
8818.1	2026.1	3.3467	Zn II	5.0 ± 1.0
	2026.5	3.3467	Mg I	

Table 14
GRB 050922C ($z = 2.1995$)

λ_{obs} (Å)	λ_{rest} (Å)	z	Feature	EW$_{obs}$ (Å)
3630.0	1215.7	1.9904	Lyα	
3654.6	1215.7	2.0008	Lyα	
3740.0	1215.7	2.0768	Lyα	
3893.0	1215.7	2.1995	Lyα	
3975.5	1242.8	2.1995	NV	2.5 ± 0.2
4004.1	1302.2	2.0768	O I	0.8 ± 0.2
	1304.4	2.0768	Si II	
	1250.6	2.1995	S II	
4030.3	1260.4	2.1995	Si II	2.1 ± 0.2
4042.5	1264.7	2.196	Si II*	1.6 ± 0.2
4104.9	1334.5	2.0768	C II	1.0 ± 0.2
4179.6	1302.2	2.1995	O I	7.0 ± 0.3
	1304.4	2.1995	Si II	
	1393.7	1.9904	Si IV	
	1402.7	1.9904	Si IV	
4273.0	1334.5	2.1995	C II	4.6 ± 0.2
	1335.7	2.1995	C II*	
4458.6	1393.7	2.1995	Si IV	1.5 ± 0.1
4486.8	1402.7	2.1995	Si IV	1.4 ± 0.1
4578.8	1533.4	1.9904	Si II*	0.8 ± 0.1
4630.0	1548.2	1.9904	C IV	6.2 ± 0.2
4661.1	1550.8	1.9904	C IV	
4630.0	1548.2	2.0008	C IV	
4661.1	1550.8	2.0008	C IV	
4769.2	1548.2	2.0768	C IV	1.3 ± 0.1
	1550.8	2.0768	C IV	

Table 14
(Continued)

λ_{obs} (Å)	λ_{rest} (Å)	z	Feature	EW_{obs} (Å)
4699.0	1526.7	2.0768	Si II	0.5 ± 0.2
4882.7	1526.7	2.1995	Si II	2.0 ± 0.1
4908.7	1533.4	2.1995	Si II*	0.9 ± 0.1
4957.6	1548.2	2.1995	C IV	4.1 ± 0.1
	1550.8	2.1995	C IV	
5146.5	1608.4	2.1995	Fe II	0.6 ± 0.1
5346.9	1670.7	2.1995	Al II	2.7 ± 0.1
5896.5	2796.3	1.1083	Mg II	1.98 ± 0.17
5909.7	2803.5	1.1083	Mg II	

Table 15
GRB 060115 ($z = 3.5328$)

λ_{obs} (Å)	λ_{rest} (Å)	z	Feature	EW_{obs} (Å)
5507.0	1215.7	3.5328	Lyα	
5634.3	1242.8	3.5328	N V	4 ± 2
5713.1	1260.4	3.5328	Si II	8 ± 3
5735.2	1264.7	3.5328	Si II*	5 ± 2
5909.3	1302.2	3.5328	O I	11.5 ± 1.8
	1304.4	3.5328	Si II	
6030.0				2.8 ± 1.4
6051.0	1334.5	3.5328	C II	8.6 ± 1.8
6918.5	1526.7	3.5328	Si II	6.3 ± 1.6
7022.5	1548.8	3.5328	C IV	6.0 ± 1.6
	1550.2	3.5328	C IV	
7572.8	1670.8	3.5328	Al II	8.1 ± 1.5

Table 16
GRB 060124 ($z = 2.3000$)

λ_{obs} (Å)	λ_{rest} (Å)	z	Feature	EW_{obs} (Å)
LRIS/R300				
4011.7	1215.7	2.3000	Lyα	13.12 ± 2.44
4231.2				10.03 ± 1.70
4598.5	1393.8	2.3000	Si IV	4.73 ± 1.08
4846.6				5.73 ± 0.84
4862.6				2.43 ± 0.71
5108.8	1548.2	2.3000	C IV	9.68 ± 0.74
	1550.8	2.3000	C IV	
6873.6				2.56 ± 0.70

Table 17
GRB 060206 ($z = 4.0559$)

λ_{obs} (Å)	λ_{rest} (Å)	z	Feature	EW_{obs} (Å)
6147.9	1215.7	4.0559	Lyα	
6370.8	1260.4	4.0559	Si II	11.99 ± 0.09
6395.2	1264.7	4.0559	Si II*	
6421.5	2586.7	1.4822	Fe II	0.29 ± 0.09
6453.7	2600.2	1.4822	Fe II	0.68 ± 0.09
6589.0	1302.2	4.0559	O I	14.04 ± 0.09
	1304.4	4.0559	Si II	
6746.0	1334.5	4.0559	C II	11.45 ± 0.14

Table 18
GRB 060210 ($z = 3.9122$)

λ_{obs} (Å)	λ_{rest} (Å)	z	Feature	EW_{obs} (Å)
		GMOS/R400		
5963.5	2026.1	1.9253	Zn II	174.46 ± 1.59
	1215.7	3.9133	Lyα	
6088.3	1238.8	3.9133	N V	5.02 ± 0.53
	1239.9	3.9133	Mg II	
	1240.4	3.9133	Mg II	
6106.9	1242.8	3.9133	N V	4.93 ± 0.46
6154.4	1250.6	3.9133	S II	8.32 ± 0.49
	1253.8	3.9133	S II	
6196.5	1259.5	3.9133	S II	21.69 ± 0.42
	1260.4	3.9133	Si II	
	1260.5	3.9133	Fe II	
	1260.7	3.9133	C I	
6214.0	1264.7	3.9133	Si II*	7.30 ± 0.29
	1265.0	3.9133	Si II*	
6280.0	1302.2	3.8186	O I	3.52 ± 0.36
	1304.4	3.8186	Si II	
	1276.5	3.9133	C I	
	1277.2	3.9133	C I	
	1280.1	3.9133	C I	
6407.3	1301.9	3.9133	P II	23.82 ± 0.41
	1302.2	3.9133	O I	
	1304.4	3.9133	Si II	
	1304.9	3.9133	O I*	
	1306.0	3.9133	O I**	
6432.6	1334.5	3.8186	C II	2.85 ± 0.24
	1309.3	3.9133	Si II*	
6561.3	1328.8	3.9133	C I	21.23 ± 0.40
	1334.5	3.9133	C II	
	1335.7	3.9133	C II*	
6536.1				1.27 ± 0.21
6759.6				1.31 ± 0.17
6848.5	2344.2	1.9253	Fe II	14.99 ± 0.28
	1393.8	3.9133	Si IV	
6873.9				4.45 ± 0.19
6885.9	1400.4	3.9133	Sn II	2.91 ± 0.11
6892.8	1402.8	3.9133	Si IV	9.74 ± 0.14
6895.1				2.24 ± 0.16
6946.7	2374.5	1.9253	Fe II	1.58 ± 0.16
	1414.4	3.9133	Ga II	
6970.1	1419.0	3.9133	CO	0.88 ± 0.15
7400.2				0.96 ± 0.14
7460.3	1548.2	3.8186	C IV	3.51 ± 0.13
7471.8	1550.8	3.8186	C IV	2.35 ± 0.13
7505.2	1526.7	3.9133	Si II	18.04 ± 0.19
7534.4	1532.5	3.9133	P II	5.17 ± 0.14
	1533.4	3.9133	Si II*	
7566.1	2586.7	1.9253	Fe II	1.21 ± 0.13
7614.2	2600.2	1.9253	Fe II	42.36 ± 0.24
	1544.3	3.9133	CO	
	1548.2	3.9133	C IV	
	1550.8	3.9133	C IV	
7677.5	1560.3	3.9133	C I	3.83 ± 0.16
7909.2	1608.5	3.9133	Fe II	7.91 ± 0.22
	1611.2	3.9133	Fe II	
	1612.8	3.9133	Fe II*	
	1613.4	3.9133	C I	

Table 19
GRB 060502A ($z = 1.5025$)

λ_{obs} (Å)	λ_{rest} (Å)	z	Feature	EW$_{obs}$ (Å)
			GMOS/R400	
5688.2	2796.4	1.0323	Mg II	5.11 ± 0.47
	2803.5	1.0323	Mg II	
5727.5				3.53 ± 0.48
5860.6	2338.7	1.5026	Fe II*	1.31 ± 0.43
5897.1				1.96 ± 0.40
5936.4	2374.5	1.5026	Fe II	2.73 ± 0.30
5957.8	2381.5	1.5026	Fe II*	2.82 ± 0.26
5970.9	2382.8	1.5026	Fe II	6.01 ± 0.28
	2383.8	1.5026	Fe II*	
6013.0	2396.2	1.5026	Fe II*	12.57 ± 0.52
	2396.4	1.5026	Fe II*	
	2400.0	1.5026	Fe II*	
	2405.2	1.5026	Fe II*	
	2405.6	1.5026	Fe II*	
	2407.4	1.5026	Fe II*	
	2411.3	1.5026	Fe II*	
	2411.8	1.5026	Fe II*	
	2414.1	1.5026	Fe II*	
6090.6				1.13 ± 0.23
6445.6	2576.9	1.5026	Mn II	0.83 ± 0.21
6470.2	2586.7	1.5026	Fe II	2.08 ± 0.25
6504.7	2599.2	1.5026	Fe II*	3.91 ± 0.23
	2600.2	1.5026	Fe II	
6521.0	2606.5	1.5026	Mn II	0.77 ± 0.22
	2607.9	1.5026	Fe II*	
6535.6	2612.7	1.5026	Fe II*	1.10 ± 0.25
6839.2				2.38 ± 0.33
6884.7	2740.4	1.5026	Fe II*	7.74 ± 0.46
	2747.3	1.5026	Fe II*	
	2747.9	1.5026	Fe II*	
	2750.2	1.5026	Fe II*	
	2756.6	1.5026	Fe II*	
6998.0	2796.4	1.5026	Mg II	4.73 ± 0.18
7016.0	2803.5	1.5026	Mg II	4.26 ± 0.21
7033.5				3.34 ± 0.24
7139.9	2853.0	1.5026	Mg I	2.26 ± 0.20
7208.9				1.08 ± 0.30

Table 20
GRB 060512 ($z = 2.1$)

λ_{obs} (Å)	λ_{rest} (Å)	z	Feature	EW$_{obs}$ (Å)
3750	1215.7	2.1	Lyα	

Table 21
GRB 060526 ($z = 3.2213$)

λ_{obs} (Å)	λ_{rest} (Å)	z	Feature	EW$_{obs}$ (Å)
5131.0	1215.7	3.2213	Lyα	
5248.0	1242.8	3.2213	N V	1.1 ± 0.3
5319.8	1260.4	3.2213	Si II	6.0 ± 0.3
5500.7	1302.2	3.2213	O I	7.5 ± 0.4
	1304.4	3.2213	Si II	
5633.4	1334.4	3.2213	C II	7.5 ± 0.4
6443.9	1526.7	3.2213	Si II	3.3 ± 0.4
6539.0	1548.2	3.2213	C IV	1.9 ± 0.4
	1550.8	3.2213	C IV	
6788.7	1608.4	3.2213	Fe II	1.9 ± 0.4
7053.2	1670.7	3.2213	Al II	3.6 ± 0.4

Table 22
GRB 060604

λ_{obs} (Å)	λ_{rest} (Å)	z	Feature	EW$_{obs}$ (Å)
5217.0				13 ± 4

Table 23
GRB 060607A ($z = 3.0749$)

λ_{obs} (Å)	λ_{rest} (Å)	z	Feature	EW$_{obs}$ (Å)
6308.8	1548.2	3.0746	C IV	1.13 ± 0.05
6319.4	1550.8	3.0746	C IV	0.83 ± 0.05

Table 24
GRB 060707 ($z = 3.4240$)

λ_{obs} (Å)	λ_{rest} (Å)	z	Feature	EW$_{obs}$ (Å)
5342.6	1215.7	3.4240	Lyα	
5538.8	1250.6	3.4240	S II	6.7 ± 1.3
5724.4				4.5 ± 1.2
5760.8	1302.2	3.4240	O I	9.2 ± 1.1
5768.8	1304.4	3.4240	Si II	6.0 ± 2.0
5902.1	1334.5	3.4240	C II	10.4 ± 1.3
5909.0	1335.7	3.4240	C II*	
6755.7	1526.7	3.4240	Si II	10.2 ± 1.4
6851.6	1548.2	3.4240	C IV	5.7 ± 1.2
6858.3	1550.8	3.4240	C IV	
7391.4	1670.8	3.4240	Al II	9.4 ± 1.6
8002.1	1808.0	3.4240	Si II	3.8 ± 1.9

Table 25
GRB 060714 ($z = 2.7108$)

λ_{obs} (Å)	λ_{rest} (Å)	z	Feature	EW$_{obs}$ (Å)
4503.8	1215.7	2.7108	Lyα	
4640.2	1250.6	2.7108	S II	3.3 ± 0.7
4651.6	1253.8	2.7108	S II	3.5 ± 0.6
4676.5	1260.4	2.7108	Si II	7.2 ± 0.6
4693.8	1264.7	2.7108	Si II*	3.7 ± 0.6
4837.3	1302.2	2.7108	O I	12.7 ± 0.6
	1304.4	2.7108	Si II	
4859.7	1309.3	2.7108	Si II*	1.0 ± 0.4
4954.3	1335.3	2.7108	C II	10.5 ± 0.5
5171.4	1393.8	2.7108	Si IV	5.8 ± 0.4
5205.1	1402.8	2.7108	Si IV	5.0 ± 0.4
5665.5	1526.7	2.7108	Si II	6.8 ± 0.5
5691.1	1533.4	2.7108	Si II*	2.2 ± 0.4
5749.1	1549.1	2.7108	C IV	13.1 ± 0.4
5969.9	1608.4	2.7108	Fe II	5.0 ± 0.5
6200.3	1670.8	2.7108	Al II	7.6 ± 0.5
6345.1	1709.6	2.7108	Ni II	0.7 ± 0.3
6462.8	1741.6	2.7108	Ni II	1.0 ± 0.3
6709.0	1808.0	2.7108	Si II	2.2 ± 0.4
6880.9	1854.7	2.7108	Al III	9.1 ± 0.5
6912.0	1862.8	2.7108	Al III	4.3 ± 0.5
7516.9	2026.1	2.7108	Zn II	1.8 ± 0.6
	2026.5	2.7108	Mg I	
7652.9	2062.7	2.7108	Zn II	In telluric band
8227.8				3.1 ± 0.7
8700.2	2344.2	2.7108	Fe II	8.0 ± 1.1
8812.1	2374.5	2.7108	Fe II	6.8 ± 1.0
8843.4	2382.8	2.7108	Fe II	9.6 ± 1.0

Table 26
GRB 060729 ($z = 0.5428$)

λ_{obs} (Å)	λ_{rest} (Å)	z	Feature	EW$_{obs}$ (Å)
4010.7	2600.2	0.5428	Fe II	0.7 ± 0.2
4314.7	2796.3	0.5428	Mg II	2.80 ± 0.06
4325.5	2803.5	0.5428	Mg II	
4402.1	2853.0	0.5428	Mg I	0.91 ± 0.06
6070.1	3934.8	0.5428	Ca II (K)	1.16 ± 0.04
6123.7	3969.6	0.5428	Ca II (H)	0.85 ± 0.04

Table 27
GRB 060807

λ_{obs} (Å)	λ_{rest} (Å)	z	Feature	EW$_{obs}$ (Å)
5200.0				0.6 ± 0.3

Table 28
GRB 060904B ($z = 0.7029$)

λ_{obs} (Å)	λ_{rest} (Å)	z	Feature	EW$_{obs}$ (Å)
4383.5	2576.9	0.7029	Mn II	0.6 ± 0.3
4404.0	2586.7	0.7029	Fe II	1.6 ± 0.3
4427.3	2600.2	0.7029	Fe II	3.1 ± 0.3
4763.7	2796.3	0.7029	Mg II	7.9 ± 0.2
4772.6	2803.5	0.7029	Mg II	
4858.4	2853.0	0.7029	Mg I	1.7 ± 0.2
6352.6	3727.7	0.7029	[O II]	Emission
6701.7	3934.8	0.7029	Ca II (K)	2.3 ± 0.2
6760.6	3969.6	0.7029	Ca II (H)	1.8 ± 0.2
8531.7	5008.2	0.7029	[O III]	Emission

Table 29
GRB 060906 ($z = 3.6856$)

λ_{obs} (Å)	λ_{rest} (Å)	z	Feature	EW$_{obs}$ (Å)
5689.8	1215.7	3.6856	Lyα	
5904.0	1260.4	3.6856	Si II	4.0 ± 1.0
6108.2	1302.2	3.6856	O I	5.5 ± 1.1
	1304.4	3.6856	Si II	
6254.6	1334.5	3.6856	C II	6.1 ± 0.9
6335.9	2796.3	1.2659	Mg II	3.7 ± 0.7
6352.5	2803.5	1.2659	Mg II	
6529.2	1393.8	3.6856	Si IV	3.2 ± 0.8
7153.6	1526.7	3.6856	Si II	2.2 ± 0.9
7258.1	1548.2	3.6856	C IV	3.4 ± 0.9
	1550.8	3.6856	C IV	

Table 30
GRB 060908 ($z = 1.8836$)

λ_{obs} (Å)	λ_{rest} (Å)	z	Feature	EW$_{obs}$ (Å)
4464.8	1548.2	1.8836	C IV	9.3 ± 1.5
4471.5	1550.8	1.8836	C IV	

Table 31
GRB 060926 ($z = 3.2086$)

λ_{obs} (Å)	λ_{rest} (Å)	z	Feature	EW$_{obs}$ (Å)
5116.2	1215.7	3.2086	Lyα	
5382.1	2796.3	0.9242	Mg II	4.8 ± 1.8
5393.1	2803.5	0.9242	Mg II	
5614.3	1334.5	3.2086	C II	5.5 ± 1.4
5625.1	1335.7	3.2086	C II*	
5863.7	1393.8	3.2086	Si IV	3.9 ± 1.4
6426.2	1526.7	3.2086	Si II	4.0 ± 1.1
6517.7	1548.2	3.2086	C IV	8.0 ± 1.2
	1550.8	3.2086	C IV	
6637.5	2374.5	1.7954	Fe II	4.8 ± 1.0
6660.6	2382.8	1.7954	Fe II	4.7 ± 1.4
7232.3	2586.7	1.7954	Fe II	7.3 ± 1.5
7267.9	2600.2	1.7954	Fe II	4.6 ± 1.5
7816.2	2796.3	1.7954	Mg II	7.5 ± 2.0
7837.1	2803.5	1.7954	Mg II	7.8 ± 2.0

Table 32
GRB 060927 ($z = 5.4636$)

λ_{obs} (Å)	λ_{rest} (Å)	z	Feature	EW$_{obs}$ (Å)
7865.	1215.7	5.4636	Lyα	
8146.7	1260.4	5.4636	Si II	9.0 ± 4.0

Table 33
GRB 061007 ($z = 1.2622$)

λ_{obs} (Å)	λ_{rest} (Å)	z	Feature	EW$_{obs}$ (Å)
5302.8	2344.2	1.2622	Fe II	6.4 ± 1.7
5370.4	2374.5	1.2622	Fe II	8.0 ± 2.0
5389.5	2382.8	1.2622	Fe II	5.1 ± 1.5
5777.2	2796.3	1.0660	Mg II	13.9 ± 1.8
5788.2	2803.5	1.0660	Mg II	
5827.7	2576.9	1.2622	Mn II	2.8 ± 1.3
5852.0	2586.7	1.2622	Fe II	7.3 ± 1.3
5884.5	2600.2	1.2622	Fe II	5.9 ± 1.4
6324.5	2796.3	1.2622	Mg II	5.8 ± 1.1
6341.9	2803.5	1.2622	Mg II	6.4 ± 1.1
8134.3	3934.8	1.0660	Ca II	3.5 ± 1.1
8429.3	3726.0	1.2622	[O II]	Emission
8440.3	3728.8	1.2622	[O II]	Emission

Table 34
GRB 061021 ($z = 0.3463$)

λ_{obs} (Å)	λ_{rest} (Å)	z	Feature	EW$_{obs}$ (Å)
3767.9	2796.4	0.3463	Mg II	2.5 ± 0.7
	2803.5	0.3463	Mg II	

Table 35
GRB 061110A ($z = 0.7578$)

λ_{obs} (Å)	λ_{rest} (Å)	z	Feature	EW$_{obs}$ (Å)
4914.	2796.3	0.7578	Mg II	6.4 ± 1.4
	2803.5	0.7578	Mg II	
6551.8	3727.7	0.7578	Hβ	Emission
8719.7	4960.3	0.7578	[O III]	Emission
8803.3	5008.2	0.7578	[O III]	Emission

Table 36
GRB 061110B ($z = 3.4344$)

λ_{obs} (Å)	λ_{rest} (Å)	z	Feature	EW_{obs} (Å)
5350.7	1215.7	3.4344	Lyα	
5774.2	1302.2	3.4344	O I	4.7 ± 1.0
5785.8	1304.4	3.4344	Si II	6.9 ± 1.1
5919.3	1334.5	3.4344	C II	6.7 ± 1.4
	1335.7	3.4344	C II*	
6182.1	1393.8	3.4344	Si IV	6.6 ± 1.2
6221.4	1402.8	3.4344	Si IV	5.9 ± 1.3
6767.8	1526.7	3.4344	Si II	3.2 ± 0.8
6802.2	1533.4	3.4344	Si II*	3.5 ± 0.9
6862.5	1548.2	3.4344	C IV	9.6 ± 1.5
6875.3	1550.8	3.4344	C IV	
7409.6	1670.8	3.4344	Al II	4.1 ± 1.3

Table 37
GRB 061121 ($z = 1.3145$)

λ_{obs} (Å)	λ_{rest} (Å)	z	Feature	EW_{obs} (Å)
			LRISb/B600	
3534.1	1526.7	1.3145	Si II	4.74 ± 0.13
3549.0	1532.5	1.3145	P II	1.75 ± 0.13
	1533.4	1.3145	Si II*	
3587.2	1548.2	1.3145	C IV	10.20 ± 0.14
	1550.8	1.3145	C IV	
3609.2	1560.3	1.3145	C I	1.14 ± 0.10
3722.7	1608.5	1.3145	Fe II	4.26 ± 0.08
3732.4	1611.2	1.3145	Fe II	1.16 ± 0.09
	1612.8	1.3145	Fe II*	
	1613.4	1.3145	C I	
3745.8	1618.5	1.3145	Fe II*	0.33 ± 0.07
3753.0	1621.7	1.3145	Fe II*	0.61 ± 0.07
3762.3				0.31 ± 0.07
3770.7	1629.2	1.3145	Fe II*	0.49 ± 0.07
3785.3	1637.4	1.3145	Fe II*	1.38 ± 0.11
	1634.4	1.3145	Fe II*	
	1636.3	1.3145	Fe II*	
3817.6				0.20 ± 0.07
3836.6	1656.9	1.3145	C I	0.57 ± 0.09
3867.7	1670.8	1.3145	Al II	5.42 ± 0.08
3939.0	1702.0	1.3145	Fe II*	0.49 ± 0.05
3957.3	1709.6	1.3145	Ni II	0.77 ± 0.07
4031.7	1741.6	1.3145	Ni II	1.22 ± 0.08
4044.8	1747.8	1.3145	Mg I	0.23 ± 0.06
4056.3	1751.9	1.3145	Ni II	0.71 ± 0.08
4185.4	1807.3	1.3145	S I	2.82 ± 0.07
	1808.0	1.3145	Si II	
4205.6	1816.9	1.3145	Si II*	0.38 ± 0.06
	1817.5	1.3145	Si II*	
4231.1	1827.9	1.3145	Mg I	0.49 ± 0.05
4293.4	1854.7	1.3145	Al III	4.68 ± 0.06
4312.1	1862.8	1.3145	Al III	3.75 ± 0.06
4690.0	2026.1	1.3145	Zn II	2.43 ± 0.06
	2026.3	1.3145	Cr II	
	2026.5	1.3145	Mg I	
4759.7	2056.3	1.3145	Cr II	1.70 ± 0.06
4774.0	2062.2	1.3145	Cr II	2.31 ± 0.06
	2062.7	1.3145	Zn II	
4782.2	2066.2	1.3145	Cr II	1.09 ± 0.06
5013.1	2166.2	1.3145	Ni II*	0.68 ± 0.05
5020.8	2169.8	1.3145	Ni II*	0.24 ± 0.05
5034.3	2175.4	1.3145	Ni II*	0.31 ± 0.06

Table 37
(Continued)

λ_{obs} (Å)	λ_{rest} (Å)	z	Feature	EW_{obs} (Å)
5131.1	2217.2	1.3145	Ni II*	1.32 ± 0.05
5146.0	2223.6	1.3145	Ni II*	0.53 ± 0.05
5152.8				0.32 ± 0.05
5207.7	2249.9	1.3145	Fe II	1.44 ± 0.06
5215.7				0.64 ± 0.06
5233.1	2260.8	1.3145	Fe II	1.76 ± 0.06
5277.3				0.38 ± 0.05
5331.5				0.20 ± 0.05
5361.8	2316.8	1.3145	Ni II*	0.93 ± 0.05
5387.8	2328.1	1.3145	Fe II*	0.92 ± 0.06
5400.1	2333.5	1.3145	Fe II*	2.11 ± 0.07
5412.7	2338.7	1.3145	Fe II*	1.16 ± 0.06
5426.7	2344.2	1.3145	Fe II	6.53 ± 0.06
	2345.0	1.3145	Fe II*	
5436.5	2349.0	1.3145	Fe II*	1.80 ± 0.05
5452.6				0.20 ± 0.05
5463.3	2359.8	1.3145	Fe II*	2.09 ± 0.06
5475.1	2365.6	1.3145	Fe II*	1.34 ± 0.06
5483.7				0.51 ± 0.05
5497.3	2374.5	1.3145	Fe II	6.01 ± 0.07
5515.9	2381.5	1.3145	Fe II*	8.53 ± 0.07
	2382.8	1.3145	Fe II	
	2383.8	1.3145	Fe II*	
5530.5	2389.4	1.3145	Fe II*	1.62 ± 0.06
5546.8	2396.2	1.3145	Fe II*	2.86 ± 0.06
	2396.4	1.3145	Fe II*	
5555.1	2400.0	1.3145	Fe II*	1.69 ± 0.06
5568.2	2405.3	1.3145	Fe II*	2.45 ± 0.06
	2405.6	1.3145	Fe II*	
5572.4	2407.4	1.3145	Fe II*	1.46 ± 0.05
5582.0	2411.3	1.3145	Fe II*	2.34 ± 0.08
	2411.8	1.3145	Fe II*	
5587.8	2414.1	1.3145	Fe II*	1.30 ± 0.06
5608.5				0.26 ± 0.06
			LRISr/R400	
5570.8	2405.2	1.3145	Fe II*	2.41 ± 0.21
	2405.6	1.3145	Fe II*	
	2407.4	1.3145	Fe II*	
5583.1	2411.3	1.3145	Fe II*	2.71 ± 0.21
	2411.8	1.3145	Fe II*	
	2414.1	1.3145	Fe II*	
5935.1				1.47 ± 0.09
5966.8	2576.9	1.3145	Mn II	3.08 ± 0.09
5989.2	2586.7	1.3145	Fe II	7.34 ± 0.09
6006.8	2594.5	1.3145	Mn II	3.01 ± 0.08
6020.0	2599.2	1.3145	Fe II*	8.80 ± 0.07
	2600.2	1.3145	Fe II	
6035.8	2606.6	1.3145	Mn II	3.49 ± 0.08
	2607.9	1.3145	Fe II*	
6049.4	2612.7	1.3145	Fe II*	3.61 ± 0.07
	2614.6	1.3145	Fe II*	
6061.4	2618.4	1.3145	Fe II*	1.13 ± 0.08
	2621.2	1.3145	Fe II*	
	2622.5	1.3145	Fe II*	
6083.6	2621.2	1.3145	Fe II*	5.16 ± 0.13
	2622.5	1.3145	Fe II*	
	2626.5	1.3145	Fe II*	
	2629.1	1.3145	Fe II*	
	2631.8	1.3145	Fe II*	
	2632.1	1.3145	Fe II*	

Table 37
(Continued)

λ_{obs} (Å)	λ_{rest} (Å)	z	Feature	EW_{obs} (Å)
6284.7				0.88 ± 0.09
6315.2				0.84 ± 0.09
6343.0	2740.4	1.3145	Fe II*	1.55 ± 0.08
6361.6	2747.3	1.3145	Fe II*	4.45 ± 0.10
	2747.9	1.3145	Fe II*	
	2750.2	1.3145	Fe II*	
6380.3	2756.6	1.3145	Fe II*	1.49 ± 0.09
6473.6	2796.4	1.3145	Mg II	10.25 ± 0.09
6490.3	2803.5	1.3145	Mg II	9.71 ± 0.07
6603.9	2853.0	1.3145	Mg I	5.70 ± 0.09
6873.2	2967.8	1.3145	Fe I	2.33 ± 0.10
6897.3				1.10 ± 0.11
7839.8	3384.7	1.3145	Ti II	1.52 ± 0.15
8231.0				1.84 ± 0.11
9106.0	3934.8	1.3145	Ca II	4.07 ± 0.19
9186.8	3969.6	1.3145	Ca II	3.30 ± 0.16

Table 38
GRB 070110 ($z = 2.3521$)

λ_{obs} (Å)	λ_{rest} (Å)	z	Feature	EW_{obs} (Å)
4067.7	1215.7	2.3521	Lyα	
4224.2	1260.4	2.3521	Si II	4.5 ± 0.4
4240.7	1264.7	2.3521	Si II*	2.4 ± 0.4
4368.6	1302.2	2.3521	O I	7.1 ± 0.4
	1304.4	2.3521	Si II	
4425.1	1548.2	1.856	C IV	8.2 ± 0.4
	1550.8	1.856	C IV	
4474.1	1334.5	2.3521	C II	3.8 ± 0.3
	1335.7	2.3521	C II*	
4672.1	1393.8	2.3521	Si IV	1.4 ± 0.3
4702.8	1402.8	2.3521	Si IV	1.4 ± 0.3
4773.7	1670.8	1.856	Al II	1.1 ± 0.3
5116.3	1526.7	2.3521	Si II	3.5 ± 0.3
5141.7	1533.4	2.3521	Si II*	1.2 ± 0.3
5193.5	1548.2	2.3521	C IV	3.1 ± 0.3
	1550.8	2.3521	C IV	
5391.1	1608.4	2.3521	Fe II	2.5 ± 0.3
5600.4	1670.8	2.3521	Al II	3.0 ± 0.3
5730.3	1709.6	2.3521	Ni II	1.2 ± 0.3
5838.9	1741.6	2.3521	Ni II	0.9 ± 0.3
6059.4	1808.0	2.3521	Si II	1.4 ± 0.3
6215.6	1854.7	2.3521	Al III	1.1 ± 0.3
6246.4	1862.8	2.3521	Al III	1.0 ± 0.3
6790.1	2026.1	2.3521	Zn II	2.0 ± 0.4
	2026.5	2.3521	Mg I	
7860.9	2344.2	2.3521	Fe II	2.9 ± 0.8
7959.6	2374.5	2.3521	Fe II	3.3 ± 0.6
7985.9	2382.8	2.3521	Fe II	7.1 ± 0.8
8670.6	2586.7	2.3521	Fe II	1.9 ± 0.9
8714.4	2600.2	2.3521	Fe II	6.8 ± 0.6

Table 39
GRB 070125 ($z = 1.5471$)

λ_{obs} (Å)	λ_{rest} (Å)	z	Feature	EW_{obs} (Å)
3950.3	1548.2	1.5471	C IV	1.7 ± 0.3
	1550.8	1.5471	C IV	
7122.4	2796.3	1.5471	Mg II	0.5 ± 0.1
7140.8	2803.5	1.5471	Mg II	0.4 ± 0.1

Table 40
GRB 070306 ($z = 1.4965$)

λ_{obs} (Å)	λ_{rest} (Å)	z	Feature	EW_{obs} (Å)
9306.3	3727.7	1.4965	[O II]	Emission

Table 41
GRB 070318 ($z = 0.8397$)

λ_{obs} (Å)	λ_{rest} (Å)	z	Feature	EW_{obs} (Å)
4313.1	2344.2	0.8397	Fe II	1.4 ± 0.3
4365.2	2374.5	0.8397	Fe II	0.8 ± 0.2
4381.7	2382.8	0.8397	Fe II	2.2 ± 0.3
4743.5	2576.9	0.8397	Mn II	6.7 ± 0.4
4758.1	2586.7	0.8397	Fe II	
4772.6	2594.5	0.8397	Mn II	
4783.6	2600.2	0.8397	Fe II	
4795.0	2606.5	0.8397	Mn II	
5145.4	2796.4	0.8397	Mg II	4.8 ± 0.3
5157.9	2803.5	0.8397	Mg II	
5247.8	2853.0	0.8397	Mg I	1.2 ± 0.2
6228.2	3384.7	0.8397	Ti II	1.0 ± 0.3
7238.4	3934.8	0.8397	Ca II	3.8 ± 0.4
7305.5	3969.6	0.8397	Ca II	1.8 ± 0.4

Table 42
GRB 070411 ($z = 2.9538$)

λ_{obs} (Å)	λ_{rest} (Å)	z	Feature	EW_{obs} (Å)
4806.5	1215.7	2.9538	Lyα	
4983.9	1260.4	2.9538	Si II	1.1 ± 0.3
5156.9	1302.2	2.9538	O I	1.3 ± 0.3
	1304.4	2.9538	Si II	
5276.6	1334.5	2.9538	C II	2.1 ± 0.3
5280.6	1335.7	2.9538	C II*	0.7 ± 0.2
5509.3	1393.8	2.9538	Si IV	3.1 ± 0.4
5545.9	1402.8	2.9538	Si IV	2.6 ± 0.4
6033.8	1526.7	2.9538	Si II	1.7 ± 0.4
6120.5	1548.2	2.9538	C IV	10.1 ± 0.5
6131.8	1550.8	2.9538	C IV	
6358.8	1608.4	2.9538	Fe II	0.9 ± 0.3
6606.3	1670.8	2.9538	Al II	1.8 ± 0.3

Table 43
GRB 070419A ($z = 0.9705$)

λ_{obs} (Å)	λ_{rest} (Å)	z	Feature	EW_{obs} (Å)
		GMOS/R831		
7753.8	3934.8	0.9705	Ca II	2.46 ± 0.31
7822.2	3969.6	0.9705	Ca II	1.21 ± 0.29
8332.3	4227.9	0.9705	Ca I	0.84 ± 0.18

Table 44
GRB 070506 ($z = 2.3090$)

λ_{obs} (Å)	λ_{rest} (Å)	z	Feature	EW_{obs} (Å)
4017.1	1215.7	2.3090	Lyα	
4166.8	1260.4	2.3090	Si II	9.0 ± 2.0
4314.5	1302.2	2.3090	O I	8.5 ± 2.0
	1304.4	2.3090	Si II	

Table 44
(Continued)

λ_{obs} (Å)	λ_{rest} (Å)	z	Feature	EW_{obs} (Å)
4641.3	1402.7	2.3090	Si IV	4.4 ± 1.5
4758.7	1548.2	2.0709	C IV	7.5 ± 1.4
	1550.8	2.0709	C IV	
5049.5	1526.7	2.3090	Si II	6.7 ± 0.9
5085.2				6.4 ± 0.9
5122.	1548.2	2.3090	C IV	6.4 ± 1.0
	1550.8	2.3090	C IV	
5324.7	1608.4	2.3090	Fe II	4.4 ± 0.7
5528.4	1670.7	2.3090	Al II	4.7 ± 0.6
5694.2	1854.7	2.0709	Al III	3.1 ± 0.5
5721.4	1862.7	2.0709	Al III	3.1 ± 0.5
6140.1	1854.7	2.3090	Al III	2.6 ± 0.5
6706.8	2026.1	2.3090	Zn II	2.8 ± 0.5
	2026.5	2.3090	Mg I	
6824.8	2062.2	2.3090	Cr II	2.9 ± 0.5
	2062.6	2.3090	Zn II	

Table 45
GRB 070611 ($z = 2.0394$)

λ_{obs} (Å)	λ_{rest} (Å)	z	Feature	EW_{obs} (Å)
3694.8	1215.7	2.0394	Lyα	
4359.4	2796.3	0.5588	Mg II	2.5 ± 1.0
4369.8	2803.5	0.5588	Mg II	2.5 ± 1.0
4708.8	1548.2	2.0394	C IV	2.9 ± 1.0
	1550.8	2.0394	C IV	
5472.6	2382.8	1.2973	Fe II	2.2 ± 0.7
6425.4	2796.3	1.2973	Mg II	3.9 ± 0.7
6440.4	2803.5	1.2973	Mg II	3.2 ± 0.7
8497.0	2796.3	2.0394	Mg II	2.8 ± 1.2
8523.2	2803.5	2.0394	Mg II	3.6 ± 0.9

Table 46
GRB 070721B ($z = 3.6298$)

λ_{obs} (Å)	λ_{rest} (Å)	z	Feature	EW_{obs} (Å)
4970.0	1215.7	3.0939	Lyα	
5590.0	1215.7	3.6298	Lyα	
6028.1	1302.2	3.6298	O I	6.5 ± 1.9
	1304.4	3.6298	Si II	
6179.8	1334.5	3.6298	C II	5.0 ± 2.0
6248.7	1526.7	3.0939	Si II	7.0 ± 2.2
6337.3	1548.2	3.0939	C IV	19.0 ± 3.0
6349.9	1550.8	3.0939	C IV	
6450.2	1393.8	3.6298	Si IV	6.0 ± 1.9
6492.7	1402.8	3.6298	Si IV	7.0 ± 2.2
6584.2	1608.5	3.0939	Fe II	9.0 ± 1.9
6842.2	1670.8	3.0939	Al II	7.6 ± 2.0
7066.2	1526.7	3.6298	Si II	5.8 ± 1.9
7104.6	1533.4	3.6298	Si II*	5.9 ± 1.8
7167.5	1548.2	3.6298	C IV	14.6 ± 2.6
7180.8	1550.8	3.6298	C IV	

Table 47
GRB 070802 ($z = 2.4511$)

λ_{obs} (Å)	λ_{rest} (Å)	z	Feature	EW_{obs} (Å)
4200.0	1215.7	2.4541	Lyα	
4607.9	1334.5	2.4541	C II	16 ± 6
5141.4	1670.7	2.0785	Al II	6.0 ± 1.7
5273.9	1526.7	2.4541	Si II	10 ± 2

Table 47
(Continued)

λ_{obs} (Å)	λ_{rest} (Å)	z	Feature	EW_{obs} (Å)
5350.9	1548.2	2.4541	C IV	7.3 ± 1.8
	1550.8	2.4541	C IV	
5390.7	1560.3	2.4541	C I	2.4 ± 1.2
5556.4	1608.4	2.4541	Fe II	10.5 ± 1.6
5724.5	1656.9	2.4541	C I	4.7 ± 1.1
5771.2	1670.7	2.4541	Al II	14.3 ± 1.2
6246.5	1808.8	2.4541	Si II	3.9 ± 1.0
6404.9	1854.7	2.4541	Al III	2.4 ± 1.0
7000.1	2026.1	2.4541	Zn II	4.2 ± 1.0
	2026.5	2.4541	Mg I	
7104.1	2056.3	2.4541	Cr II	2.0 ± 0.9
7124.8	2062.2	2.4541	Cr II	2.53 ± 0.9
7126.3	2062.7	2.4541	Zn II	
7218.7	2344.2	2.0785	Fe II	3.4 ± 1.0
7311.4	2374.5	2.0785	Fe II	4.5 ± 1.0
7335.7	2382.8	2.0785	Fe II	4.9 ± 1.0
7810.7	2260.8	2.4541	Fe II	6.6 ± 1.0
8005.9	2600.2	2.0785	Fe II	4.7 ± 1.1
8094.1	2344.2	2.4541	Fe II	16.5 ± 2.0
8200.5	2374.5	2.4541	Fe II	12.7 ± 1.5
8228.0	2382.8	2.4541	Fe II	18.8 ± 1.5
8277.1	2396.4	2.4541	Fe II*	2.9 ± 1.4
8308.7	2405.6	2.4541	Fe II**	2.8 ± 1.4
8515.5	2586.7	2.2921	Fe II	2.3 ± 0.6
8560.6	2600.2	2.2921	Fe II	2.2 ± 0.6
8607.0	2796.3	2.0785	Mg II	11.3 ± 0.6
8631.0	2803.5	2.0785	Mg II	11.5 ± 0.6
8780.1	2853.0	2.0785	Mg I	2.7 ± 1.1
8902.8	2576.9	2.4541	Mn II	5.0 ± 1.2
8934.4	2586.7	2.4541	Fe II	19.5 ± 1.3
8979.5	2600.2	2.4541	Fe II	29.0 ± 1.3
9208.6	2796.3	2.2921	Mg II	1.8 ± 0.6
9226.5	2803.5	2.2921	Mg II	1.4 ± 0.6

Table 48
GRB 071020 ($z = 2.1462$)

λ_{obs} (Å)	λ_{rest} (Å)	z	Feature	EW_{obs} (Å)
5254.7	1670.8	2.1462	Al II	6 ± 2
7376.8	2344.2	2.1462	Fe II	5 ± 2
7498.3	2382.8	2.1462	Fe II	6 ± 2
8136.8	2586.7	2.1462	Fe II	7 ± 2
8181.6	2600.2	2.1462	Fe II	11 ± 2
8274.5				6 ± 2
8797.7	2796.3	2.1462	Mg II	14 ± 2
8820.9	2803.5	2.1462	Mg II	10 ± 2

Table 49
GRB 071031 ($z = 2.6918$)

λ_{obs} (Å)	λ_{rest} (Å)	z	Feature	EW_{obs} (Å)
4483.0	1215.7	2.6918	Lyα	
4652.0	1260.4	2.6918	Si II	2.65 ± 0.15
4670.0	1264.7	2.6918	Si II*	2.00 ± 0.15
4815.2	1302.2	2.6918	O I	4.91 ± 0.11
	1304.4	2.6918	Si II	
4833.5	1309.3	2.6918	Si II*	1.45 ± 0.13
4862.9	1317.2	2.6918	Ni II	0.46 ± 0.15
4900.1	1854.7	1.6421	Al III	0.56 ± 0.12

Table 49
(Continued)

λ_{obs} (Å)	λ_{rest} (Å)	z	Feature	EW_{obs} (Å)
4928.5	1334.5	2.6918	C II	4.45 ± 0.13
	1335.7	2.6918	C II*	
5056.8	1370.1	2.6918	Ni II	0.62 ± 0.14
5145.1	1393.8	2.6918	Si IV	3.70 ± 0.15
5178.9	1402.8	2.6918	Si IV	2.76 ± 0.15
5224.5	1549.1	2.3726	C IV	1.40 ± 0.14
5636.1	1526.7	2.6918	Si II	1.99 ± 0.11
5661.1	1533.4	2.6918	Si II*	1.75 ± 0.11
5717.1	1549.1	2.6918	C IV	8.05 ± 0.16
5755.5	1559	2.6918	Fe II*****	1.22 ± 0.12
5938.2	1608.4	2.6918	Fe II	3.25 ± 0.16
5976.9	1618.5	2.6918	Fe II*	0.93 ± 0.12
5987.0	1621.7	2.6918	Fe II*	
6015.9	1629.2	2.6918	Fe II**	0.94 ± 0.12
6041.9	1636.3	2.6918	Fe II***	1.37 ± 0.12
6168.3	1670.8	2.6918	Al II	2.33 ± 0.11
6429.7	1741.6	2.6918	Ni II	0.59 ± 0.12
6466.7	1751.9	2.6918	Ni II	0.42 ± 0.12
6674.6	1808.0	2.6918	Si II	0.94 ± 0.10
6848.3	1854.7	2.6918	Al III	0.96 ± 0.12
7032.1	2382.8	1.9514	Fe II	1.48 ± 0.12
7388.5	2796.3	1.6421	Mg II	1.83 ± 0.13
7407.3	2803.5	1.6421	Mg II	1.42 ± 0.15
7479.6	2026.1	2.6918	Zn II	0.31 ± 0.15
	2026.5	2.6918	Mg I	
7673.6	2600.2	1.9514	Fe II	0.40 ± 0.20
7996.0	2166.2	2.6918	Ni II**	1.50 ± 0.20
8252.9	2796.3	1.9514	Mg II	2.40 ± 0.19
8275.0	2803.5	1.9514	Mg II	1.47 ± 0.19
8553.0	2316.7	2.6918	Ni II**	0.90 ± 0.20
8594.7	2328.1	2.6918	Fe II**	0.90 ± 0.20
8614.1	2333.5	2.6918	Fe II*	2.70 ± 0.18
8635.7	2338.7	2.6918	Fe II***	0.73 ± 0.22
8655.8	2344.2	2.6918	Fe II	4.30 ± 0.25
8672.1	2349.0	2.6918	Fe II**	2.60 ± 0.25
8714.7	2359.8	2.6918	Fe II***	2.30 ± 0.17
8733.5	2365.6	2.6918	Fe II*	1.68 ± 0.17
8766.4	2374.5	2.6918	Fe II	2.43 ± 0.35
8797.0	2382.8	2.6918	Fe II	4.47 ± 0.20
8821.5	2389.4	2.6918	Fe II*	1.35 ± 0.35
8846.5	2396.4	2.6918	Fe II*	1.77 ± 0.35
8860.2	2400.0	2.6918	Fe II**	1.79 ± 0.35
8883.5	2405.6	2.6918	Fe II**	3.96 ± 0.35
8902.2	2411.3	2.6918	Fe II***	3.30 ± 0.35
9549.1	2586.7	2.6918	Fe II	3.43 ± 0.60
9596.5	2600.2	2.6918	Fe II	5.17 ± 0.32

Table 50
GRB 071112C ($z = 0.8227$)

λ_{obs} (Å)	λ_{rest} (Å)	z	Feature	EW_{obs} (Å)
4273.4	2344.2	0.8227	Fe II	2.0 ± 0.5
4328.7	2374.5	0.8227	Fe II	1.0 ± 0.5
4345.0	2382.8	0.8227	Fe II	1.6 ± 0.5
4715.9	2586.7	0.8227	Fe II	2.0 ± 0.5
4741.0	2600.2	0.8227	Fe II	2.4 ± 0.5
5096.4	2796.3	0.8227	Mg II	4.9 ± 0.6
5110.1	2803.5	0.8227	Mg II	
6795.8	3727.7	0.8227	[O II]	Emission
7051.2	3869.8	0.8227	[Ne III]	Emission
7170.0	3934.8	0.8227	Ca II	2.4 ± 0.5

Table 50
(Continued)

λ_{obs} (Å)	λ_{rest} (Å)	z	Feature	EW_{obs} (Å)
7233.1	3969.6	0.8227	Ca II	2.8 ± 0.8
9038.5	4960.3	0.8227	[O III]	Emission
9127.7	5008.2	0.8227	[O III]	Emission

Table 51
GRB 080210 ($z = 2.6419$)

λ_{obs} (Å)	λ_{rest} (Å)	z	Feature	EW_{obs} (Å)
4406.6	1215.7	2.6419	Lyα	
4591.5	1260.4	2.6419	Si II	4.2 ± 0.7
4609.3	1264.7	2.6419	Si II*	2.3 ± 0.6
4652.8				1.4 ± 0.4
4747.6	1302.2	2.6419	O I	9.7 ± 0.6
	1304.4	2.6419	Si II	
4768.8	1309.3	2.6419	Si II*	1.3 ± 0.5
4862.5	1334.5	2.6419	C II	8.7 ± 0.5
5076.3	1393.8	2.6419	Si IV	5.7 ± 0.4
5109.4	1402.8	2.6419	Si IV	4.7 ± 0.4
5354.3	1526.7	2.5084	Si II	1.0 ± 0.3
5437.0	1549.1	2.5084	C IV	4.3 ± 0.4
5559.2	1526.7	2.6419	Si II	5.1 ± 0.3
5642.3	1548.2	2.6419	C IV	12.7 ± 0.4
	1550.8	2.6419	C IV	
5857.5	1608.4	2.6419	Fe II	3.7 ± 0.3
6083.9	1670.8	2.6419	Al II	6.2 ± 0.3
6582.7	1808.0	2.6419	Si II	2.1 ± 0.3
6753.9	1854.7	2.6419	Al III	3.9 ± 0.3
6782.0	1862.8	2.6419	Al III	2.4 ± 0.3
7379.5	2026.1	2.6419	Zn II	2.3 ± 0.4
	2026.5	2.6419	Mg I	
8533.8	2344.2	2.6419	Fe II	6.3 ± 0.4
8644.7	2374.5	2.6419	Fe II	1.8 ± 0.5
8675.2	2382.8	2.6419	Fe II	6.8 ± 0.5

Table 52
GRB 080310 ($z = 2.4274$)

λ_{obs} (Å)	λ_{rest} (Å)	z	Feature	EW_{obs} (Å)
		Kast/B830		
4167.8	1215.7	2.4293	Lyα	11.51 ± 0.54
4222.8				1.82 ± 0.46
4263.6				1.87 ± 0.45
		Kast/R600		
4562.6	1393.8	2.2810	Si IV	15.89 ± 1.21
	1334.3	2.4293	C II	
4756.5				1.73 ± 0.41
4778.0	1393.8	2.4293	Si IV	2.37 ± 0.36
4809.1				1.81 ± 0.37
5084.2	1548.2	2.2810	C IV	7.26 ± 0.37
	1550.8	2.2810	C IV	
5314.8	1548.2	2.4293	C IV	7.77 ± 0.31
	1550.8	2.4293	C IV	
5726.0	1670.8	2.4293	Al II	2.28 ± 0.25
6485.3				1.60 ± 0.25
6550.1				1.67 ± 0.25
6895.2				4.16 ± 0.27

Table 53
GRB 080319B ($z = 0.9382$)

λ_{obs} (Å)	λ_{rest} (Å)	z	Feature	EW_{obs} (Å)
4543.3	2344.2	0.9382	Fe II	1.4 ± 0.6
4798.6	2796.3	0.716	Mg II	3.0 ± 0.6
	2803.5	0.716	Mg II	
5013.5	2586.7	0.9382	Fe II	1.8 ± 0.5
5040.9	2600.2	0.9382	Fe II	1.4 ± 0.5
5419.6	2796.3	0.9382	Mg II	2.0 ± 0.5
5433.6	2803.5	0.9382	Mg II	1.7 ± 0.5

Table 54
GRB 080319C ($z = 1.9492$)

λ_{obs} (Å)	λ_{rest} (Å)	z	Feature	EW_{obs} (Å)
4502.5	1526.7	1.9492	Si II	3.9 ± 1.7
4565.4	1548.2	1.9492	C IV	10.6 ± 0.7
	1550.8	1.9492	C IV	
4743.9	1608.5	1.9492	Fe II	3.4 ± 1.3
4926.7	1670.8	1.9492	Al II	5.7 ± 0.9
5062.5	2796.4	0.8104	Mg II	4.0 ± 0.8
5075.3	2803.5	0.8104	Mg II	3.7 ± 0.8
5137.5	1741.6	1.9492	Ni II	3.0 ± 0.6
5332.1	1808.0	1.9492	Si II	3.5 ± 0.7
5470.3	1854.7	1.9492	Al III	4.3 ± 0.6
5493.6	1862.8	1.9492	Al III	4.2 ± 0.6
5976.4	2026.1	1.9492	Zn II	2.3 ± 0.7
	2026.5	1.9492	Mg I	
6064.3	2056.3	1.9492	Cr II	1.9 ± 0.6
6083.3	2062.2	1.9492	Cr II	2.3 ± 0.6
	2062.7	1.9492	Zn II	
6634.0	2249.9	1.9492	Fe II	2.3 ± 0.6

Table 55
GRB 080330 ($z = 1.5119$)

λ_{obs} (Å)	λ_{rest} (Å)	z	Feature	EW_{obs} (Å)
3889.4	1548.2	1.5119	C IV	4.3 ± 0.7
	1550.8	1.5119	C IV	
4028.8	1608.4	1.5119	Fe II	2.0 ± 0.7
4198.2	1670.8	1.5119	Al II	2.0 ± 0.7
5093.5	2026.1	1.5119	Zn II	4.3 ± 0.4
	2026.5	1.5119	Mg I	
5190.3	2062.2	1.5119	Cr II	0.6 ± 0.3
5190.3	2062.7	1.5119	Zn II	
5883.4	2344.2	1.5119	Fe II	1.4 ± 0.5
5983.0	2382.8	1.5119	Fe II	2.2 ± 0.5
6497.5	2586.7	1.5119	Fe II	11 ± 2
6527.0	2600.2	1.5119	Fe II	
7031.1	2796.3	1.5119	Mg II	5.2 ± 0.3
	2803.5	1.5119	Mg II	

Table 56
GRB 080411 ($z = 1.0301$)

λ_{obs} (Å)	λ_{rest} (Å)	z	Feature	EW_{obs} (Å)
3780.1	1862.8	1.0301	Al III	1.43 ± 0.11
4112.2	2026.1	1.0301	Zn II	1.30 ± 0.07
	2026.5	1.0301	Mg I	
4188.4	2062.2	1.0301	Cr II	1.12 ± 0.08
4188.4	2062.7	1.0301	Zn II	

Table 56
(Continued)

λ_{obs} (Å)	λ_{rest} (Å)	z	Feature	EW_{obs} (Å)
4398.0	2166.2	1.0301	Ni II**	0.62 ± 0.06
4439.8				1.33 ± 0.06
4500.8	2217.2	1.0301	Ni II**	0.61 ± 0.06
4516.3	2223.0	1.0301	Ni II	0.20 ± 0.06
4566.8	2249.9	1.0301	Fe II	0.69 ± 0.06
4591.6	2260.8	1.0301	Fe II	0.68 ± 0.06
4705.2	2316.7	1.0301	Ni II**	0.26 ± 0.05
4734.8	2333.5	1.0301	Fe II*	0.91 ± 0.05
4761.2	2338.7	1.0301	Fe II***	2.87 ± 0.06
	2344.7	1.0301	Fe II	
	2349.0	1.0301	Fe II**	
4795.7	2359.8	1.0301	Fe II***	1.37 ± 0.06
	2365.6	1.0301	Fe II**	
4822.2	2374.5	1.0301	Fe II	9.31 ± 0.11
4836.3	2382.8	1.0301	Fe II	
4867.3	2396.4	1.0301	Fe II*	
4885.9	2400.0	1.0301	Fe II**	
	2405.6	1.0301	Fe II**	
	2411.3	1.0301	Fe II***	
5203.3				0.21 ± 0.08
5231.0	2576.9	1.0301	Mn II	0.45 ± 0.05
5252.1	2586.7	1.0301	Fe II	8.37 ± 0.20
5277.7	2600.2	1.0301	Fe II	
5294.8	2607.9	1.0301	Fe II**	
5302.8	2612.7	1.0301	Fe II*	
5314.2	2614.6	1.0301	Fe II***	
	2618.4	1.0301	Fe II**	
5337.5	2622.5	1.0301	Fe II****	2.32 ± 0.10
	2626.5	1.0301	Fe II*	
	2629.1	1.0301	Fe II****	
	2631.9	1.0301	Fe II**	
5677.1	2796.3	1.0301	Mg II	6.43 ± 0.15
5690.6	2805.3	1.0301	Mg II	
5791.5	2853.0	1.0301	Mg I	1.17 ± 0.10
7984.6	3934.8	1.0301	Ca II (K)	2.19 ± 0.30
8055.6	3969.6	1.0301	Ca II (H)	2.25 ± 0.30

Table 57
GRB 080413A ($z = 2.4330$)

λ_{obs} (Å)	λ_{rest} (Å)	z	Feature	EW_{obs} (Å)
5241.9	1526.7	2.4330	Si II	1.9 ± 0.3
5314.6	1548.2	2.4330	C IV	2.8 ± 0.3
5323.3	1550.8	2.4330	C IV	2.5 ± 0.3

Table 58
GRB 080413B ($z = 1.1014$)

λ_{obs} (Å)	λ_{rest} (Å)	z	Feature	EW_{obs} (Å)
3374.5	1608.4	1.1014	Fe II	0.9 ± 0.4
3508.7	1670.8	1.1014	Al II	4.9 ± 1.0
3799.4	1808.0	1.1014	Si II	1.12 ± 0.20
3896.7	1854.7	1.1014	Al III	0.76 ± 0.20
3915.0	1862.8	1.1014	Al III	0.76 ± 0.20
4258.2	2026.1	1.1014	Zn II	1.39 ± 0.15
	2026.5	1.1014	Mg I	
4287.5				0.30 ± 0.10

Table 58
(Continued)

λ_{obs} (Å)	λ_{rest} (Å)	z	Feature	EW$_{obs}$ (Å)
4322.5	2056.3	1.1014	Cr II	1.41 ± 0.10
4334.1	2062.2	1.1014	Cr II	
	2062.7	1.1014	Zn II	
4659.9	2217.2	1.1014	Ni II**	0.29 ± 0.08
4726.6	2249.9	1.1014	Fe II	0.49 ± 0.08
4751.4	2260.8	1.1014	Fe II	0.72 ± 0.08
4926.3	2344.2	1.1014	Fe II	4.56 ± 0.08
4990.4	2374.5	1.1014	Fe II	3.04 ± 0.15
5006.9	2382.8	1.1014	Fe II	5.08 ± 0.15
5038.5	2396.4	1.1014	Fe II*	0.52 ± 0.15
5057.1	2405.6	1.1014	Fe II**	0.45 ± 0.15
5414.7	2576.9	1.1014	Mn II	15.84 ± 0.30
5436.0	2586.7	1.1014	Fe II	
5463.3	2600.2	1.1014	Fe II	
5488.4	2612.7	1.1014	Fe II*	
5525.6	2626.5	1.1014	Fe II*	0.82 ± 0.10
5877.0	2796.3	1.1014	Mg II	13.40 ± 0.20
5889.0	2803.5	1.1014	Mg II	
5995.1	2853.0	1.1014	Mg I	2.18 ± 0.10

Table 59
GRB 080520 ($z = 1.5457$)

λ_{obs} (Å)	λ_{rest} (Å)	z	Feature	EW$_{obs}$ (Å)
7116.6	2796.3	1.5457	Mg II	6 ± 3
7137.0	2803.5	1.5457	Mg II	8 ± 3
7266.0	2853.0	1.5457	Mg I	6 ± 3
9481.5	3727.1	1.5457	[O II]	Emission
9494.4	3727.9	1.5457	[O II]	Emission

Table 60
GRB 080603B ($z = 2.6892$)

λ_{obs} (Å)	λ_{rest} (Å)	z	Feature	EW$_{obs}$ (Å)
4493.3	1215.7	2.6892	Lyα	
4668.0	1264.7	2.6892	Si II*	0.52 ± 0.25
4712.5				1.51 ± 0.20
4720.8				
4740.9				
4775.2				0.30 ± 0.15
4807.5	1302.2	2.6892	O I	2.67 ± 0.15
4815.0	1304.4	2.6892	Si II	
4831.5	1309.3	2.6892	Si II*	0.54 ± 0.15
4925.8	1335.3	2.6892	C II	3.88 ± 0.15
5141.3	1393.8	2.6892	Si IV	1.87 ± 0.14
5174.5	1402.8	2.6892	Si IV	1.25 ± 0.14
5628.6	1526.7	2.6892	Si II	0.56 ± 0.14
5656.4	1533.4	2.6892	Si II*	0.58 ± 0.14
5711.3	1548.2	2.6892	C IV	4.39 ± 0.16
	1550.8	2.6892	C IV	
5912.4	2796.4	1.1156	Mg II	1.21 ± 0.13
5930.4	2803.5	1.1156	Mg II	
	1608.4	2.6892	Fe II	
6040.0	2853.0	1.1156	Mg I	0.92 ± 0.15
6160.8	1670.8	2.6892	Al II	1.55 ± 0.13

Table 61
GRB 080604 ($z = 1.4171$)

λ_{obs} (Å)	λ_{rest} (Å)	z	Feature	EW$_{obs}$ (Å)
5665.8	2344.2	1.4171	Fe II	4.8 ± 0.7
5739.4	2374.5	1.4171	Fe II	4.3 ± 0.6
5759.4	2382.8	1.4171	Fe II	4.7 ± 0.6
6252.4	2586.6	1.4171	Fe II	6.4 ± 0.5
6285.0	2600.2	1.4171	Fe II	6.4 ± 0.5
6758.4	2796.4	1.4171	Mg II	7.6 ± 0.7
6777.4	2803.5	1.4171	Mg II	5.4 ± 0.5
6896.	2853.0	1.4171	Mg I	In telluric band

Table 62
GRB 080605 ($z = 1.6403$)

λ_{obs} (Å)	λ_{rest} (Å)	z	Feature	EW$_{obs}$ (Å)
3927.4				2.8 ± 0.8
4030.4	1526.7	1.6403	Si II	5.2 ± 0.6
4050.2	1533.4	1.6403	Si II*	2.8 ± 0.6
4090.1	1548.2	1.6403	C IV	13.5 ± 0.8
	1550.8	1.6403	C IV	
4121.5	1560.3	1.6403	C I	1.7 ± 0.6
4151.5				1.3 ± 0.5
4238.1				1.4 ± 0.5
4247.6	1608.4	1.6403	Fe II	1.6 ± 0.5
4375.2	1656.9	1.6403	C I	1.0 ± 0.4
4411.0	1670.8	1.6403	Al II	6.1 ± 0.5
4773.7	1808.0	1.6403	Si II	1.2 ± 0.3
4897.0	1854.7	1.6403	Al III	5.6 ± 0.3
4918.4	1862.8	1.6403	Al III	4.1 ± 0.3
5351.2	2026.1	1.6403	Zn II	1.6 ± 0.3
	2026.5	1.6403	Mg I	
5429.1	2056.4	1.6403	Cr II	1.0 ± 0.3
5445.2	2062.2	1.6403	Cr II	1.0 ± 0.3
	2062.7	1.6403	Zn II	
5973.1	2600.2	1.2987	Fe II	1.4 ± 0.3
6189.2	2344.2	1.6403	Fe II	6.6 ± 0.3
6269.3	2374.5	1.6403	Fe II	11.6 ± 0.4
6290.5	2382.8	1.6403	Fe II	
6430.1	2796.4	1.2987	Mg II	1.77 ± 0.2
6446.4	2803.5	1.2987	Mg II	1.27 ± 0.2
6803.0	2576.9	1.6403	Mn II	1.35 ± 0.2
6828.8	2586.7	1.6403	Fe II	5.6 ± 0.3
6865.8	2600.2	1.6403	Fe II	In telluric band
7380.7	2796.4	1.6403	Mg II	22.6 ± 0.6
7400.7	2803.5	1.6403	Mg II	
7531.4	2853.0	1.6403	Mg I	6.1 ± 0.3

Table 63
GRB 080607 ($z = 3.0368$)

λ_{obs} (Å)	λ_{rest} (Å)	z	Feature	EW$_{obs}$ (Å)
		LRIS/R400		
5626.1	1393.8	3.0368	Si IV	10.78 ± 0.41
5663.2	1402.8	3.0368	Si IV	5.86 ± 0.28
5693.6				3.23 ± 0.32
5713.6	1414.4	3.0368	Ga II	1.42 ± 0.21
5735.8	1419.0	3.0368	CO	5.40 ± 0.26
5753.4	1425.0	3.0368	S I	1.00 ± 0.17
5772.1	2344.2	1.4618	Fe II	4.63 ± 0.19
5802.0	1433.9	3.0368	Pb II	6.62 ± 0.29

Table 63
(Continued)

λ_{obs} (Å)	λ_{rest} (Å)	z	Feature	EW$_{obs}$ (Å)
5848.9	2374.5	1.4618	Fe II	10.09 ± 0.20
	1447.4	3.0368	CO	
5868.1	2382.8	1.4618	Fe II	9.45 ± 0.21
	1454.8	3.0368	Ni II	
5899.3				6.09 ± 0.29
5924.2	1466.2	3.0368	Co II	1.88 ± 0.20
	1467.3	3.0368	Ni II	
	1467.8	3.0368	Ni II	
5943.1				1.53 ± 0.21
5975.2	1477.5	3.0368	CO	10.27 ± 0.24
6006.4				3.21 ± 0.20
6045.1	2586.7	1.3406	Fe II	12.94 ± 0.29
6086.4	2600.2	1.3406	Fe II	1.52 ± 0.13
6100.5	1509.6	3.0368	CO	8.03 ± 0.18
6132.1				7.78 ± 0.27
6163.0	1526.7	3.0368	Si II	7.85 ± 0.15
6189.4	1532.5	3.0368	P II	6.10 ± 0.15
	1533.4	3.0368	Si II*	
6220.6				1.43 ± 0.17
6252.0	1544.3	3.0368	CO	20.82 ± 0.25
	1548.2	3.0368	C IV	
	1550.8	3.0368	C IV	
6301.5	1560.3	3.0368	C I	8.76 ± 0.31
6325.3	1566.8	3.0368	Fe II*	2.53 ± 0.14
6338.4	2576.9	1.4618	Mn II	4.38 ± 0.14
6369.4	2586.7	1.4618	Fe II	13.04 ± 0.25
	2594.5	1.4618	Mn II	
	1574.6	3.0368	Co II	
6400.8	2600.2	1.4618	Fe II	5.42 ± 0.13
6414.4	2606.5	1.4618	Mn II	3.35 ± 0.12
	1589.2	3.0368	Si I	
6441.7	1595.8	3.0368	Si I	0.49 ± 0.12
6469.8	1602.5	3.0368	Ge I	5.28 ± 0.14
6500.9	1608.5	3.0368	Fe II	14.81 ± 0.19
	1611.2	3.0368	Fe II	
	1612.8	3.0368	Fe II*	
	1613.4	3.0368	CI	
6534.6	1618.5	3.0368	Fe II*	2.74 ± 0.12
6545.7	2796.4	1.3406	Mg II	6.88 ± 0.13
	1621.7	3.0368	Fe II*	
6562.1	2803.5	1.3406	Mg II	3.59 ± 0.13
6575.9	1629.2	3.0368	Fe II*	2.17 ± 0.12
6616.6	1637.4	3.0368	Fe II*	17.98 ± 0.26
	1631.1	3.0368	Fe II*	
	1634.4	3.0368	Fe II*	
	1636.3	3.0368	Fe II*	
	1639.4	3.0368	Fe II*	
6660.2				3.71 ± 0.13
6678.2	2853.0	1.3406	Mg I	2.18 ± 0.10
6692.1	1656.9	3.0368	C I	8.21 ± 0.15
6713.3				1.45 ± 0.19
6744.1	1670.8	3.0368	Al II	9.25 ± 0.10
6758.9				2.25 ± 0.12
6807.3				1.62 ± 0.12
6834.8				1.62 ± 0.18
6849.2				0.71 ± 0.12
6871.8	1702.0	3.0368	Fe II*	3.88 ± 0.11
6884.0	2796.4	1.4618	Mg II	8.59 ± 0.11
	1703.4	3.0368	Ni II	
	1707.1	3.0368	Mg I	

Table 63
(Continued)

λ_{obs} (Å)	λ_{rest} (Å)	z	Feature	EW$_{obs}$ (Å)
6901.1	2803.5	1.4618	Mg II	7.51 ± 0.11
	1707.1	3.0368	Mg I	
	1709.6	3.0368	Ni II	
6914.4				1.57 ± 0.12
6930.7				1.25 ± 0.13
6945.4				1.39 ± 0.14
6964.8				2.05 ± 0.13
6989.2				0.75 ± 0.12
7013.1	2853.0	1.4618	Mg I	1.82 ± 0.15
7030.2	1741.6	3.0368	Ni II	3.62 ± 0.10
7055.8	1747.8	3.0368	Mg I	2.36 ± 0.12
7072.1	1751.9	3.0368	Ni II	2.56 ± 0.12
7160.7	1772.3	3.0368	Ni II	1.06 ± 0.12
	1774.0	3.0368	Ni II	
7187.9	3073.9	1.3406	Ti II	0.74 ± 0.12
7204.0	3073.9	1.3406	Ti II	0.85 ± 0.13
	1783.3	3.0368	Ni II	
7284.8	1804.5	3.0368	Ni II	0.97 ± 0.14
7298.9	1807.3	3.0368	S I	5.72 ± 0.13
	1808.0	3.0368	Si II	
7334.4	1816.9	3.0368	Si II*	2.93 ± 0.17
	1817.5	3.0368	Si II*	
7378.6	1827.9	3.0368	Mg I	1.64 ± 0.14
7486.0	1854.7	3.0368	Al III	7.43 ± 0.14
7518.8	1862.8	3.0368	Al III	6.13 ± 0.15
7568.6	3230.1	1.3406	Ti II	0.63 ± 0.17
	3073.9	1.4618	Ti II	
7637.5	3242.9	1.3406	Ti II	25.95 ± 0.34
	1892.0	3.0368	Si III	
	1901.8	3.0368	Fe II	
7776.5				1.01 ± 0.18
7982.5	3242.9	1.4618	Ti II	1.74 ± 0.22
8122.6	2012.2	3.0368	Co II	1.20 ± 0.18
8180.1	2026.1	3.0368	Zn II	6.35 ± 0.18
	2026.3	3.0368	Cr II	
	2026.5	3.0368	Mg I	
8232.8				2.09 ± 0.23
8316.6	3384.7	1.4618	Ti II	16.66 ± 0.70
	2056.3	3.0368	Cr II	
	2062.2	3.0368	Cr II	
	2062.7	3.0368	Zn II	
	2066.2	3.0368	Cr II	
8398.3				5.94 ± 0.49
8434.2				2.56 ± 0.40
8443.2				1.15 ± 0.24
8480.9				2.10 ± 0.37
8513.3				1.93 ± 0.30
8606.0				5.68 ± 0.38
8749.4	2166.2	3.0368	Ni II*	6.05 ± 0.53
	2169.8	3.0368	Ni II*	
	2167.5	3.0368	Fe I	
8780.5	2175.4	3.0368	Ni II*	5.19 ± 0.64
8827.5				8.93 ± 0.77
8948.9	2217.2	3.0368	Ni II*	4.32 ± 0.56
8979.8	2223.6	3.0368	Ni II*	6.94 ± 0.60
9085.3	2249.9	3.0368	Fe II	4.53 ± 0.37
9097.4				3.20 ± 0.42
9134.1	2260.8	3.0368	Fe II	6.27 ± 0.53

Table 64
GRB 080707 ($z = 1.2322$)

λ_{obs} (Å)	λ_{rest} (Å)	z	Feature	EW$_{obs}$ (Å)
5236.7	2344.2	1.2322	Fe II	5.1 ± 0.9
5300.4	2374.5	1.2322	Fe II	2.4 ± 0.9
5320.4	2382.8	1.2322	Fe II	5.3 ± 0.9
5779.2	2586.7	1.2322	Fe II	3.9 ± 0.8
5799.2	2600.2	1.2322	Fe II	4.6 ± 0.8
6241.6	2796.3	1.2322	Mg II	16.4 ± 1.1
6257.3	2805.3	1.2322	Mg II	
6366.1	2853.0	1.2322	Mg I	4.9 ± 0.8

Table 65
GRB 080710 ($z = 0.8454$)

λ_{obs} (Å)	λ_{rest} (Å)	z	Feature	EW$_{obs}$ (Å)
		GMOS/B600		
4326.5	2344.2	0.8454	Fe II	0.77 ± 0.05
	2345.0	0.8454	Fe II*	
4382.0	2374.5	0.8454	Fe II	0.39 ± 0.04
4397.6	2381.5	0.8454	Fe II*	1.05 ± 0.04
	2382.8	0.8454	Fe II	
	2383.8	0.8454	Fe II*	
4773.6	2586.7	0.8454	Fe II	0.76 ± 0.03
4788.6	2594.5	0.8454	Mn II	0.21 ± 0.04
4798.6	2599.2	0.8454	Fe II*	1.32 ± 0.04
	2600.2	0.8454	Fe II	
5160.5	2796.4	0.8454	Mg II	2.23 ± 0.03
5173.8	2803.5	0.8454	Mg II	1.95 ± 0.03
5264.9	2853.0	0.8454	Mg I	0.67 ± 0.03
5895.2				0.58 ± 0.04
6281.2				0.47 ± 0.03

Table 66
GRB 080721 ($z = 2.5914$)

λ_{obs} (Å)	λ_{rest} (Å)	z	Feature	EW$_{obs}$ (Å)
4358.0	1215.7	2.5914	Lyα	
4527.1	1260.4	2.5914	Si II	6.3 ± 0.7
4680.5	1302.2	2.5914	O I	6.1 ± 0.7
	1304.4	2.5914	Si II	
4796.5	1335.3	2.5914	C II	7.1 ± 0.7
5005.7	1393.8	2.5914	Si IV	4.8 ± 0.5
5038.9	1402.8	2.5914	Si IV	3.0 ± 0.5
5482.9	1526.7	2.5914	Si II	6.0 ± 0.4
5561.0	1548.2	2.5914	C IV	16.0 ± 0.6
5571.4	1550.8	2.5914	C IV	
5776.3	1608.4	2.5914	Fe II	8.8 ± 0.5
5787.9	1611.2	2.5914	Fe II	
6000.1	1670.8	2.5914	Al II	5.1 ± 0.4
7271.6	2026.1	2.5914	Zn II	3.1 ± 0.4
	2026.5	2.5914	Mg I	
7405.3	2062.2	2.5914	Cr II	2.53 ± 0.9
	2062.7	2.5914	Zn II	

Table 67
GRB 080804

λ_{obs} (Å)	λ_{rest} (Å)	z	Feature	EW$_{obs}$ (Å)
4648.5	1526.7	2.0446	Si II	4.10 ± 0.10
4961.3	1548.2	2.0446	C IV	2.37 ± 0.10
5323.3	1550.8	2.0446	C IV	1.90 ± 0.10

Table 68
GRB 080805 ($z = 1.5042$)

λ_{obs} (Å)	λ_{rest} (Å)	z	Feature	EW$_{obs}$ (Å)
4184.0	1670.8	1.5042	Al II	15 ± 4
6150.6	2796.3	1.197	Mg II	18.2 ± 3.0
	2803.5	1.197	Mg II	
6479.8	2586.7	1.5042	Fe II	5.6 ± 1.9
6511.8	2600.2	1.5042	Fe II	7.2 ± 2.0
6999.8	2796.3	1.5042	Mg II	8.2 ± 2.0
7019.4	2803.5	1.5042	Mg II	12.5 ± 2.0
7146.0	2853.0	1.5042	Mg I	6.9 ± 1.6

Table 69
GRB 080810 ($z = 3.3604$)

λ_{obs} (Å)	λ_{rest} (Å)	z	Feature	EW$_{obs}$ (Å)
5047.6	1215.7	3.1585	Lyα	
5291.8	1215.7	3.3604	Lyα	
5551.7	1334.5	3.1585	C II	1.4 ± 0.6
6012.8				1.8 ± 0.6
6117.6	1402.7	3.3604	Si IV	1.7 ± 0.6
6346.3	1526.7	3.1585	Si II	2.6 ± 0.6
6438.3	1548.2	3.1585	C IV	1.7 ± 0.6
	1550.8	3.1585	C IV	
6655.6	1526.7	3.3604	Si II	2.1 ± 0.6
6754.4	1548.2	3.3604	C IV	13.6 ± 0.9
	1550.8	3.3604	C IV	

Table 70
GRB 080905B ($z = 2.3739$)

λ_{obs} (Å)	λ_{rest} (Å)	z	Feature	EW$_{obs}$ (Å)
4402.0	1302.2	2.3739	O I	9 ± 2
	1304.4	2.3739	Si II	
5148.0	1526.7	2.3739	Si II	2.5 ± 0.8
5227.2	1548.2	2.3739	C IV	5.6 ± 0.7
	1550.8	2.3739	C IV	
5429.8	1608.4	2.3739	Fe II	2.7 ± 0.7
5436.6	1611.2	2.3739	Fe II	
5635.6	1670.8	2.3739	Al II	3.4 ± 0.6
6099.7	1808.0	2.3739	Si II	1.5 ± 0.6
6256.3	1854.7	2.3739	Al III	2.7 ± 0.6
6284.6	1862.8	2.3739	Al III	1.7 ± 0.6
6777.7				1.2 ± 0.5
6833.7	2026.1	2.3739	Zn II	2.0 ± 0.6
	2026.5	2.3739	Mg I	
6876.9	2796.3	1.4588	Mg II	3.7 ± 0.6
6896.2	2805.3	1.4588	Mg II	2.2 ± 0.5
6959.7	2062.2	2.3739	Cr II	2.8 ± 0.5
	2062.7	2.3739	Zn II	
7307.1	2166.2	2.3739	Ni II**	2.0 ± 0.7
7815.8	2316.7	2.3739	Ni II**	2.8 ± 0.7
7906.9	2344.2	2.3739	Fe II	5.1 ± 1.0
8010.8	2374.5	2.3739	Fe II	5.3 ± 0.6
8040.1	2382.8	2.3739	Fe II	4.3 ± 0.7
8085.9	2396.4	2.3739	Fe II*	2.8 ± 0.5
8117.5	2405.6	2.3739	Fe II**	2.1 ± 0.6
8136.2	2411.3	2.3739	Fe II***	2.4 ± 0.6
8696.2	2576.9	2.3739	Mn II	2.8 ± 0.6
8727.1	2586.7	2.3739	Fe II	5.1 ± 0.6
8770.7	2600.2	2.3739	Fe II	5.6 ± 1.4

Table 70
(Continued)

λ_{obs} (Å)	λ_{rest} (Å)	z	Feature	EW_{obs} (Å)
9442.5	2796.3	2.3739	Mg II	20 ± 4
	2803.5	2.3739	Mg II	

Note. The afterglow spectrum is blended with the spectrum of another object on the slit. Hence, the EWs in this table will be affected by this contaminating light.

Table 71
GRB 080916A ($z = 0.6887$)

λ_{obs} (Å)	λ_{rest} (Å)	z	Feature	EW_{obs} (Å)
4727.2	2796.3	0.6887	Mg II	8.2 ± 1.4
	2803.5	0.6887	Mg II	
6295.6	3727.7	0.6887	[O II]	Emission
8210.7	4862.7	0.6887	Hβ	Emission
8456.8	5008.2	0.6887	[O III]	Emission

Table 72
GRB 080928 ($z = 1.6919$)

λ_{obs} (Å)	λ_{rest} (Å)	z	Feature	EW_{obs} (Å)
4133.8	2382.8	0.7359	Fe II	8.5 ± 0.7
4172.8	1548.2	1.6919	C IV	5.7 ± 0.7

Table 72
(Continued)

λ_{obs} (Å)	λ_{rest} (Å)	z	Feature	EW_{obs} (Å)
	1550.8	1.6919	C IV	
4287.8				1.6 ± 0.4
4327.8	1608.4	1.6919	Fe II	1.4 ± 0.4
4490.8	2586.7	0.7359	Fe II	3.8 ± 0.4
4513.9	2600.2	0.7359	Fe II	6.7 ± 0.4
4857.7	2796.3	0.7359	Mg II	16.5 ± 0.4
4865.3	2803.5	0.7359	Mg II	
4953.2	2853.0	0.7359	Mg I	4.0 ± 0.3
5041.1				1.0 ± 0.3
5092.6				1.0 ± 0.3
5117.4				1.1 ± 0.3
5709.2				0.7 ± 0.3
5830.3	2166.2	1.6919	Ni II**	0.8 ± 0.3
6310.4	2344.2	1.6919	Fe II	2.0 ± 0.4
6392.7	2374.5	1.6919	Fe II	1.7 ± 0.3
6415.6	2382.8	1.6919	Fe II	1.2 ± 0.2
6828.8	3934.8	0.7359	Ca II	1.5 ± 0.3
6893.4	3969.6	0.7359	Ca II	In telluric band
6938.0	2576.9	1.6919	Mn II	0.8 ± 0.3
6964.5	2586.7	1.6919	Fe II	1.4 ± 0.2
6999.2	2600.2	1.6919	Fe II	2.2 ± 0.3
7526.6	2796.3	1.6919	Mg II	3.7 ± 0.3
7547.5	2803.5	1.6919	Mg II	2.7 ± 0.3

Table 73
Statistical Sample

GRB	z	z class	N_X [10^{21} cm^{-2}]	β_{OX}	Reference
080928	1.69	a	. . .	1.00	Vreeswijk et al. (2008e)
080916B	. . .	. . .	0	< 0.90	. . .
080916A	0.69	ah	. . .	0.69	Fynbo et al. (2008b)
080913	6.70	a	. . .	< 0.48	Greiner et al. (2009)
080905B	2.37	a	. . .	0.64	Vreeswijk et al. (2008a)
080810	3.35	a	. . .	0.96	de Ugarte Postigo et al. (2008)
080805	1.51	a	. . .	0.40	Jakobsson et al. (2008e)
080804	2.20	a	. . .	0.78	Thöne et al. (2008d)
080727A	. . .	. . .	0	< 0.76	. . .
080721	2.59	a	. . .	0.60	Jakobsson et al. (2008d)
080710	0.85	a	. . .	1.04	Perley et al. (2008)
080707	1.23	a	. . .	0.83	Fynbo et al. (2008f)
080703	< 5.5	a	. . .	0.42	Ward & Ziaeepour (2008)
080613B	. . .	. . .	0	< 0.79	. . .
080607	3.04	a	. . .	0.24	Prochaska et al. (2009)
080605	1.64	a	. . .	0.38	Jakobsson et al. (2008c)
080604	1.42	a	. . .	0.90	Wiersema et al. (2008b)
080603B	2.69	a	. . .	0.92	Fynbo et al. (2008e)
080602	. . .	. . .	1.0	< 0.28	. . .
080523	< 3.0	a	. . .	0.71	Fynbo et al. (2008c)
080520	1.55	ah	. . .	0.77	Jakobsson et al. (2008a)
080430	0.77	a	. . .	0.77	Cucchiara & Fox (2008)
080413B	1.10	a	. . .	0.89	Vreeswijk et al. (2008d)
080330	1.51	a	. . .	0.99	Guidorzi et al. (2009)
080325	. . .	. . .	1.5	< 0.79	. . .
080320	< 6.4	a	. . .	< 0.15	Tanvir et al. (2008a)
080319C	1.95	a	. . .	0.31	Wiersema et al. (2008a)
080319B	0.94	a	. . .	0.67	Vreeswijk et al. (2008c)
080319A	< 4.2	h	. . .	0.49	Perley et al. (2009b)
080310	2.43	a	. . .	0.88	Fox et al. (2008)
080307	< 6.1	a	. . .	0.40	Xin et al. (2008)
080212	< 3.5	a	. . .	0.66	Kuepcue Yoldas et al. (2008)
080210	2.64	a	. . .	0.74	Jakobsson et al. (2008b)
080207	< 3.5 (XRT)	. . .	6.1	< 0.43	. . .

Table 73
(Continued)

GRB	z	z class	N_X [10^{21} cm^{-2}]	β_{OX}	Reference
080205	< 5.5	a	. . .	0.79	Oates & Markwardt (2008)
071122	1.14	a	. . .	0.83	Cucchiara et al. (2007a)
071117	1.33	h	. . .	0.58	Jakobsson et al. (2007e)
071112C	0.82	ah	. . .	0.72	Jakobsson et al. (2007a)
071031	2.69	a	. . .	0.97	Ledoux et al. (2008)
071025	5.2	ap	. . .	0.50	This work
071021	< 5.6	a	. . .	. . .	Piranomonte et al. (2007)
071020	2.15	a	. . .	0.56	Jakobsson et al. (2007c)
070808	< 3.5 (XRT)	. . .	6.5	< 0.48	. . .
070802	2.45	a	. . .	0.49	Elíasdóttir et al. (2009)
070721B	3.63	a	. . .	0.72	Malesani et al. (2007)
070621	< 3.5 (XRT)	. . .	3.2	< 0.53	. . .
070611	2.04	a	. . .	0.73	Thöne et al. (2007a)
070521	1.35	h	. . .	< −0.06	Perley et al. (2009b)
070520B	. . .	. . .	0.6	< 0.88	. . .
070518	< 2.0	a	. . .	0.81	Cucchiara et al. (2007c)
070506	2.31	a	. . .	0.93	Thöne et al. (2007b)
070419B	< 5.9	a	. . .	0.25	de Ugarte Postigo et al. (2007)
070419A	0.97	a	. . .	0.94	Cenko et al. (2007)
070412	. . .	. . .	0.7	< 0.17	. . .
070330	< 5.5	a	. . .	0.68	Kuin et al. (2007)
070328	. . .	. . .	1.8	< 0.31	. . .
070318	0.84	a	. . .	0.78	Jaunsen et al. (2007a)
070306	1.50	h	. . .	< 0.23	Jaunsen et al. (2008)
070224	< 6.1	a	. . .	0.92	Thöne et al. (2007c)
070223	< 6.1	a	. . .	. . .	Rol et al. (2007b)
070219	< 3.5 (XRT)	. . .	2.2	< 0.38	. . .
070208	1.17	ah	. . .	0.68	Cucchiara et al. (2007b)
070129	< 3.4	a	. . .	0.62	This work
070110	2.35	ah	. . .	0.77	Jaunsen et al. (2007b)
070103	< 3.5 (XRT)	. . .	2.1	< 0.48	. . .
061222A	2.09	h	. . .	< 0.22	Perley et al. (2009b)
061121	1.31	a	. . .	0.64	Bloom et al. (2006b)
061110B	3.44	a	. . .	0.55	Fynbo et al. (2006b)
061110A	0.76	ah	. . .	0.99	Fynbo et al. (2007)
061102	. . .	. . .	0	< 0.91	. . .
061021	0.35	a	. . .	0.75	This work
061007	1.26	ah	. . .	0.79	Jakobsson et al. (2006a)
061004	. . .	. . .	0	< 0.47	. . .
061002	. . .	. . .	0.6	< 0.93	. . .
060929	. . .	. . .	0.4	< 0.67	. . .
060927	5.47	a	. . .	0.55	Ruiz-Velasco et al. (2007)
060923C	< 11.0	a	. . .	< 0.31	Fox (2006)
060923B	. . .	. . .	1.9	< 0.68	. . .
060923A	< 2.8	h	. . .	< 0.11	Tanvir et al. (2008b)
060919	< 3.5 (XRT)	. . .	5.5	< 1.02	. . .
060912A	0.94	h	. . .	0.62	Levan et al. (2007)
060908	1.88	a	. . .	0.38	This work
060904A	. . .	. . .	0	< 0.52	. . .
060814	0.84	h	. . .	< −0.06	Thöne et al. (2007d)
060807	< 3.4	a	. . .	0.54	This work
060805A	. . .	. . .	0.1	< 1.07	. . .
060729	0.54	a	. . .	0.80	Thöne et al. (2006c)
060719	< 4.6	a	. . .	< −0.13	This work
060714	2.71	ah	. . .	0.77	Jakobsson et al. (2006c)
060712	. . .	. . .	1.1	< 0.96	. . .
060708	1.92	p	. . .	1.04	Oates et al. (2009)
060707	3.43	a	. . .	0.73	Jakobsson et al. (2006c)
060614	0.13	h	. . .	0.79	Della Valle et al. (2006)
060607A	3.08	a	. . .	0.53	Fox et al. (2008)
060605	3.78	a	. . .	1.00	Savaglio et al. (2006)
060604	< 2.8	a	. . .	0.75	Blustin & Page (2006)
060526	3.21	a	. . .	1.03	Jakobsson et al. (2006c)
060522	5.11	a	. . .	0.74	Cenko et al. (2006)
060512	2.1	a	. . .	0.98	This work
060502A	1.51	a	. . .	0.65	Cucchiara et al. (2006a)

Table 73
(Continued)

GRB	z	z class	N_X [10^{21} cm^{-2}]	β_{OX}	Reference
060428B	< 5.5	a	. . .	1.00	de Pasquale & Campana (2006)
060427	. . .	. . .	0.7	< 0.81	. . .
060323	< 4.4	a	. . .	0.76	Marshall & Vetere (2006)
060319	1.15	h	. . .	< 0.41	D. Perley (2009a)
060306	< 3.5 (XRT)	. . .	3.2	< 0.54	. . .
060219	< 3.5 (XRT)	. . .	2.6	< 0.54	. . .
060218	0.03	h	. . .	. . .	Sollerman et al. (2006)
060210	3.91	a	. . .	0.37	Cucchiara et al. (2006b)
060206	4.05	a	. . .	0.95	Fynbo et al. (2006c)
060204B	< 4.8	a	. . .	0.47	Fynbo et al. (2006a)
060202	0.78	h	. . .	< 0.20	Butler (2007)
060124	2.30	a	. . .	0.80	Mirabal & Halpern (2006)
060115	3.53	a	. . .	0.78	Piranomonte et al. (2006a)
060111A	< 5.5	a	. . .	0.70	Blustin et al. (2006)
060108	< 3.2	a	. . .	0.51	Oates et al. (2006)
051117B	. . .	. . .	0.6	< 1.06	. . .
051016B	0.94	h	. . .	0.63	Soderberg et al. (2005)
051006	< 3.5 (XRT)	. . .	5.1	< 1.30	. . .
051001	. . .	. . .	0.9	< 0.56	. . .
050922C	2.20	a	. . .	0.99	Jakobsson et al. (2006c)
050922B	. . .	. . .	1.1	< 0.58	. . .
050915A	< 15.0	a	. . .	< 0.44	Bloom (2005)
050908	3.34	a	. . .	1.14	Fugazza et al. (2005)
050904	6.30	a	. . .	< 0.41	Kawai et al. (2006)
050824	0.83	ah	. . .	0.91	Sollerman et al. (2007)
050822	. . .	. . .	0.6	. . .	. . .
050820A	2.61	a	. . .	0.77	Fox et al. (2008)
050819	. . .	. . .	0	< 0.90	. . .
050814	5.3	p	. . .	0.51	Jakobsson et al. (2006b)
050803	. . .	. . .	1.2	< −0.15	. . .
050802	1.71	a	. . .	0.51	Fynbo et al. (2005)
050801	1.38	p	. . .	0.95	Oates et al. (2009)
050730	3.97	a	. . .	0.79	D'Elia et al. (2005)
050726	< 5.5	a	. . .	< 0.89	Poole et al. (2005)
050716	< 11.0	a	. . .	< 0.28	Rol et al. (2007a)
050714B	< 3.5 (XRT)	. . .	2.2	< 0.48	. . .
050525A	0.61	ah	. . .	0.92	Foley et al. (2005)
050505	4.28	a	. . .	0.53	Berger et al. (2006)
050502B	< 6.4	a	. . .	< 0.58	Cenko et al. (2005)
050416A	0.65	h	. . .	0.70	Soderberg et al. (2007)
050412	. . .	. . .	0	< 0.60	. . .
050406	2.7	p	. . .	1.02	Schady et al. (2006)
050401	2.90	a	. . .	0.36	Watson et al. (2006)
050319	3.24	a	. . .	0.90	Jakobsson et al. (2006c)
050318	1.44	a	. . .	0.75	Berger et al. (2005)
050315	1.95	a	. . .	0.63	Berger et al. (2005)

Notes. The z classes are a: afterglow spectrum; h: host galaxy emission; p: photometric redshift from afterglow imaging. For bursts where the OA is not detected we provide the excess X-ray absorption and the corresponding redshift limit when appropriate (see the main text). We also provide references for redshift measurements.

REFERENCES

Akerman, C. J., Ellison, S. L., Pettini, M., & Steidel, C. C. 2005, A&A, 440, 499

Aoki, K., et al. 2008, PASJ, 61, 387

Berger, E., Fox, D. B., Kulkarni, S. R., Frail, D. A., & Djorgovski, S. G. 2007, ApJ, 660, 504

Berger, E., Penprase, B. E., Cenko, S. B., Kulkarni, S. R., Fox, D. B., Steidel, C. C., & Reddy, N. A. 2006, ApJ, 642, 979

Berger, E., et al. 2005, ApJ, 634, 501

Bloom, J. S. 2003, AJ, 125, 2865

Bloom, J. S. 2005, GCN Circ., 3990, 1

Bloom, J. S., Foley, R. J., Koceveki, D., & Perley, D. 2006a, GCN Circ., 5217, 1

Bloom, J. S., Kulkarni, S. R., & Djorgovski, S. G. 2002, AJ, 123, 1111

Bloom, J. S., Perley, D. A., & Chen, H.-W. 2006b, GCN Circ., 5826, 1

Bloom, J. S., et al. 2009, ApJ, 691, 723

Blustin, A. J., & Page, M. J. 2006, GCN Circ., 5219, 1

Blustin, A. J., Zane, S., & Rosen, S. R. 2006, GCN Circ., 4482, 1

Butler, N. 2006, GCN Circ., 5435, 1

Butler, N. R. 2007, ApJ, 656, 1001

Campana, S., et al. 2006, Nature, 442, 1008

Castro-Tirado, A., et al. 2006, GCN Circ., 5218, 1

Cenko, S. B., Berger, E., Djorgovski, S. G., Mahabal, A. A., & Fox, D. B. 2006, GCN Circ., 5155, 1

Cenko, S. B., Fox, D. B., Rich, J., Schmidt, B., Christiansen, J., & Berger, E. 2005, GCN Circ., 3357, 1

Cenko, S. B., Gezari, S., Small, T., Fox, D. B., & Chornock, R. 2007, GCN Circ., 6322, 1

Cenko, S. B., et al. 2008, ApJ, 677, 441

Chen, H.-W., Prochaska, J. X., Bloom, J. S., & Thompson, I. B. 2005, ApJ, 634, L25

Chen, H.-W., Prochaska, J. X., & Gnedin, N. Y. 2007a, ApJ, 667, L125

Chen, H.-W., Prochaska, J. X., Ramirez-Ruiz, E., Bloom, J. S., Dessauges-Zavadsky, M., & Fole, R. J. 2007b, ApJ, 663, 420

Chen, H.-W., et al. 2009, ApJ, 691, 152

Christensen, L., Hjorth, J., & Gorosabel, J. 2004, A&A, 425, 913

Costa, E., et al. 1997, Nature, 387, 783

Coward, D. M. 2009, MNRAS, 393, L65

Cucchiara, A., & Fox, D. B. 2008, GCN Circ., 7654, 1

Cucchiara, A., Fox, D. B., & Cenko, S. B. 2007a, GCN Circ., 7124, 1

Cucchiara, A., Fox, D. B., Cenko, S. B., & Price, P. A. 2007b, GCN Circ., 6083, 1

Cucchiara, A., Marshall, F. E., & Guidorzi, C. 2007c, GCN Circ., 6419, 1

Cucchiara, A., Price, P. A., Fox, Cenko, S. B., & Schmidt, B. P. 2006a, GCN Circ., 5052, 1

Cucchiara, A., et al. 2006b, Nuovo Cimento B, 121, 1455

Cucchiara, A., et al. 2009, ApJ, 697, 345

Curran, P. A., et al. 2007, A&A, 467, 1049

D'Elia, M., et al. 2005, GCN Circ., 3746, 1

D'Elia, M., et al. 2007, A&A, 467, 629

D'Elia, M., et al. 2009a, ApJ, 694, 332

D'Elia, M., et al. 2009b, A&A, 503, 437

Della Valle, M., et al. 2006, Nature, 444, 1050

De Pasquale, M., & Cummings, J. 2006, GCN Circ., 5130, 1

de Pasquale, M., & Campana, S. 2006, GCN Circ., 5035, 1

de Ugarte Postigo, A., Jelinek, M., Tristram, P., Bond, I., Yock, P., Hearnshaw, J., & Castro-Tirado, A. J. 2007, GCN Circ., 6321, 1

de Ugarte Postigo, A., Thöne, C. C., Fynbo, J. P. U., Jaunsen, A. O., & Ledoux, C. 2008, GCN Circ., 8089, 1

Dessauges-Zavadsky, M., Chen, H.W., Prochaska, J. X., Bloom, J. S., & Barth, A. J. 2006, ApJ, 648, L89

Elíasdóttir, Á., et al. 2009, ApJ, 697, 1725

Ellison, S., York, B. A., Pettini, M., & Kanekar, N. 2008, MNRAS, 388, 1349

Ellison, S. L., et al. 2001, A&A, 379, 393

Evans, P., et al. 2009, MNRAS, 397, 1177

Fiore, F., Guetta, D., Piranomonte, S., D'Elia, V., & Antonelli, L. A. 2007, A&A, 470, 515

Foley, R. J., Chen, H.-W., Bloom, J., & Prochaska, J. X. 2005, GCN Circ., 3483, 1

Foley, R. J., et al. 2007, ApJ, 645, 450

Fox, D. B. 2006, GCN Circ., 5607, 1

Fox, A. J., Ledoux, C., Vreeswijk, A., Smette, A., & Jaunsen, A. O. 2008, A&A, 491, 189

Fruchter, A. S., Krolik, J. H., & Rhoads, J. E. 2001, ApJ, 563, 597

Fruchter, A. S., et al. 2006, Nature, 441, 463

Fugazza, D., et al. 2005, GCN Circ., 3948, 1

Fugazza, D., et al. 2006, GCN Circ., 5513, 1

Fynbo, J. P. U., Gorosabel, J., Jensen, B. L., & Naeraenen, J. 2006a, GCN Circ., 4677, 1

Fynbo, J. P. U., Greiner, J., Kruehler, T., Rossi, A., Vreeswijk, P. M., & Malesani, D. 2008a, GCN Circ., 8225, 1

Fynbo, J. P. U., Malesani, D., Hjorth, J., Sollerman, J., & Thöne, C. C. 2008b, GCN Circ., 8254, 1

Fynbo, J. P. U., Malesani, D., Jakobsson, P., Milvang-Jensen, B., & Hjorth, J. 2008c, GCN Circ., 7770, 1

Fynbo, J. P. U., Malesani, D., Thöne, C. C., Vreeswijk, P. M., Hjorth, J., & Henriksen, C. 2006b, GCN Circ., 5809, 1

Fynbo, J. P. U., Prochaska, J. X., Sommer-Larsen, J., Dessauges-Zavadsky, M., & Møller, P. 2008d, ApJ, 683, 321

Fynbo, J. P. U., Thöne, C. C., Malesani, D., Hjorth, J., Vreeswijk, P. M., & Jakobsson, P. 2007, GCN Circ., 6759, 1

Fynbo, J. P. U., et al. 2001, A&A, 369, 373

Fynbo, J. P. U., et al. 2005, GCN Circ., 3749, 1

Fynbo, J. P. U., et al. 2006c, A&A, 451, L47

Fynbo, J. P. U., et al. 2006d, Nature, 444, 1047

Fynbo, J. P. U., et al. 2008e, GCN Circ., 7797, 1

Fynbo, J. P. U., et al. 2008f, GCN Circ., 7949, 1

Gal-Yam, A., et al. 2006, Nature, 444, 1053

Gehrels, N., et al. 2004, ApJ, 611, 1005

Gnedin, N., Kravtsov, A. V., & Chen, H.-W. 2008, ApJ, 672, 765

Greiner, J., et al. 2009, ApJ, 693, 1610

Groot, P., et al. 1998, ApJ, 493, L27

Grupe, D., et al. 2007, ApJ, 133, 1216

Guetta, D., & Piran, T. 2007, J. Cosmol. Astropart. Phys., JCAP7(2007)3

Guidorzi, C., et al. 2009, A&A, 499, 439

Hao, H., et al. 2007, ApJ, 659, L99

Hirschi, R., Meynet, G., & Maeder, A. 2005, A&A, 443, 581

Hjorth, J., et al. 2003, Nature, 423, 847

Hogg, D. W., & Fruchter, A. S. 1999, ApJ, 520, 54

Jakobsson, P., Fynbo, J. P. U., Malesani, D., Hjorth, J., & Milvang-Jensen, B. 2008a, GCN Circ., 7757, 1

Jakobsson, P., Fynbo, J. P. U., Tanvir, N., & Rol, E. 2006a, GCN Circ., 5716, 1

Jakobsson, P., Fynbo, J. P. U., Vreeswijk, P. M., Malesani, D., & Sollerman, J. 2007a, GCN Circ., 7076, 1

Jakobsson, P., Malesani, D., Thöne, C. C., Fynbo, J. P. U., Hjorth, J., Jaunsen, A. O., Andersen, M. I., & Vreeswijk, P. M. 2007b, GCN Circ., 6283, 1

Jakobsson, P., Vreeswijk, P. M., Hjorth, J., Malesani, D., Fynbo, J. P. U., & Thöne, C. C. 2007c, GCN Circ., 6952, 1

Jakobsson, P., Vreeswijk, P. M., Malesani, D., Jaunsen, A. O., Fynbo, J. P. U., Hjorth, J., & Tanvir, N. R. 2008b, GCN Circ., 7286, 1

Jakobsson, P., Vreeswijk, P. M., Xu, D., & Thöne 2008c, GCN Circ., 7832, 1

Jakobsson, P., et al. 2004, ApJ, 617, L21

Jakobsson, P., et al. 2005, MNRAS, 362, 245

Jakobsson, P., et al. 2006b, A&A, 447, 897

Jakobsson, P., et al. 2006c, A&A, 460, L13

Jakobsson, P., et al. 2006d, GCN Circ., 5319, 1

Jakobsson, P., et al. 2007d, GCN Circ., 6398, 1

Jakobsson, P., et al. 2007e, GCN Circ., 7117, 1

Jakobsson, P., et al. 2008d, GCN Circ., 7998, 1

Jakobsson, P., et al. 2008e, GCN Circ., 8062, 1

Jaunsen, A. O., Fynbo, J. P. U., Andersen, M. I., & Vreeswijk, P. M. 2007a, GCN Circ., 6216, 1

Jaunsen, A. O., Malesani, D., Fynbo, J. P. U., Sollerman, J., & Vreeswijk, P. M. 2007b, GCN Circ., 6010, 1

Jaunsen, A. O., et al. 2008, ApJ, 681, 453

Jensen, B. L., et al. 2001, A&A, 370, 909

Kaper, L., et al. 2009, in Astrophysics and Space Science Proceedings, Science with the VLT in the ELT Era, ed. A. Moorwood (Netherlands: Springer), 319

Kawai, N., et al. 2006, Nature, 440, 184

Kistler, M. D., Yuksel, H., Beacom, J. F., & Stanek, K. Z. 2008, ApJ, 673, L119

Kouveliotou, C., et al. 1993, ApJ, 413, L101

Krühler, T., et al. 2008, ApJ, 685, 376

Krumholz, M. R., Ellison, S. L., Prochaska, J. X., & Tumlinson, J. 2009, ApJ, 701, L12

Kuepcue Yoldas, A., Yoldas, A., Greiner, J., Kruehler, T., & Rossi, A. 2008, GCN Circ., 7303, 1

Kuin, N. P. M., Grupe, D., & Brown, P. 2007, GCN Circ., 6238, 1

Lazzati, D., Covino, S., & Ghisellini, G. 2002, MNRAS, 330, 583

Ledoux, C., Jakobsson, P., Jaunsen, A. O., Thöne, C. C., Vreeswijk, P. M., Malesani, D., Fynbo, J. P. U., & Hjorth, J. 2007, GCN Circ., 7023, 1

Ledoux, C., Petitjean, P., Fynbo, J. P. U., Møller, P., & Srianand, R 2006a, A&A, 457, 71

Ledoux, C., et al. 2005, GCN Circ., 3860, 1

Ledoux, C., et al. 2006b, GCN Circ., 5237, 1

Ledoux, C., et al. 2009, A&A, 506, 661

Levan, A. J., et al. 2006, ApJ, 647, 471

Levan, A. J., et al. 2007, MNRAS, 378, 1439

Malesani, D., Jakobsson, P., Fynbo, J. P. U., Hjorth, J., & Vreeswijk, P. M. 2007, GCN Circ., 6651, 1

Malesani, D., Jakobsson, P., Fynbo, J. P. U., Stritzinger, M., & Covino, S. 2006, GCN Circ., 5350, 1

Marshall, F. E., Godet, O., & Oates, S. R. 2008, GCN Circ., 7664, 1

Marshall, F., & Vetere, L. 2006, GCN Circ., 4917, 1

Mirabal, N., & Halpern, J. P. 2006, GCN Circ., 4591, 1

Morgan, A. N., Vanden Berk, D. E., Brown, P., & Evans, P. A. 2006, GCN Circ., 7661, 1

Møller, P., et al. 2002, A&A, 396, L21

Mundell, C. G., et al. 2007, ApJ, 660, 489

Noll, S., et al. 2004, A&A, 418, 885

Noterdaeme, P., et al. 2009, A&A, 505, 1087

Nysewander, M., Fruchter, A. S., & Peer, A. 2009, ApJ, 701, 824

Oates, S. R., & Markwardt, C. B. 2008, GCN Circ., 7253, 1

Oates, S. R., et al. 2006, MNRAS, 372, 327

Oates, S. R., et al. 2009, MNRAS, 395, 490

Oke, J. B., et al. 1995, PASP, 107, 375

Page, K. L., et al. 2009, MNRAS, in press (arXiv:0907.4578)

Pedersen, K., et al. 2006, ApJ, 636, 381

Perley, Chornock, R., & Bloom, J. S. 2008, GCN Circ., 7962, 1

Perley, D. 2009a, Gamma-Ray Burst Online Index (Berkeley, CA: UC Berkeley), http://grbox.net

Perley, D. A., et al. 2009b, AJ, 138, 1690

Piranomonte, S., et al. 2006a, GCN Circ., 4520, 1

Piranomonte, S., et al. 2006b, GCN Circ., 5626, 1
Piranomonte, S., et al. 2007, GCN Circ., 6985, 1
Piranomonte, S., et al. 2008, A&A, 492, 775
Pontzen, A., et al. 2009, MNRAS, submitted (arXiv:0909.1321)
Poole, T., Moretti, A., Holland, S. T., Chester, M., Angelini, L., & Gehrels, N. 2005, GCN Circ., 3698, 1
Prochaska, J. X., Chen, H.-W., & Bloom, J. S. 2006a, ApJ, 648, 95
Prochaska, J. X., Chen, H.-W., Dessauges-Zavadsky, M., & Bloom, J. S. 2007, ApJ, 666, 267
Prochaska, J. X., Chen, H.-W., Wolfe, A. M., Dessauges-Zavadsky, M., & Bloom, J. S. 2008a, ApJ, 672, 59
Prochaska, J. X., Dessauges-Zavadsky, M., Ramirez-Ruiz, E., & Chen, H.-W. 2008b, ApJ, 685, 344
Prochaska, J. X., Foley, R., Tran, H., Bloom, J. S., & Chen, H.-W. 2006b, GCN Circ., 4593, 1
Prochaska, J. X., Murphy, M., Malec, A., & Miller, S. 2008c, GCN Circ., 7388, 1
Prochaska, J. X., et al. 2009, ApJ, 691, L27
Prochter, G. E., et al. 2006, ApJ, 648, L93
Racusin, J. L., et al. 2008, Nature, 455, 183
Reddy, N., & Steidel, C. C. 2008, ApJ, 692, 778
Rol, E., Jakobsson, P., Tanvir, N. R., & Levan, A. 2006, GCN Circ., 5555, 1
Rol, E., et al. 2007a, MNRAS, 374, 1078
Rol, E., et al. 2007b, GCN Circ., 6221, 1
Romano, P., et al. 2006, A&A, 456, 917
Ruiz-Velasco, A. E., et al. 2007, ApJ, 669, 1
Rykoff, E. S., et al. 2007, GCN Circ., 6992, 1
Salvaterra, R., et al. 2009, Nature, 461, 1258
Savaglio, S. 2006, New J. Phys., 8, 195
Savaglio, S., Fall, S. M., & Fiore, F. 2003, ApJ, 585, 638
Savaglio, S., Palazzi, E., Ferrero, P., & Klose, S. 2006, GCN Circ., 6166, 1
Savaglio, S., et al. 2002, GCN Circ., 1633, 1
Savaglio, S., et al. 2004, ApJ, 602, 51
Schady, P., & Moretti, A. 2006, GCN Circ., 5296, 1
Schady, P., et al. 2006, ApJ, 643, 276
Schady, P., et al. 2007a, MNRAS, 377, 273
Schady, P., et al. 2007b, MNRAS, 380, 1041
Schlegel, D. J., Finkbeiner, D. P., & Davis, M. 1998, ApJ, 500, 525
Schaye, J. 2001, ApJ, 562, L95
Shapley, A., Steidel, C. C., Pettini, M., & Adelberger, K. L. 2003, ApJ, 588, 65
Sheffer, Y., Prochaska, J. X., Draine, B. T., Perley, D. A., & Bloom, J. S. 2009, ApJ, 701, L63
Soderberg, A. M., Berger, E., & Ofek, E. 2005, GCN Circ., 4186, 1
Soderberg, A. M., et al. 2007, ApJ, 661, 982
Sollerman, J., et al. 2006, A&A, 454, 503
Sollerman, J., et al. 2007, A&A, 466, 839
Stanek, K. Z., et al. 2003, ApJ, 591, L17
Starling, R., Thöne, C. C., Fynbo, J. P. U., Vreeswijk, P. M., & Hjorth, J. 2006a, GCN Circ., 5131, 1
Starling, R. L. C., et al. 2005, A&A, 442, L21

Starling, R., et al. 2006b, GCN Circ., 5149, 1
Starling, R. L. C., et al. 2009, MNRAS, in press (arXiv:0812.2490)
Sudilovsky, V., et al. 2007, ApJ, 669, 741
Tanvir, N. R., Rol, E., & Stephens, A. 2008a, GCN Circ., 7488, 1
Tanvir, N. R., et al. 2008b, MNRAS, 388, 1743
Tanvir, N. R., et al. 2009, Nature, 461, 1254
Tejos, N., Lopez, S., Prochaska, J. X., Chen, H.-W., & Dessauges-Zavadsky, M. 2007, ApJ, 671, 622
Thöne, C. C., De Cia, A., Malesani, D., & Vreeswijk, P. M. 2008a, GCN Circ., 7587, 1
Thöne, C. C., Fynbo, J. P. U., & Jakobsson, P. 2006b, GCN Circ., 5747, 1
Thöne, C. C., Fynbo, J. P. U., Jakobsson, P., Vreeswijk, P. M., & Hjorth, J. 2006c, GCN Circ., 5812, 1
Thöne, C. C., Jakobsson, P., Fynbo, J. P. U., Malesani, D., Hjorth, J., & Vreeswijk, P. M. 2007b, GCN Circ., 6499, 1
Thöne, C. C., Jaunsen, A. O., Fynbo, J. P. U., Jakobsson, P., & Vreeswijk, P. M. 2007a, GCN Circ., 6379, 1
Thöne, C. C., Kann, D. A., Augusteijn, T., & Reyle-Laffont, C. 2007c, GCN Circ., 6154, 1
Thöne, C. C., Perley, D. A., & Bloom, J. S. 2007d, GCN Circ., 6663, 1
Thöne, C. C., et al. 2006c, GCN Circ., 5373, 1
Thöne, C. C., et al. 2008b, A&A, 489, 37
Thöne, C. C., et al. 2008c, GCN Circ., 7602, 1
Thöne, C. C., et al. 2008d, GCN Circ., 8058, 1
Thöne, C. C., et al. 2008e, A&A, submitted (arXiv:0806.1182)
van Paradijs, J., et al. 1997, Nature, 386, 686
Vergani, S. D., et al. 2009, A&A, 503, 771
Vreeswijk, Fynbo, J. P. U., Malesani, D., Hjorth, J., & de Ugarte Postigo, A. 2008a, GCN Circ., 8191, 1
Vreeswijk, P. M., Jakobsson, P., Jaunsen, A. O., & Ledoux, C. 2008b, GCN Circ., 7391, 1
Vreeswijk, P. M., Møller, P., & Fynbo, J. P. U. 2003, A&A, 409, L5
Vreeswijk, P. M., et al. 2004, A&A, 419, 927
Vreeswijk, P. M., et al. 2007, A&A, 468, 83
Vreeswijk, et al. 2008c, GCN Circ., 7444, 1
Vreeswijk, et al. 2008d, GCN Circ., 7601, 1
Vreeswijk, P. M., et al. 2008e, GCN Circ., 8301, 1
Ward, P., & Ziaeepour, H. 2008, GCN Circ., 7941, 1
Watson, D., et al. 2006, ApJ, 652, 1011
Weymann, R. J., Carswell, R. F., & Smith, M. G. 1981, ARA&A, 19, 41
Wiersema, K., et al. 2008a, GCN Circ., 7517, 1
Wiersema, K., et al. 2008b, GCN Circ., 7818, 1
Wijers, R. A. M. J., Bloom, J. S., Bagla, J. S., & Natarajan, P. 1998, MNRAS, 294, L13
Wolfe, A. M., Gawaiser, E., & Prochaska, J. X. 2005, ARA&A, 43, 861
Woosley, S., & Bloom, J. S. 2006, ARA&A, 44, 507
Woosley, S. E., & Heger, A. 2006, ApJ, 637, 914
Woźniak, P. R., et al. 2009, ApJ, 691, 495
Xin, L. P., et al. 2008, GCN Circ., 7371, 1
Zheng, W., Deng, J., & Wang, J. 2009, RAA, 9, 1103

ERRATUM: "LOW-RESOLUTION SPECTROSCOPY OF GAMMA-RAY BURST OPTICAL AFTERGLOWS: BIASES IN THE *SWIFT* SAMPLE AND CHARACTERIZATION OF THE ABSORBERS[*]"
(2009, ApJS, 185, 526)

J. P. U. Fynbo[1,2], P. Jakobsson[2], J. X. Prochaska[3], D. Malesani[1], C. Ledoux[4], A. de Ugarte Postigo[4], M. Nardini[5], P. M. Vreeswijk[1,4], K. Wiersema[6], J. Hjorth[1], J. Sollerman[1,7], H.-W. Chen[8], C. C. Thöne[1,9], G. Björnsson[2], J. S. Bloom[10], A. Castro-Tirado[11], L. Christensen[12], A. De Cia[2], A. S. Fruchter[13], J. U. Gorosabel[11], J. F. Graham[13], A. O. Jaunsen[1], B. L. Jensen[1], D. A. Kann[14], C. Kouveliotou[15], A. Levan[16], J. Maund[1], N. Masetti[17], B. Milvang-Jensen[1], E. Palazzi[17], D. A. Perley[10], E. Pian[18], E. Rol[6], P. Schady[19], R. Starling[6], N. Tanvir[6], D. J. Watson[1], D. Xu[1], T. Augusteijn[20], F. Grundahl[21], J. Telting[20], AND P.-O. Quirion[21]

[1] Dark Cosmology Centre, Niels Bohr Institute, University of Copenhagen, Juliane Maries Vej 30, DK-2100 Copenhagen O, Denmark
[2] Centre for Astrophysics and Cosmology, Science Institute, University of Iceland, Dunhagi 5, IS-107 Reykjavík, Iceland
[3] Department of Astronomy and Astrophysics, UCO/Lick Observatory, University of California, 1156 High Street, Santa Cruz, CA 95064, USA
[4] European Southern Observatory, Alonso de Córdova 3107, Vitacura, Casilla 19001, Santiago 19, Chile
[5] SISSA—Via Beirut 2/4, I-34014 Trieste, Italy
[6] Department of Physics and Astronomy, University of Leicester, University Road, Leicester, LE1 7RH, UK
[7] Department of Astronomy, The Oskar Klein Centre, Stockholm University, 106 91 Stockholm, Sweden
[8] Department of Astronomy & Astrophysics and Kavli Institute for Cosmological Physics, University of Chicago, Chicago, IL 60637, USA
[9] INAF—Osservatorio Astronomico di Brera, Via Bianchi 46 I-23806 Merate, Italy
[10] Department of Astronomy, University of California, Berkeley, CA 94720-3411, USA
[11] IAA-CSIC, P.O. Box 03004, E-18080 Granada, Spain
[12] European Southern Observatory, Karl-Schwarzschildstrasse 2, D-85748 Garching, Germany
[13] Space Telescope Science Institute, Department of Physics and Astronomy, Johns Hopkins University, 3700 San Martin Drive, Baltimore, MD 21218, USA
[14] Thüringer Landessternwarte Tautenburg, Sternwarte 5, D-07778 Tautenburg, Germany
[15] NASA Marshall Space Flight Center, Huntsville, AL 35805, USA
[16] Department of Physics, University of Warwick, Coventry CV4 7AL, UK
[17] INAF—Istituto di Astrofisica Spaziale e Fisica Cosmica di Bologna, via Gobetti 101, 40129 Bologna, Italy
[18] INAF—Trieste Astronomical Observatory, 34143 Trieste, Italy
[19] The UCL Mullard Space Science Laboratory, Holmbury St Mary, Dorking, Surrey RH5 6NT, UK
[20] Nordic Optical Telescope Apartado 474, 38700 Santa Cruz de La Palma, Santa Cruz de Tenerife, Spain
[21] Institute of Physics and Astronomy, University of Århus, Ny Munkegade, DK-8000 Århus C, Denmark

In this paper, Figure 14 is incomplete due to an error during production. We here provide the missing sub-figures.

Figure 14. Shown are one- and two-dimensional spectra for GRBs 0070721B–080928, which were missed in the original paper. Lines from the GRB absorption systems are marked with vertical lines whereas unidentified lines or lines from intervening systems are marked with vertical dashed lines. Telluric features are marked with a telluric symbol. The error spectrum is plotted as a dotted line. When in the spectral range we also plot the position of the Lyman limit as a vertical dashed line.
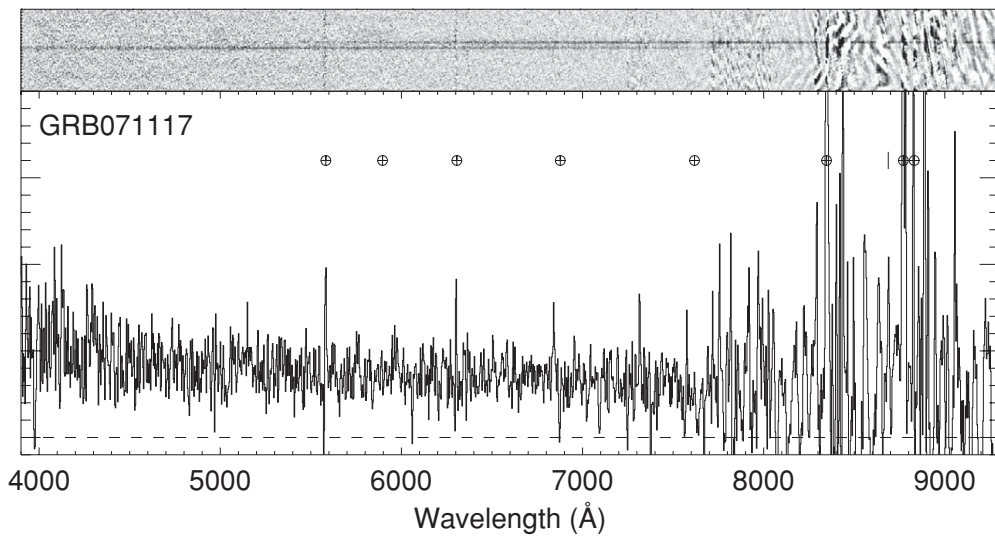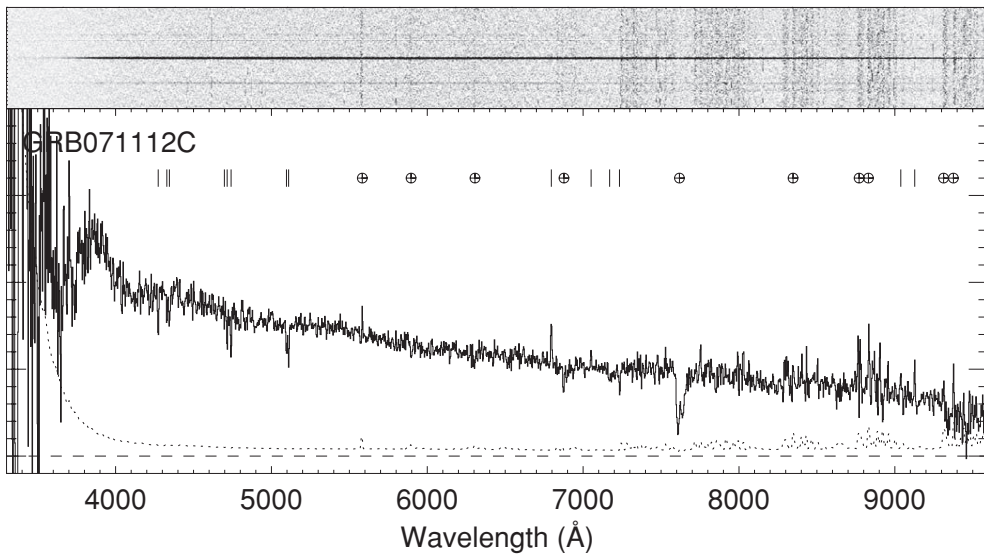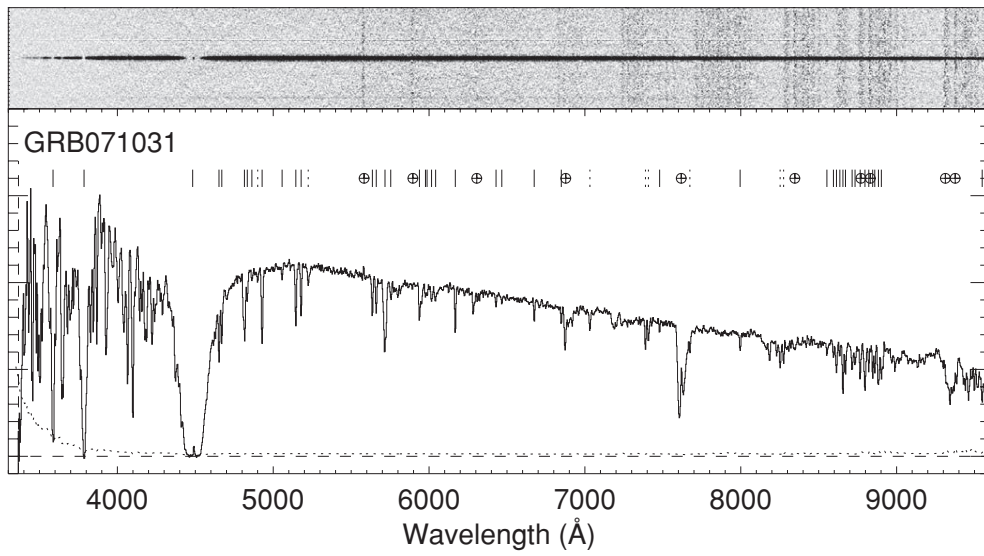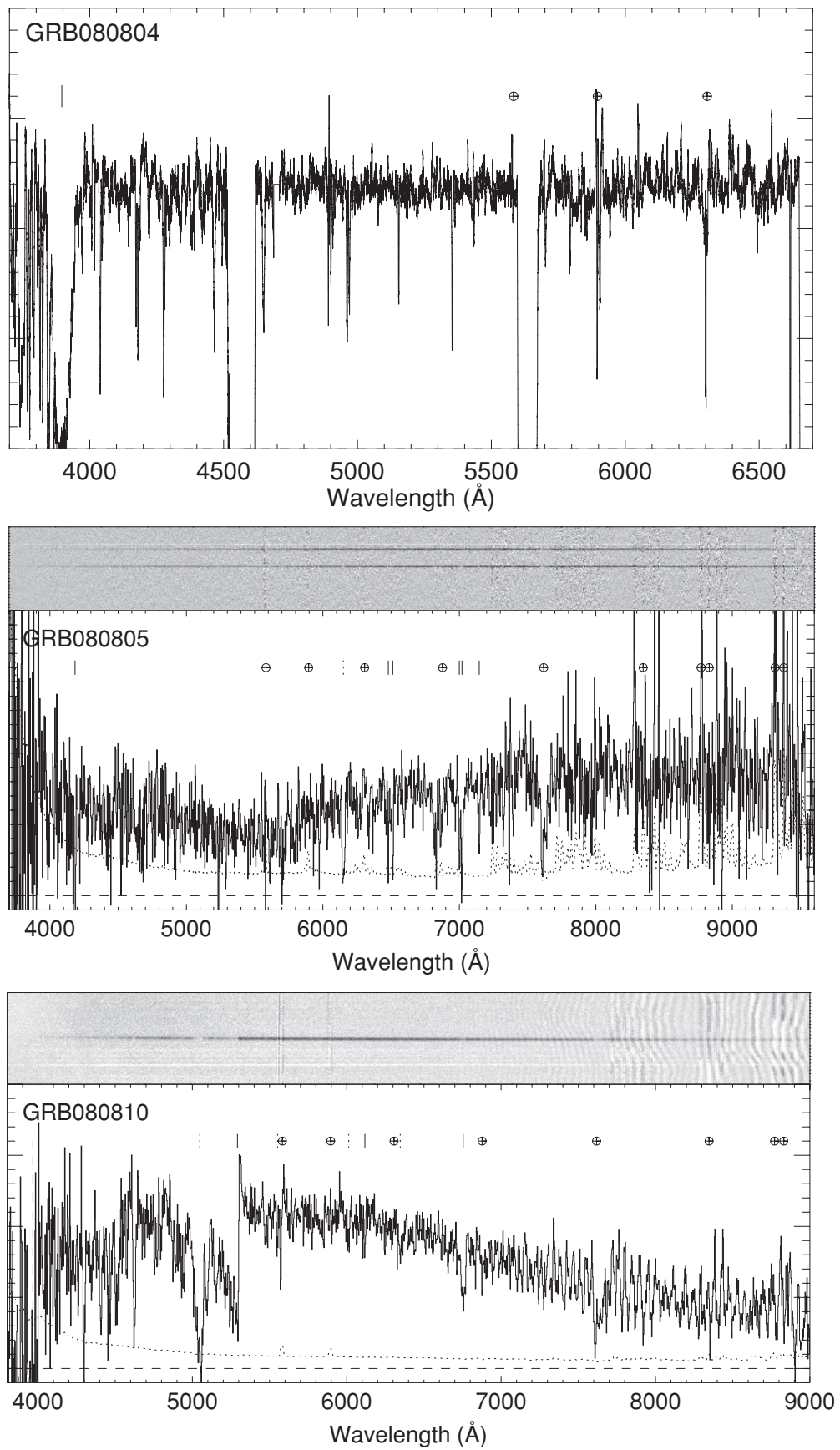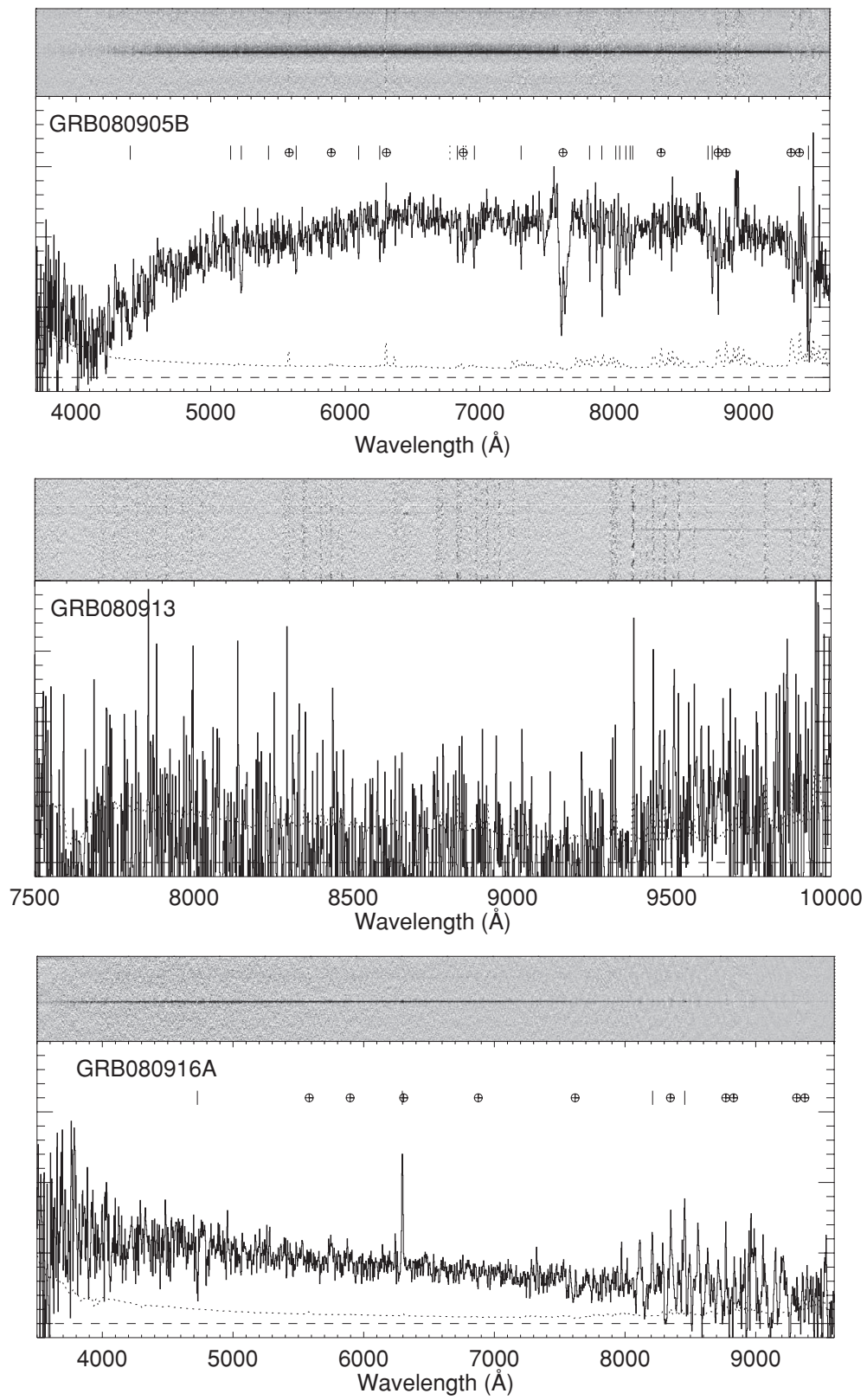
Figure 14. (Continued)

Figure 14. (Continued)

Figure 14. (Continued)

Figure 14. (Continued)

Figure 14. (Continued)

Figure 14. (Continued)

GRB080707

GRB080710

GRB080721

Figure 14. (Continued)

Figure 14. (Continued)

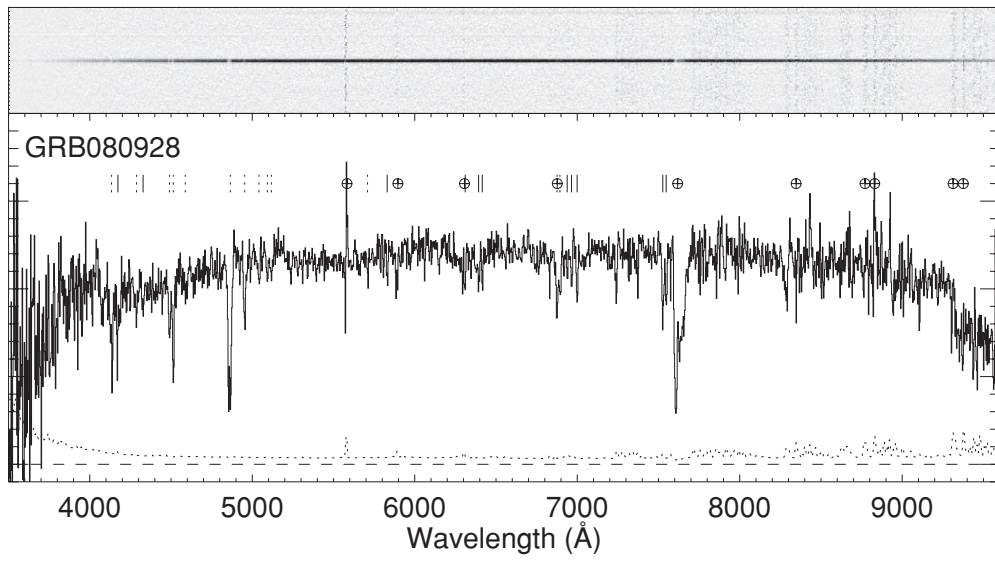**Figure 14.** (Continued)

Figure 14. (Continued)